

A UV Zeeman-Effect Polarizer

by

Robert Wallace Grant

B.Sc., The University of Manitoba, 1979

A THESIS SUBMITTED IN PARTIAL FULFILMENT OF  
THE REQUIREMENTS FOR THE DEGREE OF  
MASTER OF SCIENCE

in

THE FACULTY OF GRADUATE STUDIES  
(Department of Physics)

We accept this thesis as conforming  
to the required standard

THE UNIVERSITY OF BRITISH COLUMBIA

September 1985

© Robert Wallace Grant, 1985

In presenting this thesis in partial fulfilment of the requirements for an advanced degree at the University of British Columbia, I agree that the Library shall make it freely available for reference and study. I further agree that permission for extensive copying of this thesis for scholarly purposes may be granted by the head of my department or by his or her representatives. It is understood that copying or publication of this thesis for financial gain shall not be allowed without my written permission.

Department of Physics

The University of British Columbia  
1956 Main Mall  
Vancouver, Canada  
V6T 1Y3

Date Aug. 30 1985

ABSTRACT

It is shown that light emitted by mercury vapour at 253.7 nm can be polarized by passing the light through mercury absorption gas embedded in a magnetic field which is transverse to the direction of propagation of the light. The absorption lines of the mercury are split by the Zeeman effect, so that the absorber has an absorption coefficient which depends on both the polarization and wavelength of the transmitted light.

A complete theory for the  $\text{Hg}^{202}$  isotope is presented and the results are compared to measurements made with a natural mercury emitter and absorber. The observations are in qualitative agreement with the theory once isotope and hyperfine structure of the isotopes in natural mercury are included in the theory. Quantitative analysis was not possible because the emission line profiles could not be measured with the available equipment.

## TABLE OF CONTENTS

|  |      |   |
|--|------|---|
| Abstract .....   | ii   |   |
| Table of Contents .....                                | iii  |   |
| List of Figures .....                                  | vi   |   |
| Acknowledgements .....                                 | viii |   |
| Chapter One  |      |   |
| Introduction .....                                     | 1    |   |
| Chapter Two .....                                      |      | 3 |
| II.1 The Zeeman Effect .....                           | 4    |   |
| II.2 Line Broadening .....                             | 14   |   |
| Natural Broadening .....                               | 15   |   |
| Resonance Broadening .....                             | 17   |   |
| Doppling Broadening .....                              | 21   |   |
| The Combined Line Profile .....                        | 22   |   |
| II.3 Theory .....                                      | 24   |   |
| II.4 The Wave in a Transverse and Parallel Field ..... | 50   |   |
| The Transverse Field .....                             | 51   |   |
| Parallel Field .....                                   | 57   |   |

|   |    |
|---|----|
| II.5 The Polarization of the Transmitted Wave ..... | 58 |
| Completely Polarized Light .....                    | 65 |
| Unpolarized Light .....                             | 67 |
| Partially Polarized Light .....                     | 68 |
| Unpolarized Incident Wave .....                     | 70 |
| Simple Examples .....                               | 72 |
| Linearly Polarized Incident Wave .....              | 75 |

### Chapter Three

|   |     |
|---|-----|
| III.1 The Experimental Design .....                                 | 89  |
| The Light Source .....  | 92  |
| The Gas Cell .....  | 93  |
| The Magnet .....  | 95  |
| The Aperture Stops and Lenses .....                                 | 96  |
| Polarizer and Quarter-Wave Plate .....                              | 97  |
| Monochromator .....   | 98  |
| Detector .....  | 98  |
| Effect of the Magnetic Field on the<br>Experimental Apparatus ..... | 99  |
| III.2 The Experimental Procedure .....                              | 100 |
| The Unstable Light Source .....                                     | 104 |
| III.3 Experimental Error .....                                      | 106 |
| III.4 Experimental Results .....                                    | 110 |

## Chapter Four

|  |     |
|--|-----|
| Comparing Theory and Experiment .....                  | 120 |
| IV.1 The Effect of Using Natural Mercury               |     |
| in the Absorption Cell .....                           | 121 |
| Effect of Nuclear Spin .....                           | 121 |
| IV.2 The Shape of the Experimental Incident Line ..... | 124 |
| IV.3 The Experimental Results .....                    | 125 |

## Chapter Five

|                             |     |
|-----------------------------|-----|
| Concluding Discussion ..... | 129 |
| References .....            | 132 |
| Appendix .....              | 135 |

## LIST OF FIGURES

| Figure Numbers  | Page |
|---|------|
| 1. Relative Intensities $I^{\text{rel}}$ of the Component Lines for observations along the y-axis .....   | 12   |
| 2. Orientation of the Magnetic Field .....  | 27   |
| 3. Orientation of $ u\rangle$ Co-ordinate System .....  | 32   |
| 4. a) Polarization Measuring System   |      |
| b) Polarization Orientation .....   | 62   |
| 5. Emission, Absorption and Transmission Line Profile .....   | 73   |
| 6. Geometry of Polarization Ellipse .....   | 78   |
| 7. $J_{yy}^{\infty}$ as a function of Magnetic Field Strength for Three Gas Temperatures, 300K, 350K and 375K<br>D = 25 ( $10^{-3}$ ) $\text{cm}^{-1}$<br>$J_{xx} = J_{yy}$ at zero field and is independent of the strength of the field ..... | 86   |
| 8. $J_{yy}^{\infty}$ as a function of Magnetic Field Strength for Three Gas Temperature, 300K, 350K and 375K<br>D = 40 ( $10^{-3}$ $\text{cm}^{-1}$ )<br>$J_{xx} = J_{yy}$ at zero field and is independent of the strength of the field .....  | 87   |

9.  $J_{yy}^{\infty}$  as a function of Magnetic Field Strength for  
 Three Gas Temperatures, 300K, 350K and 375K  
 $D = 60(10^{-3}\text{cm}^{-1})$   
 $J_{xx} = J_{yy}$  at zero field and is independent of the  
 strength of the field ..... 88
10. Experimental Apparatus ..... 90
11. Temperature Regulator for the Water Bath ..... 94
12.  $\text{Im}(J_{xy})$  as a function of Magnetic Field Strength ..... 113
13.  $J'_{xx}$  and  $J'_{yy}$  as functions of magnetic field strength  
 for a natural mercury absorption gas at 22.6°C. .... 117
14.  $J'_{xx}$  and  $J'_{yy}$  as function of magnetic field strength for  
 a natural mercury absorption gas at 30°C ..... 118
15. Polarization P as a function of magnetic field strength  
 for a natural mercury gas at 22.6° and 30.0°C ..... 119

ACKNOWLEDGEMENTS

Physics demands extended periods of isolated solitary work. The reward for this effort comes from the time spent with others sharing ideas and learning. I would like to thank my friends and colleagues in the Physics Department for making my time there rewarding. I would particularly like to thank Dr. F.L. Curzon who suggested and supervised the work in this thesis. Without his unflagging support this thesis would never have been completed.

I would also like to thank Mr. A. Cheuck for his assistance in designing and constructing the experimental apparatus. The assistance of Dr. Bloom in providing laboratory space and the electromagnet used in the experiment is also acknowledged.

Finally, I would like to thank Dr. F.L. Curzon, Susan Mah, Connie Zator, Young Yuen and Don Furseth for their help in preparing this thesis.

CHAPTER I

Introduction

A number of spectroscopic techniques for analysing line shapes and transition probabilities require high quality linear polarizers. These polarizers currently exist for the visible and near ultra-violet region, but because of the properties of the dispersive media used, they have low transmissivity in the far ultra-violet region.

The object of this study is to examine the possibility of exploiting the Zeeman Effect to produce polarizers which have a high transmissivity in the ultra-violet region. The proposed technique involves the characteristics of the absorption spectra of a gas immersed in a magnetic field. The absorption spectra, when viewed in a direction transverse to the magnetic field, split into a series of Zeeman Components which are linearly polarized either transverse or parallel to the magnetic field. By adjusting the degree of splitting and the shape of the absorption lines the gas can act as a linear polarizer for incident light at or near an absorption line of the gas.

The technique is examined both theoretically and experimentally. In Chapter II a theoretical model is developed for the propagation of light in a gas immersed in a magnetic field. The derived equations are more general than is required for this study, but it is hoped that they may find application in further studies.

The theoretical model is used to calculate the effect of a gas composed of the  $\text{Hg}^{202}$  isotope, on the state of polarization of an incident 253.7 nm line of mercury. The 253.7 nm line was selected because its properties are reasonably well known and therefore the calculation could be performed with a high degree of precision. The theoretical calculations indicate that the method can be used to produce highly linearly polarized light with small transmission losses.

The technique is examined experimentally in Chapter III. The state of polarization of the 253.7 nm line of mercury is measured after the initially unpolarized light traverses a gas cell filled with natural mercury and immersed in a magnetic field traverse to the direction of propagation of the light. While the use of natural mercury rather than an even isotope introduces a number of undesirable effects, the experiment supports the conclusion that the technique can be used to produce high quality polarizers.

## CHAPTER II

In this chapter a theoretical model is developed to describe the production of polarized light through the Zeeman Effect. The purpose of this model is to account for the observed polarization and in so doing provide a framework for its study and assessment. The final result is an equation for the transmission of light through a gas immersed in a magnetic field, where the frequency of the light is at or near a resonance frequency of the atoms of the gas. The equation indicates how to optimize the polarization and in addition reveals the inherent limitations of this method of polarizing light.

The central role of the Zeeman Effect in this study necessitates a review of this phenomenon. However, since many comprehensive accounts of this effect already exist, (see Condon and Shortley 1964, Sobel'man 1972, and Kuhn 1969) only a cursory review is presented. Brevity is achieved in part by omitting the mathematical derivations of most of the equations, and by presenting only those equations which are necessary for a clear understanding of the effect, or which are required in the subsequent theoretical development.

### II.1 THE ZEEMAN EFFECT

When atoms are placed in an external magnetic field it is found that the field causes some of the spectral lines of these atoms to split into a series of component lines which are displaced about the frequency of the original line. If a spectral line is observed along an axis which is transverse to the direction of the magnetic field, it is found that a given component line is linearly polarized with its electric field vector either parallel ( $\pi$ -component), or perpendicular ( $\sigma$ -component), to the external magnetic field vector. It is these two results, the splitting of the spectral lines and the polarization of the component lines, which together comprise the Zeeman Effect.

The Zeeman Effect can only be satisfactorily accounted for by using a quantum mechanical representation of the atom in an external magnetic field as given by:

$$H = H_0 + H_m \quad (2-1)$$

where  $H_0$  is the Hamiltonian of the isolated atom, and  $H_m$  describes the interaction between the external magnetic field  $\vec{B}$  and the magnetic moment of the atom  $\vec{\mu}$ .  $H_m$  has the form

$$H_m = -\vec{\mu} \cdot \vec{B} \quad (2-2)$$

The magnetic moment of the atom is related to the total orbital angular momentum  $\vec{L}$  and the total spin angular momentum  $\vec{S}$  of the electrons in the

†

atom through the equation :

$$\vec{\mu} = \frac{\mu_o}{h} (\vec{L} + 2 \vec{S}) \quad (2-3)$$

where

$$\mu_o = \frac{eh}{2m_e} \quad (2-4)$$

is the Bohr Magneton;  $m_e$ , is the electron mass; and  $e$  is the elementary charge.

The Hamiltonian  $H$  should also contain a term  $H'_m$  which is quadratic in  $\vec{B}$ . This term would account for the induced effect of atomic diamagnetism. However, it can be shown (see Messiah 1962, page 541) that for the lower energy states of the atom:

$$\frac{H'_m}{H_m} \sim 10^{-5} ZB \quad (\text{Tesla}) \quad (2-5)$$

where  $Z$  is the atomic number of the atom. Thus, for the modest fields of less than 1 Tesla considered in this study, the term  $H'_m$  is negligibly small and can be excluded from the Hamiltonian  $H$ .

The Hamiltonian equation is solved using perturbation techniques. The eigenstates of  $H_o$  are given by  $|\alpha jm\rangle$  where  $j$  is the quantum number for the total angular momentum  $J$  of the state,  $mh$  is the eigenvalue of  $J_z$  (the component of the total angular momentum operator along the  $z$  axis), and  $\alpha$  labels all the remaining quantum numbers of the state. The eigenstates are

---

†At this point only atoms with a nuclear spin  $I = 0$  are considered.

$(2j + 1)$  - fold degenerate in the quantum number  $m$ , i.e. states from the same level have the same energy.<sup>†</sup>

The degeneracy of the states dictates the use of a degenerate perturbation technique, which reduces the problem of finding the first order change in the energy  $\Delta E_{jm}$  of each state to the diagonalization of a perturbation matrix, (see Merzbacher, 1970, page 425).

In the representation  $|\alpha jm\rangle$  the perturbation matrix, which includes all the states of a given level, is already diagonal and the equation for  $\Delta E_{jm}$  reduces to:

$$\begin{aligned}\Delta E_{jm} &= \langle \alpha jm | H_m | \alpha jm \rangle \\ &= \frac{\mu_o}{h} \langle \alpha jm | (\vec{L} + 2\vec{S}) \cdot \vec{B} | \alpha jm \rangle \\ &= \frac{\mu_o}{h} \langle \alpha jm | g_{\alpha j} \vec{J} \cdot \vec{B} | \alpha jm \rangle \\ &= \mu_o g_{\alpha j} B_m\end{aligned}\tag{2-6}$$

where, in the last step, the  $z$  axis was chosen along  $\vec{B}$ .  $g_{\alpha j}$ , known as the Landé  $g$  factor, is a constant for each level, i.e. it is independent of  $m$ .

---

<sup>†</sup>There is some ambiguity in the meanings of the terms 'level' and 'energy level', (see Condon and Shortley pages 97 and 385). To avoid confusion the term 'energy level' will refer exclusively to the energy associated with a particular state, or when the state is degenerate to the energy associated with the group of degenerate states. The term 'level' will refer to the group of states which differ only in their  $m$  quantum number, even when these states are no longer degenerate.

Implicit in this development is the assumption that the change in energy due to  $H_m$  is much less than the energy separation between the levels; or equivalently, the perturbation due to  $H_m$  is much smaller than the perturbation due to the spin-orbit interaction. Where this assumption is no longer valid the neighboring levels must also be included in the perturbation matrix. For most of the levels of heavier atoms this is necessary only for magnetic fields larger than 1 Tesla, which are not considered in this study. The assumption is easily satisfied for the 253.7 nm line of mercury (see the appendix).

The effect of the magnetic field on the states can be deduced from equation (2-6). The degenerate level splits into  $(2j+1)$  different energy levels, each of which corresponds to a unique value of  $m$ . These new energy levels are symmetrically displaced about the original energy level since  $m = \pm j, \pm j - 1, \dots$ . The magnitude of the splitting is linear in  $B$ . There is no first order change in the energy level of a state with  $j = 0$  or  $m = 0$ .

The effect of the magnetic field on the line spectra of an atom can now be examined. The absorption or emission of a photon by an atom is associated with the transition from one energy level to another. The angular frequency of a spectral line resulting from such a transition in the absence of a magnetic field is given by  $\omega_0$ , where:

$$\omega_0 = \frac{1}{h} | E_{\alpha j}^{\circ} - E_{\alpha' j'}^{\circ} | \quad (2-7)$$

and  $E_{\alpha j}^{\circ}$  and  $E_{\alpha' j'}^{\circ}$  are the energy levels of the unperturbed states  $|\alpha jm\rangle$  and  $|\alpha' j' m'\rangle$  respectively.

In the presence of a magnetic field the energy levels  $E_{\alpha jm}$  become:

$$E_{\alpha jm} = E_{\alpha j}^{\circ} + \Delta E_{jm} = E_{\alpha j}^{\circ} + g_{\alpha j} \mu_o Bm \quad (2-8)$$

and the line splits into a series of component lines<sup>†</sup> with angular frequencies  $\omega_{mm'}$ , where:

$$\omega_{mm'} = \frac{1}{h} [(E_{\alpha j}^{\circ} - E_{\alpha' j'}^{\circ}) + \mu_o B (g_{\alpha j} m - g_{\alpha' j'} m')]$$

or

$$\omega_{mm'} = \omega_0 + \frac{\mu_o}{h} B (g_{\alpha j} m - g_{\alpha' j'} m') \quad (2-9)$$

This equation describes the observed splitting of the spectral lines by the magnetic field. However, the additional property of the Zeeman effect, namely the polarization of the component lines, is only indirectly related to the presence of the magnetic field. It can only be properly accounted for by examining the radiative process which governs the transition between two states. Furthermore, while equation (2-9) describes all possible transitions between two levels, these transitions may occur with markedly different probabilities. It is the radiative process that determines the probability of a particular transition or equivalently the strength of the associated component line.

---

<sup>†</sup>The component lines are produced by the transitions between specific states of two given levels.

These observations indicate that a brief digression to the theory of radiative processes is necessary for a complete understanding of the Zeeman Effect. For the purposes of this study the only radiative processes of interest are those described by electric dipole transitions, since these produce the most intense lines.

The probability  $W_{\vec{R}}$  of an electric dipole transition between the states  $|\alpha jm\rangle$  and  $|\alpha' j' m'\rangle$  resulting in the absorption or emission of a photon polarized in the direction of the unit vector  $\vec{R}$  and travelling in the direction  $\vec{k}$  is of the form: (Sobel'man page 305)

$$W_{\vec{R}} \propto |\vec{R} \cdot \langle \alpha jm | \vec{P} | \alpha' j' m' \rangle|^2 \quad (2-10)$$

where  $\vec{P}$  is the electric dipole operator

$$\vec{P} = -e \sum_i^Z \vec{r}_i \quad (2-11)$$

and the sum is taken over the position  $\vec{r}_i$  of each electron with respect to the nucleus.

Most of the interesting properties of the transition can be deduced from the matrix element  $\langle \alpha jm | \vec{P} | \alpha' j' m' \rangle$ . In particular, by exploiting the Wigner-Eckart Theorem (see Messiah page 573), the dependence of the matrix element and hence  $W_{\vec{R}}$  on  $m$  and  $m'$  can be found as follows:

$$\langle \alpha j m | \vec{P} | \alpha' j' m' \rangle = \frac{1}{\sqrt{(2j+1)}} C(j' 1 m' q | j m) \\ \times \langle \alpha j || P || \alpha' j' \rangle e_q^* \quad (2-12)$$

where  $\langle \alpha j || P || \alpha' j' \rangle^\dagger$ , the reduced matrix element, is a scalar independent of  $m$  and  $m'$ ,  $C(j' 1 m' q | j m)$  is a Clebsch-Gordon coefficient (these are tabulated in Condon and Shortley page 76),  $q = m - m'$ ,  $e_q^*$  is the complex conjugate of the unit vector  $e_q$  defined as follows<sup>††</sup>:

$$e_1 = -\frac{1}{\sqrt{2}} (\bar{i} + i\bar{j}); \quad e_0 = \bar{k}; \quad e_{-1} = \frac{1}{\sqrt{2}} (\bar{i} - i\bar{j}) \quad (2-13)$$

From the properties of the Clebsch-Gordon coefficients it follows immediately that  $\langle \alpha j m | \vec{P} | \alpha' j' m' \rangle = 0$ , and by equation (2-10)  $W_{\vec{R}} = 0$  unless:

$$j - j' = 0, \pm 1; \quad j + j' > 1 \text{ and}; \quad q = 0, \pm 1 \quad (2-14)$$

Thus, only a restricted class of states is connected through electric dipole transitions and the selection rules contained in equations (2-14) govern equation (2-9).

<sup>†</sup> $\langle \alpha j || P || \alpha' j' \rangle$  is related to the quantities  $\langle \alpha j : P : \alpha' j' \rangle$  introduced in Condon and Shortley. The relationships are tabulated in Sobel'man (page 85). If these relations are substituted into equation 2-12 it is easily shown that equation 2-12 is equivalent to the equations given by Condon and Shortly at page 63.

<sup>††</sup>The properties of these spherical basis vectors are presented in Rose, 1957 page 103.

Equation (2-12) also accounts for the polarization and relative intensities of the Zeeman Components. This can be seen most readily by studying the special case of the emission or absorption of a photon travelling along the y-axis, i.e.  $\vec{k} = \vec{j}$ . Any direction of polarization  $\vec{R}$  can now be resolved completely into components along the x and z axis, and no further restrictions are imposed by independently examining  $W_{\vec{R}}$  along each of these axes.

Inserting equation (2-12) into equation (2-10), and letting  $\vec{R} = \vec{k}$  we find:

$$W_k \propto \frac{1}{2j+1} C(j'1m'q | jm)^2 | \langle \alpha j || P || \alpha' j' \rangle |^2 \text{ when } q = 0 \quad (2-15)$$

and  $W_k = 0$  when  $q = \pm 1$

Now letting  $\vec{R} = \vec{i}$  we find:

$$W_i = 0 \text{ when } q = 0$$

and

$$W_i \propto \frac{1}{2} \frac{1}{2j+1} C(j'1m'q | jm)^2 | \langle \alpha j || P || \alpha' j' \rangle |^2 \text{ when } q = \pm 1 \quad (2-16)$$

Thus photons polarized in the k direction result exclusively from transitions where  $q = 0$  and those polarized along the x-axis result exclusively from transitions where  $q = \pm 1$ .

Fig. 1: Relative Intensities  $I^{\text{rel}}$  of the Component Lines for Observations along the y-axis

| Transition                             | $I_Z^{\text{rel}}, (m' = m)$ | $I_X^{\text{rel}}, (m' = m \pm 1)$        |
|--|------------------------------|---|
| $\alpha j \rightarrow \alpha' j$       | $m^2$                        | $\frac{1}{4} (j \mp m) (j + 1 \pm m)$     |
| $\alpha j \rightarrow \alpha' (j - 1)$ | $j^2 - m^2$                  | $\frac{1}{4} (j \mp m) (j - 1 \mp m)$     |
| $\alpha j \rightarrow \alpha' (j + 1)$ | $(j + 1)^2 - m^2$            | $\frac{1}{4} (j + 1 \mp m) (j \mp m + 2)$ |

For transitions between two levels,  $\alpha j \rightarrow \alpha' j'$  the term  $\frac{1}{2j+1} |\langle \alpha j || P || \alpha' j' \rangle|^2$  remains fixed. Therefore the relative probabilities of transitions between the states of the two levels, or equivalently, the relative intensities of the component lines  $I^{\text{rel}}$  depend only on the square of the Clebsch-Gordon coefficients. These relative intensities for the special case of  $\vec{k}$  along the y-axis are tabulated in Fig. 1.

The origin of the observed polarization produced by the Zeeman Effect can now be understood. In the absence of an external perturbation, such as a magnetic field, the states  $|\alpha' j' m'\rangle$  are degenerate in  $m'$  and equally populated. Thus all the transitions between two levels have the same energy and all the spectral line components have the same frequency. Each of the spectral line components has a characteristic polarization, but when these components are added together to produce the observed spectral line the characteristic polarizations cancel exactly to give isotropic unpolarized light. This result is easily demonstrated for the special case studied above by noting that for every spectral line the total intensity polarized along the x axis is equal to the total intensity polarized along the z-axis. (The total intensity polarized along each axis is found by summing the relative intensities  $I_X^{\text{rel}}$  and  $I_Z^{\text{rel}}$ , given in Fig. 1, over all allowed values of  $m$ .) This is the expected result since it accords with the principle that there is no preferred direction in space for an isolated atom.

The situation changes when a magnetic field is applied. The component lines no longer have the same frequency, making it possible to observe each

component independently. Observations transverse to the magnetic field are equivalent to the special case examined earlier of photons travelling along the y-axis, since the z-axis was chosen along  $\vec{B}$  in equation (2-6). The  $\pi$ -components can be immediately identified as the  $q = 0$  transitions and the  $\sigma$ -components as the  $q = \pm 1$  transitions.

The relative intensities of the components will still be given by Fig. 1 provided the weak magnetic field approximation remains valid, implying that the states do not deviate substantially from the unperturbed states  $|\alpha jm\rangle$ . The frequency of each component line is given by equation (2-9).

These results provided a complete description of the main properties of the Zeeman Effect. They are used in a later section, after the problem of line broadening has been reviewed, to examine the feasibility of polarizing spectral lines through the selective absorption of the component lines.

## II.2 LINE BROADENING

The results presented in the previous section pertain to the idealized case of a perfectly isolated atom at rest. In this idealization the atom can only absorb or emit photons with the discrete energy of a transition between two states. In practice an atom is moving randomly through a gas and is surrounded by perturbing particles which alter its state. These deviations from the ideal have the effect of allowing an atom to absorb or

emit photons over a range of frequencies for each allowed transition. This effect is known as Line Broadening and the function which expresses the dependence of the transition probability on the angular frequency,  $\omega$ , of the photon is the Line Profile  $P(\omega)$ <sup>†</sup>

In the case of emission lines the broadening processes are intimately related to the specific mechanism used to excite the atoms and therefore cannot be described without reference to the particular light source. Even when the excitation mechanism is well understood the calculation of the resulting line profile is generally very complex. In this study our chief interest is in the absorption of light by a single element gas through resonance transition, i.e. transitions connected to the ground state. In this case the problem assumes an unusually tractable form in which the line broadening is dominated by only three well understood mechanisms. In this section these three mechanisms, Natural, Resonance, and Doppler Broadening, are treated separately and then with some qualifications the results are combined to obtain the complete line profile.

#### Natural Broadening

An atom can never be isolated from the ubiquitous photon radiation field. The field interacts with the atom allowing energy to be transferred between the atom and the field. This transfer of energy is, in turn,

---

<sup>†</sup> The Line Profile corresponds to the experimentally observed spectral line shape only in the case of lines in an optically thin material.

accompanied by a transition from one atomic state to another. The existence of these allowed transitions between states implies that the states  $\alpha j$  have a finite average or natural lifetime  $\tau_{\alpha j}$ . Applying the time-energy uncertainty principle  $\Delta E_{\alpha j} \tau_{\alpha j} \sim h$  we find that a finite lifetime implies an indeterminacy in each energy level of the order  $\Delta E_{\alpha j}$ . Thus the photon field leads to a finite lifetime and a finite lifetime means that a transition must occur at a range of energies rather than at a single discrete energy. A complete analysis (see Heitler 1954 page 181, or Messiah 1962, page 994) shows that a finite lifetime manifests itself in the form of a Lorentz Line Profile  $L(\omega)$ .

$$L(\omega)d\omega = \frac{\gamma}{2\pi} \frac{d\omega}{(\omega - \omega_0)^2 + (\frac{\gamma}{2})^2} \quad (2-17)$$

where  $\gamma$  is the full width at half maximum. This line profile occurs whenever a perturbation has the effect of altering the lifetime of a state and is therefore not unique to Natural Broadening.

For Natural Broadening  $\gamma = \gamma_N$  and is called the natural line width where

$$\gamma_N = \tau_{\alpha j}^{-1} + \tau_{\alpha' j'}^{-1}, \text{ for the transition } \alpha j \rightarrow \alpha' j' \quad (2-18)$$

When an atom is immersed in radiation which it is capable of absorbing, the lifetime of the ground state is not strictly infinite. However, excepting the case of very intense radiation, the lifetime of the ground

state is much greater than that of any excited state. Thus for resonance absorption  $\gamma_N \sim \tau_{\alpha j}^{-1}$  where  $\alpha j$  is the excited state.

Natural Broadening usually makes the least significant contribution to the final line profile.

### Resonance Broadening

Collisions among the atoms of a gas also lead to line broadening. In a gas composed primarily of atoms of one element, the broadening of the resonance lines of this element is dominated by collisions among the atoms of this element. Consider two atoms differing only in that one is in the ground state ( $\alpha_0 j_0$ ), while the other is in an excited state ( $\alpha j$ ) which has an allowed transition to the ground state. A collision between these two atoms permits a resonance transfer of energy, i.e. the excited atom decays to the ground state while the ground state atom is driven into the state  $\alpha j$ . This resonance transfer effectively creates an additional mode of decay for the state  $\alpha j$  and hence leads to a shortening of the lifetime of that state. This collision induced shortening of the lifetime will independently produce a Lorentz line Profile characterized by a full width at half-max.  $\gamma_R$ .

$\gamma_R$  has been theoretically calculated using a variety of techniques. The most complete treatments appear to be by Ali and Griem, 1965 and D'Yakonov and Perel 1965. Ali and Griem derive their result using the

impact and classical path approximations for a state  $\alpha_j$  which has an electric dipole transition to the ground state  $\alpha_0 j_0$ . They find:

$$\gamma_R = 3.84 \pi \frac{2j_0 + 1}{2j + 1} N \frac{e^2 f_a}{m_e \omega_0} \quad (2-19)$$

in cgs units, or

$$\gamma_R = 3.84\pi \frac{2j_0 + 1}{2j + 1} N \frac{e^2 f_a}{4\pi\epsilon_0 m_e \omega_0} \quad (2-20)$$

in MKS units:

where:

$N$  is the density of atoms in the ground state,

$m_e$  is the electron mass,

$e$  is the electron charge,

$f_a$  is the absorption oscillator strength, and

$\epsilon_0$  is the Permittivity constant

D'Yakonov and Perel determine  $\gamma_R$  using irreducible tensors to calculate the relaxation of the nondiagonal density matrix of an excited atom in collision with an atom in the ground state. They also use the classical path and impact approximations and assume the existence of an electric dipole transition to the ground state. Their result does not exhibit the simple dependence on  $j$  and  $j_0$  of equation (2-20) and a numerical result is provided only for the case where  $j = 1$  and  $j_0 = 0$ . However, if for this

specific case, their result is put in the same form as equation (2-20) they find that the numerical factor corresponding to 3.84 has a value of 2.55.

The impact approximation, upon which these results are based, remains valid provided the time between effective collisions is much larger than the duration of an effective collision  $Q^{-1}$ , and only frequencies within a range  $\Delta\omega$  from the line centre are considered. These two validity criteria are contained in the equation from Ali and Griem:  $\text{Max} \{ \gamma_R, \Delta\omega \} \ll Q$  where,

$$Q = \left\{ \frac{3.84\pi N}{\gamma_R} \right\}^{1/2} \left( \frac{K_B T}{M} \right)^{3/4} \quad (2-21)$$

and,  $K_B$  is the Boltzmann constant,  $T$  is the temperature in  $K^\circ$ , and  $M$  is the mass of the atom.

$\gamma_R$  has been experimentally determined by G. Stanzel 1974, for the 253.7 nm resonance line of Mercury; he found:

$$\gamma_R = (5.3 \pm 0.5) 10^{-9} \text{ N sec}^{-1} \text{ cm}^3 \quad (2-22)$$

for  $N \sim 5 \times 10^{18} \text{ cm}^{-3}$  and  $T \sim 553 \text{ K}^\circ$ . Using the characteristics of the 253.7 nm line given in the appendix, the theoretical values given by Ali and Griem and by D'Yakonov and Perel are respectively:

$$\gamma_R = 6.03 \times 10^{-9} \text{ N sec}^{-1} \text{ cm}^3 \quad (2-23)$$

and

$$\gamma_R = 4.01 \times 10^{-9} \text{ N sec}^{-1} \text{ cm}^3 \quad (2-24)$$

Thus both results are in fair agreement with experiment given that the validity criteria are only weakly satisfied at these temperatures and densities, i.e. from equation (2-21).

$$\gamma_R \sim 3 \times 10^{10} \ll 8 \times 10^{10} \sim Q \quad (2-25)$$

The theoretical equations for  $\gamma_R$  were derived assuming that the atoms were not immersed in a magnetic field. In the absence of a magnetic field a collision between two like atoms permits not only a resonance transfer of energy, but also an alteration in the excited state. The resulting excited atom can be in a state with an  $m$  quantum number different from that of the excited atom before the collision. When a magnetic field is applied the states no longer have the same energy, therefore a change in the  $m$  quantum number of the excited state must be accompanied by a change in the kinetic energy of the colliding atoms. This has the effect of decreasing the probability of a change in the resulting excited state. The theoretical equations for  $\gamma_R$  should remain valid, however, provided the magnetic field induced line splitting ( $\omega_{mm'} - \omega_0$ ), from equation (2-9) is small compared to the inverse of the duration of an effective collision, i.e.

$$\omega_{mm'} - \omega_0 \ll Q \quad (2-26)$$

(see D'Yakonov and Perel and Sobel'man page 464).

For many lines this inequality is not satisfied at even modest field strengths of less than 1 Tesla. At these field strengths the Zeeman

splitting of the line becomes sufficiently great to cause a significant decrease in the probability of a collision induced transition to a state with a different  $m$  quantum number. This in turn decreases the overall probability of a resonance transfer of excitation energy since in effect the number of states able to participate in the transfer has decreased. Thus the resonance line width  $\gamma_R$  will be smaller than predicted by equation (2-20) when the inequality (2-26) is not satisfied.

### Doppler Broadening

Doppler Broadening of spectral lines is the cumulative result of the random motion of the atoms. Ignoring all other broadening mechanisms, an atom will only absorb or emit photons of frequency  $\omega_0$  as measured in the atom's frame of reference. The frequency of these photons in the reference frame of an external observer is  $\omega$ , where according to the non-relativistic Doppler Principle  $\omega = \omega_0 + \frac{V}{c} \omega_0$ , and  $V$  is the component of the atom's velocity along the direction of observation. If the distribution function for  $V$  is  $f(V) dV$  then the Doppler line profile,  $D(\omega)$ , produced by a unit volume of atoms is:

$$D(\omega) d\omega = f\left(\frac{c}{\omega_0} (\omega - \omega_0)\right) \frac{c}{\omega_0} d\omega \quad (2-27)$$

For a gas in equilibrium  $f(V) dV$  is just the Maxwellian velocity distribution and  $D(\omega) d\omega$  becomes:

$$D(\omega)d\omega = \pi^{-1/2} D^{-1} \exp \left[ - \left( \frac{\omega - \omega_0}{D} \right)^2 \right] d\omega \quad (2-28)$$

where  $D = \omega_0 \frac{v}{c}$  is known as the Doppler Width, and  $v = \left( \frac{2K_B T}{M} \right)^{1/2}$  (2-29)

### The Combined Line Profile

The combined line profile  $P(\omega) d\omega$  is a convolution of the characteristic line profiles of each broadening process. If two broadening processes are statistically independent and have profiles  $P_1(\omega - \omega_0)$  and  $P_2(\omega - \omega_0)$ , the combined line profile  $P'(\omega - \omega_0)$  is given by:

$$P'(\mu) = \int_{-\infty}^{\infty} P_1(\phi) P_2(\mu - \phi) d\phi \quad (2-30)$$

where  $P'$ ,  $P_1$  and  $P_2$  are expressed as functions of frequency differences,  $\omega - \omega_0$ , rather than absolute frequencies  $\omega$ .

Natural and Resonance Broadening are strictly independent processes and the combined line profile  $L'(\omega)$  is again a Lorentzian with  $\gamma$  now given by:

$$\gamma = \gamma_N + \gamma_R \quad (2-31)$$

Doppler and Resonance Broadening are not statistically independent, because a single collision can produce both a resonance transfer of energy and a change in velocity. A complete analysis involving the calculation of a correlation function (Sobel'man, page 401) shows that the correlation between these two processes can lead to a collisional narrowing of the Doppler width of the combined line profile. However, where:

$$L \ll \frac{2\pi c}{\omega} \quad (2-32)$$

and  $L = \frac{1}{\sqrt{2}\sigma_0 N}$  is the mean free path and  $\sigma_0$  is the gas-kinetic cross section,

the two processes can be treated independently. The complete line profile  $P(\omega)$  is therefore given by:

$$P(\mu) = \int_{-\infty}^{\infty} L'(\theta) D(\mu-\theta) d\theta \quad (2-33)$$

or

$$P(\omega) = \frac{\gamma}{2\pi} \pi^{-1/2} D^{-1} \int_{-\infty}^{\infty} \frac{e^{-\left(\frac{x}{D}\right)^2} dx}{(\omega-\omega_0-x)^2 + \left(\frac{\gamma}{2}\right)^2} \quad (2-34)$$

This type of profile is known as a Voigt Profile.

In conclusion, where all the assumptions made in this development remain valid, we expect a unit volume of atoms in the gas to absorb photons over a range of frequencies with a probability given by the Voigt Profile of equation (2-34). In the presence of a magnetic field the line will split

and each Zeeman Component will have this same Voigt Profile, apart from a slight narrowing due to the effect of the magnetic field on the resonance broadening of each m-component.

### II.3 THEORY

In this section a theoretical model is developed for the transmission of light through a gas immersed in a magnetic field where the frequency of the light is at or near a resonant frequency of the atoms of the gas. The theory is based on a semi-classical approach similar to one used in a related context by Corney et al., 1965 and Dodd and Series 1961. While more sophisticated and rigorous methods involving quantized fields are possible, little additional information of importance to this study is gained at the cost of much greater complexity. Therefore, while acknowledging the merits of rigor, I have opted for a simpler and I hope more readily comprehensible exposition of the problem.

Conversely most of the results obtained through this development can be derived more simply by making perspicacious substitutions into the more familiar equations describing the transmission of light through a gas. It was felt however that only through the step by step development of a theory, in which all the assumptions and approximations are given explicitly, can the applicability of the result be properly determined. Thus a complete and systematic development is presented.

In this development the light is treated classically as an electromagnetic (em) wave governed by Maxwell's equations, while the atoms are treated quantum mechanically. The external (static) magnetic field is allowed to assume any orientation with respect to the direction of propagation of the light. While this provides a more general equation than is necessary for this study, and involves some additional complexity, the more general equation may be useful in future research.

For simplicity the theory is developed using c.g.s. Gaussian units; however, the important resulting equations are also expressed in MKSA units.† The electric field,  $\vec{E}(\vec{r}, t)$ , of a classical em wave travelling through a non-magnetic, current-free medium obeys the equation:

$$\nabla^2 \vec{E}(\vec{r}, t) - \nabla(\nabla \cdot \vec{E}(\vec{r}, t)) = \frac{1}{c^2} \frac{\partial^2}{\partial t^2} (\vec{E}(\vec{r}, t) + 4\pi \vec{P}_c) \quad (2-35)$$

where  $\vec{P}_c$  is the dipole moment per unit volume.

In the equation all higher electric moments have been neglected. This corresponds to the earlier approximation of considering only electric dipole transitions.

To solve equation (2-35) for  $\vec{E}(\vec{r}, t)$ ,  $\vec{P}_c$  must be determined for a gas in a magnetic field. This is accomplished by first finding the average dipole moment  $\vec{P}_c^a$  for a single atom immersed in a magnetic field and interacting

---

† J.D. Jackson's "Classical Electrodynamics" provides a table for converting any equation from one system to the other.

with an em wave. The average dipole moment  $\vec{p}_c^a$  corresponds to the expectation value of the quantum mechanical electric dipole operator  $\vec{P}$  (see equation (2-11)). Thus,

$$\vec{p}_c^a = \langle t | \vec{P} | t \rangle \quad (2-36)$$

where  $|t\rangle$  is the state of the atom at time  $t$ .

The problem has therefore been reduced to solving the time dependent Schrodinger equation:

$$i\hbar \frac{\partial}{\partial t} |t\rangle = H |t\rangle \quad (2-37)$$

The Hamiltonian,  $H$  for this atom is given by:

$$H = H_0 + H_D + \frac{\mu_0}{\hbar} g_{\alpha j} \vec{J} \cdot \vec{B} + H_I(t) \quad (2-38)$$

where:

$H_0$  is the Hamiltonian for the unperturbed atom, and  $H_0 | \alpha jm \rangle = E_{\alpha j} | \alpha jm \rangle$ .

$\frac{\mu_0}{\hbar} g_{\alpha j} \vec{J} \cdot \vec{B}$  was introduced in equation (2-6) and accounts for the effects of a weak magnetic field. With complete generality the magnetic field can be confined to the  $x$ - $z$  plane with the angle between  $\vec{B}$  and the  $z$  axis denoted by  $\beta$ . (see Fig. 2). Recall from equation (2-6) if  $\beta=0$ ,

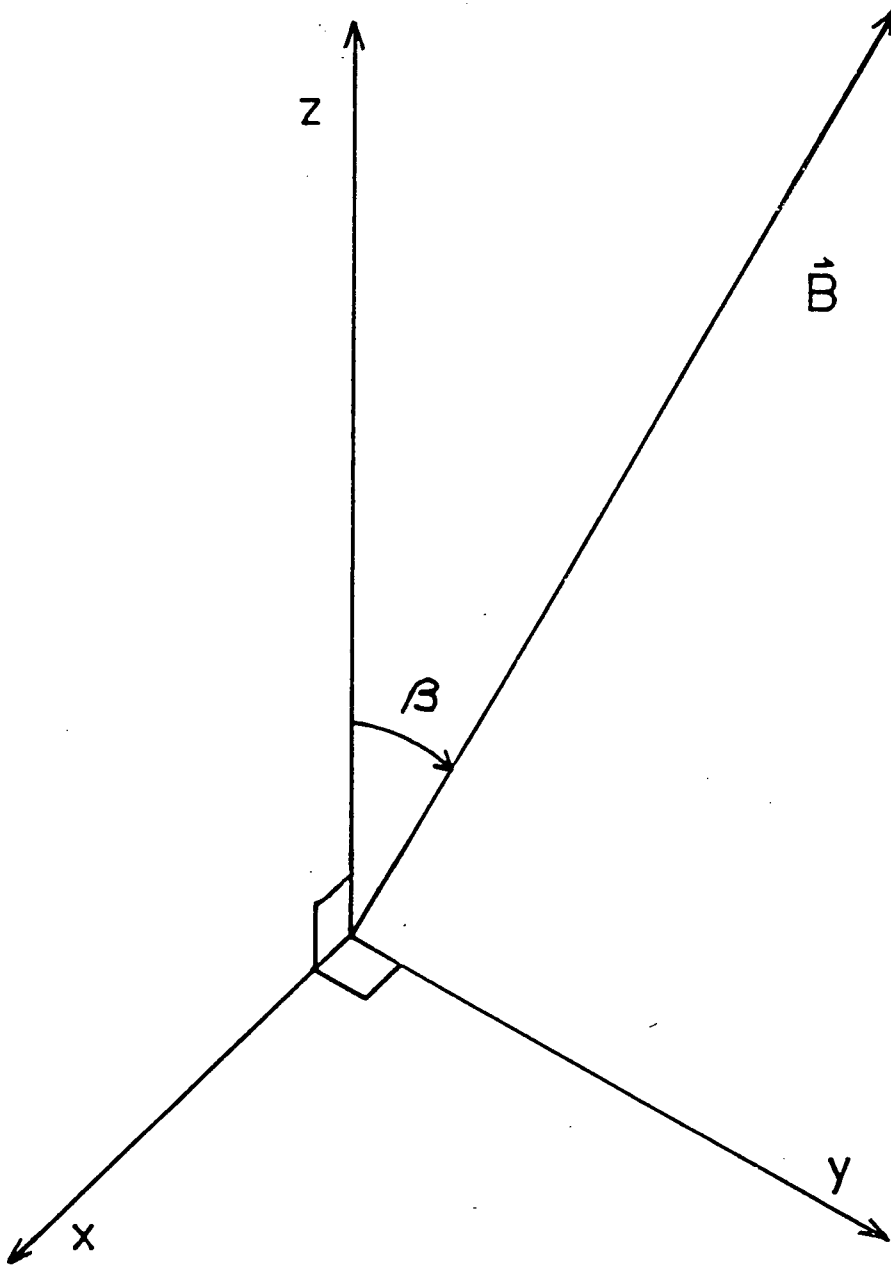


Fig. 2: Orientation of the Magnetic Field

$$\frac{\mu_0}{h} g_{\alpha j} \vec{J} \cdot \vec{B} |\alpha jm\rangle = \mu_0 g_{\alpha j} B_m |\alpha jm\rangle.$$

The operator  $H_D$  is introduced phenomenologically to provide for the exponential decay of the excited states  $e^{-\gamma t}$ , where  $1/\gamma$  is the lifetime of a given state. The finite lifetime can account for all spectral line broadening mechanisms which produce a Lorentz profile. Note that:

$$H_D |\alpha jm\rangle = -(1/2) i h \gamma_{\alpha j} |\alpha jm\rangle \quad (2-39)$$

$H_I(t)$  describes the interaction between the atom and the electromagnetic wave. If the wavelength of the em-wave is much greater than the size of the atom (which is true for optical frequencies) then  $H_I(t)$  can be given by:

$$H_I(t) = -\vec{p} \cdot \vec{E}(\vec{r}, t) \quad (2-40)$$

which is analogous to the classical expression for the energy of a dipole in an electric field.

The interaction between the atom and the em-wave's magnetic field is much weaker and has been neglected.

To solve the Schrodinger equation the techniques of time-dependent perturbation theory are employed. The state  $|\psi\rangle$  is expressed as a superposition of states which are independent of time.

$$|t\rangle = C_g(t) |g\rangle + \sum_d C_d(t) |d\rangle \quad (2-41)$$

where:

$|g\rangle$  represents the ground state which has been made non-degenerate: i.e.  $|g\rangle = |x00\rangle$ . While this restriction is not essential it greatly simplifies the derivation of  $|t\rangle$ . The solutions for degenerate ground states are introduced later in an obvious, albeit ad hoc, way for the special case of light travelling transverse to the magnetic field.

$|d\rangle$  is simply a shorter notation for the excited states  $|\alpha jm\rangle$  where "d" represents all the quantum numbers of the state.

$C_g(t)$  and  $C_d(t)$  are the time dependent probability amplitudes for the states  $|g\rangle$  and  $|d\rangle$  respectively. Since all the states are orthonormal:

$$C_g(t) = \langle g | t \rangle \quad \text{and} \quad C_d(t) = \langle d | t \rangle \quad (2-42)$$

The probability of an atom being in a state other than the ground state is very small, implying  $|C_g| \sim 1$ . This indicates that the state of the atom can be well described by just the first order terms in the perturbation expansion.

Defining the time-independent operator

$$\bar{H} = H - H_I(t) \quad (2-43)$$

it can be shown (see Messiah page 722) that to first order:

$$|t\rangle = e^{-\frac{i}{\hbar} \bar{H}(t-\tau)} |g\rangle + \frac{1}{i\hbar} \int_{\tau}^t dt_0 e^{-\frac{i}{\hbar} \bar{H}(t-t_0)} H_I(t_0) e^{-\frac{i}{\hbar} \bar{H}(t_0-\tau)} |g\rangle \quad (2-44),$$

where the oscillating electric field producing  $H_I(t)$  was switched on at time  $t = \tau$  at which time the atom was in the ground state.

The terms of the form  $e^{-\frac{i}{\hbar} \bar{H}} |g\rangle$  can be evaluated immediately since  $H_0 |g\rangle = E_0 |g\rangle$  where  $E_0$  is the energy of the ground state.  $H_D |g\rangle = 0$ , since there is no broadening of the ground state, and  $\frac{\mu_0}{h} g_{\alpha j} \vec{J} \cdot \vec{B} |g\rangle = 0$  since  $|g\rangle$  is non-degenerate. Thus:

$$e^{-\frac{i}{\hbar} \bar{H}(t-\tau)} |g\rangle = |g\rangle e^{-\frac{i}{\hbar} E_0(t-\tau)} \quad (2-45)$$

and equation (2-44) becomes

$$|t\rangle = |g\rangle e^{-\frac{i}{\hbar} E_0(t-\tau)} + \frac{1}{i\hbar} \int_{\tau}^t dt_0 e^{-\frac{i}{\hbar} \bar{H}(t-t_0)} H_I(t_0) |g\rangle e^{-\frac{i}{\hbar} E_0(t_0-\tau)} \quad (2-46)$$

This equation for  $|t\rangle$  although not directly solvable can be used with

equation (2-41) to obtain  $C_d(t)$  and  $C_g(t)$ . To first order

$$C_d(t) = \langle d | t \rangle \sim \langle d | g \rangle e^{-\frac{1}{\hbar} E_0(t-\tau)} + \frac{1}{i\hbar} \int_{\tau}^t dt_0 \langle d | e^{-\frac{1}{\hbar} \bar{H}(t-t_0)} H_I(t_0) | g \rangle e^{-\frac{1}{\hbar} E_0(t-\tau)} \quad (2-47)$$

The first term is zero since the states are orthonormal. The second term can be solved if  $\bar{H} | d \rangle$  can be found. Toward this end we consider the states  $|u\rangle'$  defined in a new co-ordinate system  $R'$ .  $R'$  is chosen such that the  $z'$ -axis is parallel to the magnetic field  $\vec{B}$ . Thus  $R'$  is generated by a rotation about the  $y$ -axis through an angle  $\beta$  with respect to the old co-ordinate system; see Fig. 3. In the new co-ordinate system the operator  $\bar{H}$  becomes:

$$\bar{H} = H_0 + H_D + \frac{\mu_0}{\hbar} g_{\alpha j} B J_{z'} \quad (2-48)$$

Therefore

$$\bar{H} |u\rangle' = (E_{\alpha j} - 1/2 i \hbar \gamma_{\alpha j} + \mu_0 g_{\alpha j} B u) |u\rangle' = \lambda_u |u\rangle' \quad (2-49)$$

$\langle d |$  is related to  $\langle u |$  through the equation

$$\langle d | = \langle \alpha j m | = \sum_u D_{mu}^j(0, \beta, 0) \langle \alpha j u | = \sum_u D_{mu}^j \langle u |' \quad (2-50)$$

where  $D_{mu}^j(0, \beta, 0)$  are elements of the rotation matrix, (see Rose, 1957).

---

†To simplify the notation the state  $|\alpha j u\rangle'$  is designated  $|u\rangle'$  with the remaining quantum numbers implied.

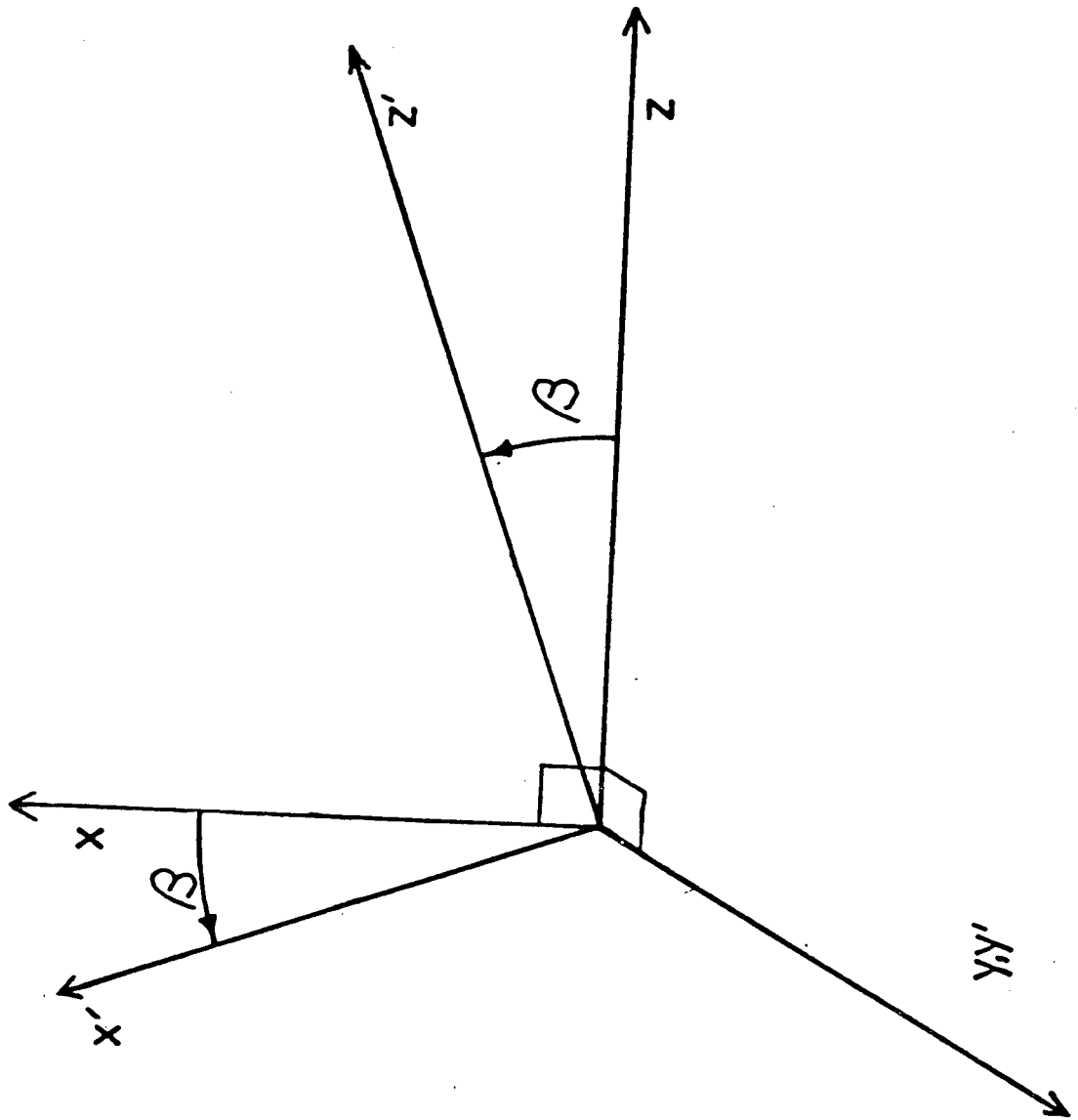


Fig. 3: Orientation of  $\{u'\}$  Co-ordinate System

Inserting these results into equation (2-47) gives:

$$C_d(t) = \frac{1}{i\hbar} \int_{\tau}^t dt_0 \sum_u D_{\mu u}^j e^{-\frac{i}{\hbar} \lambda_u (t-t_0)} \langle u | H_I(t_0) | g \rangle e^{-\frac{i}{\hbar} E_0 (t_0 - \tau)} \quad (2-51)$$

Now transforming back to the original co-ordinate system using the equation:

$$\langle u | = \sum_n D_{nu}^{j*} (0, \beta, 0) \langle \alpha j n | = \sum_n D_{nu}^{j*} \langle n | \quad (2-52)$$

we have

$$C_d(t) = \frac{1}{i\hbar} \int_{\tau}^t dt_0 \sum_{un} D_{\mu u}^j D_{nu}^{j*} e^{-\frac{i}{\hbar} \lambda_u (t-t_0)} \langle n | H_I(t_0) | g \rangle e^{-\frac{i}{\hbar} E_0 (t_0 - \tau)} \quad (2-53)$$

To evaluate the remaining matrix element  $\langle n | H_I(t_0) | g \rangle$ , the time dependence of  $\vec{E}(\vec{r}, t)$  must be given explicitly. Let  $\vec{E}(\vec{r}, t)$  be given by the sinusoidal wave;

$$\vec{E}(\vec{r}, t) = \vec{E}(\vec{r}) e^{-i\omega t} + \vec{E}^*(\vec{r}) e^{i\omega t} \quad (2-54)$$

Where  $\vec{E}(\vec{r})$  may be complex, but as defined  $E(\vec{r}, t)$  is real as required for  $H_I(t)$  to be Hermitian. With this definition

$$\begin{aligned} \langle n | H_I(t) | g \rangle &= \\ &\langle n | -\vec{p} \cdot \vec{E}(\vec{r}) | g \rangle e^{-i\omega t} + \langle n | -\vec{p} \cdot \vec{E}^*(\vec{r}) | g \rangle e^{i\omega t} \\ &= -\langle n | \vec{p} | g \rangle \cdot \vec{E}(\vec{r}) e^{-i\omega t} - \langle n | \vec{p} | g \rangle \cdot \vec{E}^*(\vec{r}) e^{i\omega t} \end{aligned} \quad (2-55)$$

The last step is permitted because  $\vec{E}(\vec{r})$  affects the states only through the operator  $\vec{P}$ . The matrix element  $\langle n | \vec{P} | g \rangle$  is just the familiar electric dipole transition matrix, and equation (2-12) is applied at a later stage to give the explicit dependence on  $n$ . Invoking the electric dipole selection rules the element  $\langle n | \vec{P} | g \rangle = 0$  except for states  $|n\rangle$  with  $j=1$  since  $|g\rangle$  is non-degenerate. Since  $\langle n | \vec{P} | g \rangle \cdot \vec{E}(\vec{r})$  is independent of time the equation for  $C_d(t)$  becomes

$$C_d(t) = \frac{-1}{i\hbar} \sum_{un} D_{mu}^{(1)} D_{nu}^{(1)*} e^{-\frac{i}{\hbar} \lambda_u t} e^{\frac{i}{\hbar} E_o \tau} \langle n | \vec{P} | g \rangle \cdot \int_{\tau}^t (\vec{E}(\vec{r}) e^{-i\omega t_0} + \vec{E}^*(\vec{r}) e^{i\omega t_0}) e^{\frac{i}{\hbar} (\lambda_u - E_o) t_0} dt_0 \quad (2-56)$$

The integral can be easily solved, with the result

$$\vec{E}(\vec{r}) \left[ \frac{e^{\frac{i}{\hbar} (\lambda_u - E_o - \hbar\omega) t_0}}{\frac{i}{\hbar} (\lambda_u - E_o - \hbar\omega)} \right]_{\tau}^t + \vec{E}^*(\vec{r}) \left[ \frac{e^{\frac{i}{\hbar} (\lambda_u - E_o + \hbar\omega) t_0}}{\frac{i}{\hbar} (\lambda_u - E_o + \hbar\omega)} \right]_{\tau}^t \quad (2-57)$$

Recall from equation (2-49)  $\frac{\lambda_u - E_o}{\hbar} = \frac{1}{\hbar} (E_{\alpha j} - E_o + \mu_o g_{\alpha j} B_u - (1/2) i \hbar \gamma_{\alpha j})$ .

The cases of interest occur when the frequency of the light is at or near a resonant frequency of the atom, i.e.  $\omega \sim \frac{E_{\alpha j} - E_o}{\hbar}$ . In this case the second term in equation (2-57) is negligible compared to the first term and the

expression for  $C_d(t)$  is given finally by:

$$C_d(t) = \frac{-1}{i\hbar} \sum_{un} D_{mu}^{(1)} D_{nu}^{(1)*} \left( e^{-\frac{i}{\hbar} \lambda_u t} \right) e^{-\frac{i}{\hbar} E_0 \tau} \langle n | \vec{p} | g \rangle \cdot$$

$$\vec{E}(\vec{r}) \left( \frac{e^{\frac{i}{\hbar} (\lambda_u - E_0 - \hbar\omega)t} - e^{\frac{i}{\hbar} (\lambda_u - E_0 - \hbar\omega)\tau}}{\frac{i}{\hbar} (\lambda_u - E_0 - \hbar\omega)} \right) \quad (2-58)$$

Equations (2-41) and (2-44) can also be used to determine  $C_g(t)$ . To first order

$$C_g(t) = \langle g | g \rangle e^{-\frac{i}{\hbar} E_0 (t-\tau)} +$$

$$\frac{1}{i\hbar} \int_{\tau}^t dt_0 \langle g | e^{-\frac{i}{\hbar} \bar{H}_0 (t-t_0)} H_I(t_0) | g \rangle e^{-\frac{i}{\hbar} E_0 (t_0-\tau)} \quad (2-59)$$

Using arguments similar to those used for  $C_d(t)$ , it is apparent that the second term is zero since  $\langle g | \vec{P} | g \rangle = 0$ . Thus,

$$C_g(t) = e^{-\frac{i}{\hbar} E_0(t-\tau)} \quad (2-60)$$

The expressions for  $C_g(t)$  and  $C_d(t)$  can now be inserted into equation (2-41) yielding  $|t\rangle$  to first order. With  $|t\rangle$  known,  $\langle t | \vec{P} | t \rangle$  can be found<sup>†</sup>.

Expanding  $\langle t | \vec{P} | t \rangle$  and retaining only first order terms:

$$\begin{aligned} \langle t | \vec{P} | t \rangle = & \langle g | \vec{P} | g \rangle C_g^*(t) C_g(t) + \sum_d \langle g | \vec{P} | d \rangle C_g^*(t) C_d(t) \\ & + \sum_d \langle d | \vec{P} | g \rangle C_g(t) C_d^*(t) \end{aligned} \quad (2-61)$$

The first term is zero since  $\langle g | \vec{P} | g \rangle = 0$

The third term is also just the complex conjugate of the second term; hence  $\langle t | \vec{P} | t \rangle$  can be written as:

$$\langle t | \vec{P} | t \rangle = 2 \operatorname{Re} \left( \sum_d \langle g | \vec{P} | d \rangle C_g^*(t) C_d(t) \right) \quad (2-62)$$

where  $\operatorname{Re}(Z)$  stands for the real part of  $Z$ .

---

<sup>†</sup>Note that  $\langle t | t \rangle \neq 1$ , since the states  $|g\rangle$  and  $|d\rangle$  were made orthonormal; i.e.  $\langle d | d \rangle = 1$ . Thus, the proper expression is  $\frac{\langle t | \vec{P} | t \rangle}{\langle t | t \rangle}$ . However, since  $\sum_d C_d^*(t) C_d \ll 1$  this small numerical correction can be ignored.

Inserting the derived expressions for  $C_g(t)$  (equation 2-60) and  $C_d(t)$  (equation 2-58) the expression in brackets in equation (2-62) becomes:

$$\sum_d \langle g | \vec{P} | d \rangle C_d^*(t) C_d(t) = \sum_{dun} \langle g | \vec{P} | d \rangle D_{mu}^{(1)} D_{nu}^{*(1)} \langle n | \vec{P} | g \rangle \cdot \vec{E}(r) \times \left( \frac{e^{-i\omega t} - e^{\frac{i}{\hbar}(\lambda_u - E_o)(\tau-t)} e^{-i\omega\tau}}{(\lambda_u - E_o - \hbar\omega)} \right) \quad (2-63)$$

The steady state solution, which is the one of interest, occurs when the electric field has been interacting with the atom long enough for all transient effects to have vanished. In the above equation this is equivalent to taking the limit of  $\tau \rightarrow -\infty$ . Examining the function which is dependent on  $\tau$ , it is clear that it contains an oscillatory component and the component  $e^{1/2\gamma\alpha_j\tau}$ . Since  $\lim_{\tau \rightarrow -\infty} e^{1/2\gamma\alpha_j\tau} = 0$  it follows that the expression in brackets in equation (2-63) becomes:

$$\left( \frac{e^{-i\omega t}}{(\lambda_u - E_o - \hbar\omega)} \right) \quad (2-64)$$

when  $\tau \rightarrow -\infty$ .

The summation over  $d$  in equation (2-63) includes all excited states. However, if the frequency of the light is near a particular resonance line, as we have assumed, the contribution from the states of neighbouring levels will be minimal and the sum can be taken only over the states of the

relevant level. (Where the levels are closely spaced the sum should include the states of the neighbouring levels.) With these modifications equation (2-63) becomes.

$$\sum_{\mu\nu} \langle g | \vec{P} | m \rangle D_{\mu}^{(1)} D_{\nu}^{*(1)} \langle n | \vec{P} | g \rangle \cdot \vec{E}(\vec{r}) e^{-i\omega t} \left( \frac{1}{(\lambda_u - E_o - \hbar\omega)} \right) \quad (2-65)$$

The matrix elements  $\langle g | \vec{P} | m \rangle$ , and  $\langle n | \vec{P} | g \rangle$  can now be reduced using equation (2-12):

$$\langle g | \vec{P} | m \rangle = C(11mq|00) \langle \alpha j || P || \alpha' j' \rangle e_q^* \quad (2-66)$$

Since  $|g\rangle$  is non-degenerate,  $q = -m$ ; i.e. each unit vector corresponds to a single allowed transition. From tables (see Condon and Shortley, page 76) the Clebsch-Gordon coefficients are found to be:

$$C(11mq|00) = - \frac{(-1)^q}{\sqrt{3}} \quad (2-67)$$

Thus

$$\langle g | \vec{P} | m \rangle = - \frac{(-1)^m}{\sqrt{3}} \langle \alpha j || P || \alpha' j' \rangle e_{-m}^* \quad (2-68)$$

From the property of the unit basis vectors,  $e_{\mu}^* = (-1)^{\mu} e_{-\mu}$  this becomes:

$$\langle g | \vec{P} | m \rangle = \frac{-1}{\sqrt{3}} \langle \alpha j || P || \alpha' j' \rangle e_m \quad (2-69)$$

similarly

$$\langle n | \vec{p} | g \rangle = \frac{-1}{\sqrt{3}} \langle \alpha_j | |P| | \alpha' j' \rangle^* e_n^* \quad (2-70)$$

Using these equations, (2-65) becomes:

$$\sum_{\text{mun}} \frac{1}{3} |\langle \alpha_j | |P| | \alpha' j' \rangle|^2 e_m D_{\text{mu}}^{(1)} D_{\text{nu}}^{(1)*} e_n^* \cdot \vec{E}(\vec{r}) e^{-i\omega t} \left( \frac{1}{\lambda_u - E_o - \hbar\omega} \right) \quad (2-71)$$

As an aid to further development,  $\langle t | \vec{p} | t \rangle$  is expressed in terms of the complex polarizability tensor per atom,  $\underline{\alpha}^a$ , which is defined by the equation:

$$\langle t | \vec{p} | t \rangle = 2\text{Re}(\underline{\alpha}^a \cdot \vec{E}(\vec{r}) e^{-i\omega t}) \quad (2-72)$$

It is evident from equations (2-62) and (2-71) that  $\underline{\alpha}^a$  is most conveniently defined with respect to the unit vector basis  $e_q$ . Thus

$$\alpha_{mn}^a = \sum_u \frac{|\langle \alpha_j | |P| | \alpha' j' \rangle|^2}{3(\lambda_u - E_o - \hbar\omega)} D_{\text{mu}}^{(1)} D_{\text{nu}}^{(1)*} \quad (2-73)$$

and,

$$\langle t | \vec{p} | t \rangle \cdot e_m = P_c^a \cdot e_m = 2\text{Re}(\sum_n \alpha_{mn}^a E_n(\vec{r}) e^{-i\omega t}) \quad (2-74)$$

The dipole moment per unit volume  $\vec{p}_c$ , which is required in equation (2-35), can be found by summing  $\vec{p}_c^a$  over the atoms in a unit volume. It is

convenient to define a complex polarizability tensor per unit volume  $\underline{\alpha}$  by the equation

$$\vec{P}_c = 2\text{Re}(\underline{\alpha} \cdot \vec{E}(\vec{r})e^{-i\omega t}) \quad (2-75)$$

It follows from the definition of  $\vec{P}_c$  that  $\underline{\alpha}$  is given by the sum of  $\underline{\alpha}^a$  over a unit volume of atoms, or:

$$\alpha_{mn} = \sum_{i=1}^N \alpha_{mn}^a \quad (2-76)$$

At this point we neglect the small number of atoms in the excited state, which is equivalent to ignoring induced emissions, and take the sum over atoms in the ground state. By performing the usual macroscopic spatial averaging, (see Jackson 1975, page 226) the discrete sum can be replaced by an integral over the velocity distribution of a unit volume of atoms.

Assuming a Maxwellian velocity distribution and accounting for the Doppler shift of each atom's natural frequency as seen by an external observer, (i.e. accounting for Doppler Broadening) the integral is given by:

$$\alpha_{mn} = \frac{1}{3h} | \langle \alpha_j || P || \alpha' j' \rangle |^2 \sum_u \frac{D_{mu}^{(1)} D_{nu}^{(1)*}}{nu} \frac{N}{V_0 \pi^{1/2}} \times \int_{-\infty}^{\infty} \frac{e^{-\left(\frac{v}{V_0}\right)^2}}{\omega_0 + \frac{v}{c} \omega_0 + \frac{\mu_0}{h} g_{\alpha j} B u - \omega - (1/2)i \gamma_{\alpha j}} dv \quad (2-77)$$

$$\text{recall } V_0 = \left( \frac{2K_B T}{M} \right)^{1/2}$$

$N$  = density fo the atoms in the ground state

$M$  = mass of the atom

$V$  = component of the velocity along the direction of observation

$$\omega_0 = \frac{1}{h} (E_{\alpha j} - E_0)$$

This equation may be simplified by introducing the complex error function  $W(a + ib)$  (see Abramowitz and Stegun 1972, page 295)

$$W(a + ib) = \frac{1}{\pi} \int_{-\infty}^{\infty} \frac{e^{-t^2} dt}{(a + ib) - t} \quad (2-78)$$

whence  $\alpha_{mn}$  becomes

$$\alpha_{mn} = \frac{iNc\pi^{1/2}}{3h V_0 \omega_0} |\langle \alpha j || P || \alpha' j' \rangle|^2 \sum_u D_{mu}^{(1)} D_{nu}^{(1)*} W(a_u + ib) \quad (2-79)$$

$$\text{where } a_u = \frac{c}{V_0 \omega_0} \left( \omega - \omega_0 - \frac{\mu_0}{h} g_{\alpha j} B_u \right) \quad (2-80)$$

$$b = \frac{c}{V_0 \omega_0} (1/2)(i\gamma_{\alpha j}) \quad (2-81)$$

It is conventional to introduce the dimensionless quantity  $f_a$  the absorption oscillator strength for the transition  $\alpha j \rightarrow \alpha' j'$ , which is defined by the relation (Sobel'man page 302):

$$f_a = \frac{2m_e \omega_0}{3\hbar e^2} \frac{1}{2j+1} |\langle \alpha j || P || \alpha' j' \rangle|^2 \quad (2-82)$$

With this definition  $\alpha_{mn}$  becomes, (recall  $j=0$ ):

$$\alpha_{mn} = \frac{iNc f_a e^2 \pi^{1/2}}{2V_0 m_e \omega_0^2} \sum_u D_{\mu}^{(1)} D_{\nu}^{(1)} W(a_u + ib) \quad (2-83)$$

To facilitate future development some elements of  $\underline{\alpha}$  are given explicitly. From Rose, 1957 the matrix:

$$D_{\mu}^{(1)}(0, \beta, 0) = \begin{vmatrix} \frac{1}{2}(1 + \cos\beta) & \frac{-1}{\sqrt{2}} \sin\beta & \frac{1}{2}(1 - \cos\beta) \\ \frac{1}{\sqrt{2}} \sin\beta & \cos\beta & -\frac{1}{\sqrt{2}} \sin\beta \\ \frac{1}{2}(1 - \cos\beta) & \frac{1}{\sqrt{2}} \sin\beta & \frac{1}{2}(1 + \cos\beta) \end{vmatrix} \quad (2-84)$$

Therefore:

$$\alpha_{11} = iK_0 \left[ \frac{1}{4} (1+\cos\beta)^2 W(a_1 + ib) + \frac{1}{2} \sin^2\beta W(a_0 + ib) + \frac{1}{4} (1-\cos\beta)^2 W(a_{-1} + ib) \right] \quad (2-85)$$

$$\alpha_{-1-1} = iK_0 \left[ \frac{1}{4} (1-\cos\beta)^2 W(a_1 + ib) + \frac{1}{2} \sin^2\beta W(a_0 + ib) + \frac{1}{4} (1+\cos\beta)^2 W(a_{-1} + ib) \right] \quad (2-86)$$

$$\alpha_{-11} = \alpha_{1-1} = iK_0 \sin^2\beta \left[ \frac{1}{4} W(a_1 + ib) - \frac{1}{2} W(a_0 + ib) + \frac{1}{4} W(a_{-1} + ib) \right] \quad (2-87)$$

where:  $K_0 = \frac{Ncf_a e^{2\pi^{1/2}}}{2V_0 m_e \omega_0^2} \quad (2-88)$

or

$$K_0 = \frac{Ncf_a e^{2\pi^{1/2}}}{8\pi\epsilon_0 V_0 m_e \omega_0^2} \quad \text{in MKSA units} \quad (2-89)$$

For most lines in a gas of modest density  $|\alpha_{mn}| \ll 1$ . For example, using the information in the appendix:  $|\alpha| \sim 10^{-5}$  for the 253.7 nm. line of mercury at the vapour pressure of mercury at 20°C.

Equation (2-75) for  $\vec{P}_c$  and equation (2-83) for  $\underline{\alpha}$  together contain the

relevant quantum mechanical results in a form suitable for further analysis using the classical electromagnetic equation (2-35) given earlier. Inserting these quantities into equation (2-35) gives:

$$\begin{aligned} \nabla^2 \vec{E}(\vec{r}, t) - \nabla(\nabla \cdot \vec{E}(\vec{r}, t)) &= \frac{1}{c^2} \frac{\partial^2}{\partial t^2} (\vec{E}(\vec{r}, t) + 4\pi \vec{P}_c) \\ &= \frac{1}{c^2} \frac{\partial^2}{\partial t^2} (\vec{E}(\vec{r}, t) + 4\pi(\underline{\alpha} \cdot \vec{E}'(\vec{r})e^{-i\omega t} + \underline{\alpha}^* \cdot \vec{E}'^*(\vec{r})e^{i\omega t})) \end{aligned} \quad (2-90)$$

where  $E_{\text{local}} = \vec{E}'(\vec{r})e^{-i\omega t} + \vec{E}'^*(\vec{r})e^{i\omega t}$  is the total electric field at each atom.

Equation (2-90) has the same form as the equation which describes the propagation of an em wave through an anisotropic crystal (see Born and Wolf 1975, page 665). In an anisotropic crystal the electric field need not be perpendicular to the phase velocity; i.e. there may be a component of the electric field in the direction of the phase velocity. If this occurs the energy of the wave does not propagate in the direction of the phase velocity.

The component of the electric field along the direction of the phase velocity arises from the term  $\nabla(\nabla \cdot \vec{E}(\vec{r}, t))$  which is zero for isotropic materials. From Maxwell's equations:

$$\nabla \cdot \vec{E} = -4\pi \nabla \cdot \vec{P}_c \quad (2-91)$$

hence

$$\nabla(\nabla \cdot \vec{E}) = -4\pi\nabla \left[ \nabla \cdot (\underline{\alpha} \cdot \vec{E}'(\vec{r})e^{-i\omega t} + \underline{\alpha}^* \cdot \vec{E}'^*(\vec{r})e^{i\omega t}) \right] \quad (2-92)$$

Using this equation it can be shown that where  $|\alpha_{mn}| \ll 1$  the term  $\nabla(\nabla \cdot \vec{E})$  and the component of  $\vec{E}$  along the phase velocity is small compared to the component perpendicular to the phase velocity. Thus, in order to simplify greatly the solution to equation (2-90), the term  $\nabla(\nabla \cdot \vec{E})$  may be omitted, and the small difference between the direction of the phase velocity and energy flow may be ignored.

In the equation for  $\vec{p}_c$  the electric field interacting with the atoms must be the total field at the atom,  $E_{\text{local}}$ . This field is produced by both the field of the incident em wave  $\vec{E}(\vec{r}, t)$ , and the induced field of the neighbouring atoms. The relation between the incident field and the induced field is extremely complex for high frequencies in anisotropic materials. However where  $|\alpha_{mn}| \ll 1$  the induced field is much smaller than the incident field and the approximation  $\vec{E}(\vec{r}, t) = \vec{E}_{\text{local}}(\vec{r}, t)$  can be made. With these approximations equation (2-90) becomes:

$$\begin{aligned} \nabla^2(\vec{E}(\vec{r})e^{-i\omega t} + \vec{E}^*(\vec{r})e^{i\omega t}) &= \frac{1}{c^2} \frac{\partial^2}{\partial t^2} [(\underline{\epsilon} \cdot \vec{E}(\vec{r})e^{-i\omega t} \\ &+ \underline{\epsilon}^* \cdot \vec{E}^*(\vec{r})e^{i\omega t})] \end{aligned} \quad (2-93)$$

$$\text{where } \underline{\epsilon} = \underline{1} + 4\pi\underline{\alpha} \quad (2-94)$$

$$\begin{aligned} \text{or } \nabla^2 \vec{E}(\vec{r}) e^{-i\omega t} - \frac{1}{c^2} \frac{\partial^2}{\partial t^2} (\underline{\epsilon} \cdot \vec{E}(\vec{r}) e^{-i\omega t}) \\ + \nabla^2 \vec{E}^*(\vec{r}) e^{i\omega t} - \frac{1}{c^2} \frac{\partial^2}{\partial t^2} (\underline{\epsilon}^* \cdot \vec{E}^*(\vec{r}) e^{i\omega t}) = 0 \end{aligned} \quad (2-95)$$

Since  $\vec{E}(\vec{r})$  and  $\vec{E}^*(\vec{r})$  are linearly independent and the differential operators are linear, this equation can be true only if:

$$\nabla^2 \vec{E}(\vec{r}) e^{-i\omega t} - \frac{1}{c^2} \frac{\partial^2}{\partial t^2} (\underline{\epsilon} \cdot \vec{E}(\vec{r}) e^{-i\omega t}) = 0 \quad (2-96)$$

and likewise for the complex conjugate term.

Without loss of generality equation (2-96) can be solved for the case of a plane wave propagating along the z-axis. The solution is of the form

$$\vec{E} = E_1 e^{i(Kz - \omega t)} e_1 + E_{-1} e^{i(Kz - \omega t)} e_{-1}$$

where

$$E_{\pm 1} = \mp \left( \frac{E_x \mp iE_y}{\sqrt{2}} \right) \quad (2-98)$$

and  $E_x$  and  $E_y$  are the amplitudes of the wave along the x and y-axis respectively.

Substituting this solution into equation (2-96) yields the two homogeneous equations:

$$\frac{c^2}{\omega^2} K^2 E_1 - (\epsilon_{11} E_1 + \epsilon_{1-1} E_{-1}) = 0 \quad (2-99)$$

and

$$\frac{c^2}{\omega^2} K^2 E_{-1} - (\epsilon_{-11} E_1 + \epsilon_{-1-1} E_{-1}) = 0 \quad (2-100)$$

Solving these two simultaneous equations for  $K^2$  gives:

$$\frac{c^2}{\omega^2} K_{\pm}^2 = \frac{(\epsilon_{-1-1} + \epsilon_{11}) \pm [(\epsilon_{11} - \epsilon_{-1-1})^2 + 4\epsilon_{-1-1}^2]^{1/2}}{2} \quad (2-101)$$

where the fact that  $\epsilon_{-11} = \epsilon_{1-1}$  has been used.

Substituting this expression back into equations (2-99) gives

$$\frac{E_1}{E_{-1}} = \frac{\frac{1}{2} (\epsilon_{11} - \epsilon_{-1-1}) \pm [\frac{1}{4} (\epsilon_{11} - \epsilon_{-1-1})^2 + \epsilon_{-1-1}^2]^{1/2}}{\epsilon_{-11}} \quad (2-102)$$

where the signs + and - are associated with the solutions  $K_+^2$  and  $K_-^2$  (see eq. 2-101) respectively.

The form of the solution is greatly simplified by defining the complex function suggested by Corney, Kibble and Series, 1965:

$$\tan \theta = \frac{2\epsilon_{-11}}{\epsilon_{11} - \epsilon_{-1-1}} \quad (2-103)$$

$$\text{whence } \frac{E_1}{E_{-1}} = \frac{\cos \theta/2}{\sin \theta/2} \text{ for the solution } K_+^2 \quad (2-104)$$

$$\text{and } \frac{E_1}{E_{-1}} = \frac{-\sin \theta/2}{\cos \theta/2} \text{ for the solution } K_-^2 \quad (2-105)$$

The general solution for the differential equation (2-96) is thus

$$\begin{aligned} \vec{E} = & a_+ (\cos \theta/2 \mathbf{e}_1 + \sin \theta/2 \mathbf{e}_{-1}) e^{i(K_+z - \omega t)} \\ & + a_- (-\sin \theta/2 \mathbf{e}_1 + \cos \theta/2 \mathbf{e}_{-1}) e^{i(K_-z - \omega t)} \end{aligned} \quad (2-106)$$

The factors  $a_+$  and  $a_-$  are determined by the boundary conditions.  $K_+$  and  $K_-$  are the roots of equation (2-101) which give an exponentially decaying solution. These expressions are examined in detail in a later section.

For the purpose of this study we can select an incident e-m wave propagating along the  $z$  axis and given by the equation:

$$\vec{E} = (E_x(\omega) \bar{\mathbf{i}} + E_y(\omega) \bar{\mathbf{j}}) e^{i(K_1 z - \omega t)} \quad (2-107)$$

where,

$$E_x(\omega) = A_x(\omega) e^{i\phi_x}, \text{ and} \quad (2-108)$$

$A_x(\omega)$  is the amplitude, (a real valued function of the frequency  $\omega$ ) and  $\phi_x$  is the phase of the x component.  $E_y(\omega)$  is defined analogously.

We choose the boundary of the gas at  $z = 0$  normal to the  $z =$  axis, therefore the electric field is continuous across the boundary and there is no refraction. Equation (2-107) can now be equated to equation (2-106) at  $z = 0$  and solved for  $a_+$  and  $a_-$ . Thus:

$$\begin{aligned} & \frac{1}{\sqrt{2}} (E_x + iE_y) e_{-1} + \frac{1}{\sqrt{2}} (-E_x + iE_y) e_1 \\ = & (a_+ \cos \theta/2 - a_- \sin \theta/2) e_1 + (a_+ \sin \theta/2 + a_- \cos \theta/2) e_{-1} \end{aligned} \quad (2-109)$$

with the solutions

$$a_+ = \frac{E_x}{\sqrt{2}} (\sin \theta/2 - \cos \theta/2) + \frac{iE_y}{\sqrt{2}} (\cos \theta/2 + \sin \theta/2) \quad (2-110)$$

$$a_- = \frac{E_x}{\sqrt{2}} (\cos \theta/2 + \sin \theta/2) + \frac{iE_y}{\sqrt{2}} (\cos \theta/2 - \sin \theta/2) \quad (2-111)$$

The reflected wave has been omitted because we are primarily interested in the change in the transmitted wave with the application of the magnetic field. It is clear that the change in the reflectivity of the gas with the application of the field is small, hence there is a negligible effect on the transmitted wave.

The final solution for the em wave in the gas can now be given:

$$\begin{aligned}
 \vec{E} = & \left\{ \left[ \frac{E_x}{\sqrt{2}} (\sin \theta/2 - \cos \theta/2) \cos \theta/2 + \frac{iE_y}{\sqrt{2}} (\cos \theta/2 + \sin \theta/2) \cos \theta/2 \right] e_{-1} \right. \\
 & + \left. \left[ \frac{E_x}{\sqrt{2}} (\sin \theta/2 - \cos \theta/2) \sin \theta/2 + \frac{iE_y}{\sqrt{2}} (\cos \theta/2 + \sin \theta/2) \sin \theta/2 \right] e_{-1} \right\} \\
 & e^{i(K_+z - \omega t)} + \\
 & \left\{ \left[ \frac{-E_x}{\sqrt{2}} (\cos \theta/2 + \sin \theta/2) \sin \theta/2 + \frac{-iE_y}{\sqrt{2}} (\cos \theta/2 - \sin \theta/2) \sin \theta/2 \right] e_1 \right. \\
 & + \left. \left[ \frac{E_x}{\sqrt{2}} (\cos \theta/2 + \sin \theta/2) \cos \theta/2 + \frac{iE_y}{\sqrt{2}} (\cos \theta/2 - \sin \theta/2) \cos \theta/2 \right] e_{-1} \right\} e^{i(K_-z - \omega t)}
 \end{aligned}
 \tag{2-112}$$

#### II.4 THE WAVE IN A TRANSVERSE AND PARALLEL FIELD

The physical effects of the gas upon the incident light can now be ascertained from equations (2-112). While the equation is quite complex, it reduces considerably in the case where the magnetic field is either transverse or parallel to the direction of propagation. Since these two cases are of particular interest they are examined in detail.

The Transverse Field

When the magnetic field is parallel to the x-axis, it is transverse to the direction of propagation. From our earlier definition of the orientation of the field this corresponds to an angle  $\beta = \pi/2$ . Returning to equations (2-85), (2-86) and (2-87) and substituting this value for  $\beta$  we find

$$\alpha_{11} = \alpha_{-1-1} = iK_0 \left( \frac{1}{4} W(a_1 + ib) + \frac{1}{2} W(a_0 + ib) + \frac{1}{4} W(a_{-1} + ib) \right) \quad (2-113)$$

$$\alpha_{1-1} = \alpha_{-11} = iK_0 \left( \frac{1}{4} W(a_1 + ib) - \frac{1}{2} W(a_0 + ib) + \frac{1}{4} W(a_{-1} + ib) \right) \quad (2-114)$$

This increased symmetry simplifies equation (2-112). Recall from equation (2-94):

$$\epsilon_{mn} = \delta_{mn} + 4\pi\alpha_{mn} \quad (2-115)$$

hence

$$\epsilon_{11} = \epsilon_{-1-1} \quad \text{and} \quad \epsilon_{-11} = \epsilon_{1-1}$$

Thus the complex function [equation (2-103)]

$$\tan \theta = \frac{2\epsilon_{1-1}}{\epsilon_{11} - \epsilon_{-1-1}} \rightarrow \infty \text{ (REAL)} \quad (2-116)$$

and we have the simple result  $\theta = \pi/2$ . Substituting this value into equation (2-112) yields:

$$\vec{E} = \frac{iE_y}{\sqrt{2}} (e_1 + e_{-1}) e^{i(K_+ - \omega t)} + \frac{E_x}{\sqrt{2}} (e_{-1} - e_1) e^{i(K_- - \omega t)} \quad (2-117)$$

but from the definition of  $e_q$  this is simply

$$\vec{E} = E_x(\omega) e^{i(K_- z - \omega t)} \hat{i} + E_y(\omega) e^{i(K_+ z - \omega t)} \hat{j} \quad (2-118)$$

Thus the electric field of the incident wave divides naturally into two components along the x and y axis. The properties of these two components in general will be different as they are governed by the two different factors  $K_-$  and  $K_+$ .

The effect of the magnetic field is contained in the expressions for  $K_-$  and  $K_+$ . Recall equation (2-101):

$$\frac{c^2}{\omega^2} K_{\pm}^2 = \frac{(\epsilon_{-1-1} + \epsilon_{11}) \pm [(\epsilon_{11} - \epsilon_{-1-1})^2 + 4\epsilon_{1-1}^2]^{1/2}}{2}$$

Invoking the unique symmetry of  $\epsilon_{mn}$  for the transverse field we have:

$$\frac{c^2}{\omega^2} K_{\pm}^2 = \epsilon_{11} \pm \epsilon_{1-1} \quad (2-119)$$

hence:

$$\frac{c^2}{\omega^2} K_{\pm}^2 = 1 + 4\pi (\alpha_{11} \pm \alpha_{1-1}) \quad (2-120)$$

The physical consequences of this equation are most readily demonstrated by introducing the conventional parameters  $n_{\pm}$ , the index of refraction and  $k_{\pm}$ , the absorption coefficient where<sup>†</sup>:

$$\frac{c}{\omega} K_{\pm} = (n_{\pm} + i \frac{1}{2} \frac{c}{\omega} k_{\pm}) \quad (2-121)$$

It follows that:

$$n_{\pm}^2 - \frac{1}{4} \frac{c^2}{\omega^2} k_{\pm}^2 = \frac{\omega^2}{c^2} \operatorname{Re} (K_{\pm}) \quad (2-122)$$

$$\frac{c}{\omega} n_{\pm} k_{\pm} = \frac{\omega^2}{c^2} \operatorname{Im} (K_{\pm}) \quad (2-123)$$

Solving these equations for  $n_{\pm}$  and  $k_{\pm}$  using the approximation  $|\alpha_{mn}| \ll 1$  we find

$$n_{\pm} \sim 1 + 2\pi \operatorname{Re} (\alpha_{11} \pm \alpha_{1-1}) \quad (2-124)$$

$$k_{\pm} \sim 4\pi \frac{\omega}{c} \operatorname{Im} (\alpha_{11} \pm \alpha_{1-1}) \quad (2-125)$$

Thus from equation (2-121):

---

<sup>†</sup>The factor  $1/2 \frac{c}{\omega}$  multiplying the absorption coefficient  $k_{\pm}$  is introduced to conform with the conventional definition of  $k$  as the coefficient governing the exponential damping of the intensity,  $I$ , which is proportional to the square of the electric field, i.e.  $I = I_0 e^{-kz}$ .

$$\frac{c}{\omega} K_{\pm} = 1 + 2\pi (\alpha_{11} \pm \alpha_{1-1}) \quad (2-126)$$

Substituting the complete expressions for  $\alpha_{11}$  and  $\alpha_{1-1}$  from equations (2-113) and (2-114), we find

$$\frac{c}{\omega} K_{+} = 1 + 2\pi i K_0 \left( \frac{1}{2} W(a_1 + ib) + \frac{1}{2} W(a_{-1} + ib) \right) \quad (2-127)$$

$$\frac{c}{\omega} K_{-} = 1 + 2\pi i K_0 W(a_0 + ib) \quad (2-128)$$

With these expressions inserted into equation (2-118) the equation for propagation transverse to the magnetic field assumes its final form.

Let us now examine the physical content of this equation. The magnetic field manifests itself through the term  $a_u$  in the functions  $W(a_u + ib)$ .

Recall from equation (2-80)

$$a_u = \frac{c}{V_0 \omega_0} \left( \omega - \omega_0 - \frac{\mu_0}{h} g_{\alpha j} B u \right)$$

The consequences of this are clearly illustrated by considering first the absorption coefficients  $k_{+}$  and  $k_{-}$  from equations (2-125), (2-113) and (2-114):

$$k_{+} = 4\pi K_0 \frac{\omega}{c} \operatorname{Re} \left( \frac{1}{2} W(a_1 + ib) + \frac{1}{2} W(a_{-1} + ib) \right) \quad (2-129)$$

$$k_{-} = 4\pi K_0 \frac{\omega}{c} \operatorname{Re} \left( W(a_0 + ib) \right) \quad (2-130)$$

Examining  $k_-$ , which determines the amplitude of the x component of the wave, we find that the magnitude of the absorption varies over a frequency range determined by  $\text{Re}(W(a_0 + ib))$  which is independent of the field. (Note that  $\text{Re}(W(z))$  is proportional to a Voigt function.) In contrast the amplitude of the y component of the wave depends on  $k_+$  which is a function of the magnetic field. As the field is increased the peaks of the two functions  $\text{Re}(W(a_1 + ib))$  and  $\text{Re}(W(a_{-1} + ib))$  shift to the frequencies  $\omega_0 + \frac{\mu_0}{h} g_{\alpha j} B$  and  $\omega_0 - \frac{\mu_0}{h} g_{\alpha j} B$  respectively. Hence the magnitude of the absorption will decrease at the frequency  $\omega_0$  while increasing at the two frequencies displaced symmetrically about  $\omega_0$ . Note that when  $\vec{B} = 0$ ,  $k_+ = k_- = k$  where  $k$  is the familiar absorption coefficient for a gas not immersed in a magnetic field, (See Sobel'man, 1972 p. 381)

The indices of refraction  $n_-$  and  $n_+$  determine the phase velocity of the x and y components of the wave respectively. In the presence of a magnetic field  $n_+ \neq n_-$  and a wave propagating through the gas will experience a relative phase shift between its x and y components.

Examining the equations for  $k_+$  and  $k_-$  in the light of our earlier discussions of the Zeeman effect (section II.1) leads to an obvious extension of the equations for  $K_+$  and  $K_-$  to the more general instance of a degenerate ground state. In that discussion we noted that  $\sigma$ -components could only absorb photons polarized perpendicular to the magnetic field (i.e. along the y-axis), while  $\pi$  components could only absorb photons parallel to the field (i.e. along the x-axis). It is therefore not surprising to observe that the expression for  $k_+$  is simply proportional to

sum of the line broadened  $\sigma$ -components while  $k_-$  is proportional to the sum of the line broadened  $\pi$ -components for this non-degenerate case. Thus there emerges an intimate relationship between the absorption coefficients and the Zeeman components. This relationship can be demonstrated rigorously, (see Sobel'man 1972).

Extrapolating this relationship to the more general degenerate case  $K_+$  and  $K_-$  become

$$\frac{c}{\omega} K_+ = 1 + 2\pi i K_0 \sum_{mm'} C^1_{mm'} W(a_{mm'} + ib) \quad (2-131)$$

where  $m - m' = \pm 1$

$$\frac{c}{\omega} K_- = 1 + 2\pi i K_0 \sum_{mm'} C^0_{mm'} W(a_{mm'} + ib) \quad (2-132)$$

where  $m - m' = 0$

$$a_{mm'} = \omega - \omega_0 - \frac{\mu_0}{h} B (g_{\alpha j^m} - g_{\alpha' j', m'}) \quad (2-133)$$

The constants  $C^0_{mm'}$ , and  $C^1_{mm'}$ , are the relative intensities of the  $\pi$  and  $\sigma$  components respectively, which have been normalized such that

$$\sum_{mm'} C^0_{mm'} = 1 \quad \text{and} \quad \sum_{mm'} C^1_{mm'} = 1 \quad (2-134)$$

where  $m' - m = 0$

where  $m' - m = \pm 1$

In the next section propagation parallel to the magnetic field is examined.

The Parallel Field

The magnetic field is parallel to the direction of propagation when  $\beta = 0$ . From equations (2-85), (2-86) and (2-87),

$$\alpha_{1-1} = \alpha_{-11} = 0 \quad (2-135)$$

$$\alpha_{11} = iK_0 W(a_1 + ib) \quad (2-136)$$

$$\alpha_{-1-1} = iK_0 W(a_{-1} + ib) \quad (2-137)$$

hence from equation (2-94)

$$\epsilon_{1-1} = 0 \quad (2-138)$$

and from equation (2-103)  $\tan\theta = 0 \quad (2-139)$

and therefore  $\theta = 0$

Using this result, equation (2-112) reduces to

$$\vec{E} = \frac{-E_x + i E_y}{\sqrt{2}} e^{i(K_+ - \omega t)} e_1 + \frac{E_x + i E_y}{\sqrt{2}} e^{i(K_- - \omega t)} e_{-1} \quad (2-140)$$

Thus the wave divides naturally into two circularly polarized components.

From equation (2-101)

$$\frac{c^2}{\omega^2} K_+^2 = \epsilon_{11} \quad \text{and} \quad \frac{c^2}{\omega^2} K_-^2 = \epsilon_{-1-1} \quad (2-141)$$

Again making the assumption  $|\alpha| \ll 1$  we find

$$\frac{c}{\omega} K_+ = 1 + 2\pi i K_0 W(a_+ + ib) \quad (2-142)$$

$$\frac{c}{\omega} K_- = 1 + 2\pi i K_0 W(a_- + ib) \quad (2-143)$$

These expressions together with equation (2-140) completely describe the propagation of light parallel to the magnetic field. Note that each circularly polarized component is affected by a specific transition,  $u = \pm 1$ , of the atom.

When a magnetic field is applied these two components have different indices of refraction and will absorb light over a different range of frequencies. The differing indices of refraction lead to the familiar effect of faraday rotation of linearly polarized incident light. These results can be extended to the situation of a degenerate ground state by analogy with the case of a transverse field. When this is done the final equation is in complete agreement with that obtained by Camm and Curzon, 1972, using a different approach.

In the next section these results are used to examine the polarizing effect of a gas on an incident em - wave.

## II.5 THE POLARIZATION OF THE TRANSMITTED WAVE

To this point the theory has been developed for the special case of a monochromatic plane wave. Recall equation (2-118) for the case of a transverse magnetic field.

$$\vec{E} = E_x(\omega) e^{i(K_- z - \omega t)} \bar{i} + E_y(\omega) e^{i(K_+ z - \omega t)} \bar{j} \quad (2-118)$$

where  $K_+$  and  $K_-$  are given by equations (2-127) and (2-128) and from equation

$$(2-108): E_x(\omega) = A_x(\omega) e^{i\phi_x} \quad E_y(\omega) = A_y(\omega) e^{i\phi_y}$$

where  $A_x$  and  $A_y$  are the amplitudes and  $\phi_y$  and  $\phi_x$  are the phases of the incident em wave.

A characteristic of monochromatic plane waves is that three quantities, examined at a given point  $z$  in space, remain constant for all time. They are the two amplitudes,

$$A_x e^{-1/2 k_- z} \quad \text{and} \quad A_y e^{-1/2 k_+ z} \quad \text{and the phase difference given by;}$$

$$\delta = \left( \frac{\omega}{c} n_- z + \phi_x \right) - \left( \frac{\omega}{c} n_+ z + \phi_y \right)$$

These three independent quantities are sufficient to determine completely the state of polarization of the light represented by this wave, (Klein, 1970, p. 485). Since for a monochromatic plane wave these quantities are constant in time, a monochromatic plane wave must have a fixed state of polarization.

A strictly monochromatic plane wave is, however, a mathematical idealization which is never realized in practice. Consequently equation (2-118) must be modified slightly to accord with reality. This is most readily accomplished by transforming equation (2-118) into the quasi-monochromatic plane wave:

$$\vec{E} = E_x(\omega, t) e^{i(K_z z - \omega t)} \vec{i} + E_y(\omega, t) e^{i(K_+ z - \omega t)} \vec{j} \quad (2-144)$$

where  $E_x(\omega, t)$  and  $E_y(\omega, t)$  are slowly varying functions of time compared to  $e^{i\omega t}$  and are defined by the expressions:

$$E_x(\omega, t) = A_x(\omega, t) e^{i\phi_x(t)} \quad (2-145)$$

$$E_y(\omega, t) = A_y(\omega, t) e^{i\phi_y(t)} \quad (2-146)$$

where the modified amplitudes and phases are now stochastic functions of time.

This new representation of the light wave requires a more sophisticated definition of polarization than was necessary for strictly nonchromatic plane waves since it admits the possibility of unpolarized light.

A number of equivalent schemes have been devised to represent the state of polarization of light. The scheme used in this study is after a method presented in Born & Wolf (1975), p. 544 where the polarization is related to the degree of correlation between the irregular fluctuations of  $A_x$ ,  $A_y$ ,  $\phi_x$ , and  $\phi_y$ . An attractive feature of this scheme is that the theoretical parameters are closely related to the experimentally measured quantities because the theoretical development closely models the experimental technique used to analyse the light. This feature proves to be particularly advantageous when we compare the results of theory with experiment.

The theory is developed by considering the following idealized experiment, (see Fig. 4). The incident light, having traversed a length,  $l$ , of gas in a transverse magnetic field, passes through a compensator (such as a quarter wave plate) which retards the phase of the y-component by an amount  $\xi$  with respect to the phase of the x component. Using equation (2-144) the wave is given by:

$$\vec{E} = [E_x(\omega, t)e^{iK_-l} \bar{i} + E_y(\omega, t)e^{iK_+l} e^{i\xi} \bar{j}] \cdot e^{i(\frac{\omega}{c}z - \omega t)} \quad (2-147)$$

The wave next passes through a polarizer with its pass direction inclined at an angle  $\psi$  with respect to the x axis. Whence the component passing through the polarizer is given by:

$$E(\psi, \xi, t) = [E_x(\omega, t)e^{iK_-l} \cos \psi + E_y(\omega, t)e^{iK_+l} e^{i\xi} \sin \psi] \cdot e^{i(\frac{\omega}{c}z - \omega t)} \quad (2-148)$$

Finally, the intensity of the wave is measured by a detector. The instantaneous intensity<sup>†</sup>,  $I'$ , of the wave is proportional to the square of the real part of the complex electric field function,  $E(\psi, \xi, t)$ , i.e.

$$I' \propto \text{Re}^2 (E(\psi, \xi, t)) \quad (2-149)$$

---

<sup>†</sup>Technically, this quantity is the flux density or irradiance and not the intensity, (see Klein, 1970 at pp. 122 and 508). However, the two are closely related and many authors including Born and Wolf use the term intensity. Therefore, for convenience, the term intensity is used here.

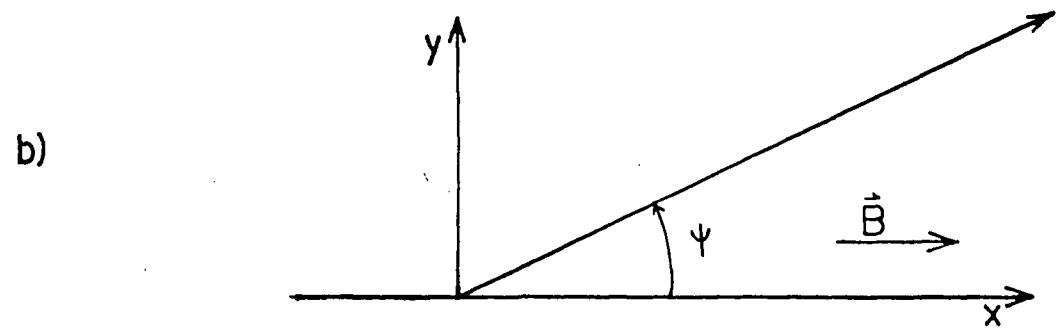
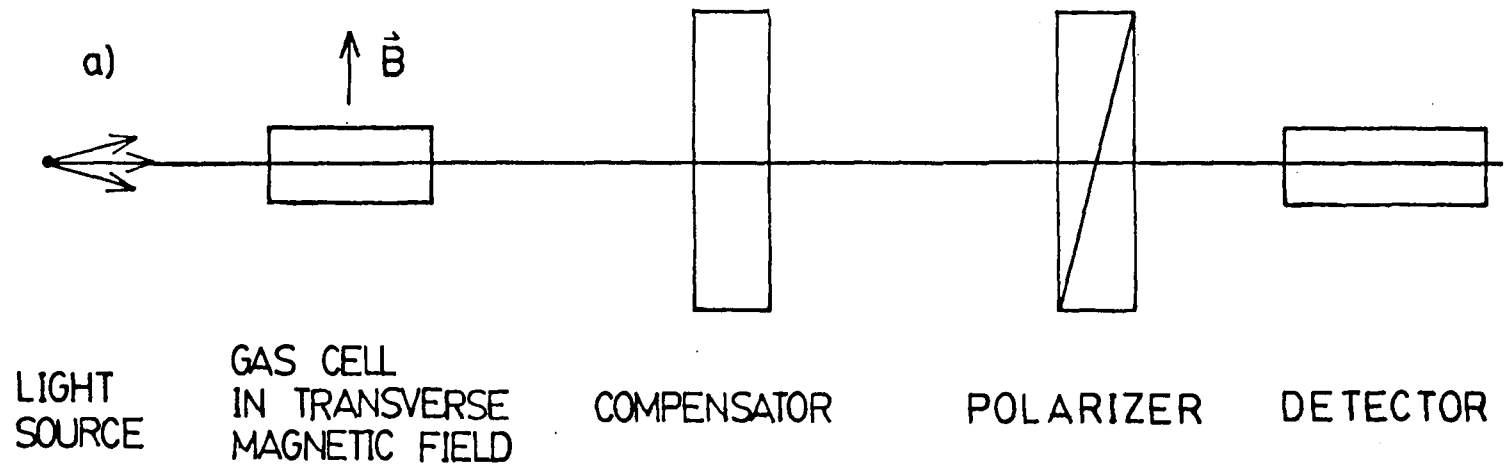


Fig. 4: a) Polarization Measuring System  
 b) Polarization Orientation

However, a real detector, such as a photomultiplier or a photographic plate, does not measure the instantaneous intensity; it measures a time averaged intensity  $I$ . This experimentally measured intensity,  $I$ , is theoretically described by taking the time average of  $I'$  as described by the expression:

$$I = \langle I'(t) \rangle = \frac{1}{2T} \int_{-T}^T I'(t) dt \quad (2-150)$$

where  $T$  is the averaging time period.

With the light source and detector used in this study, the functions  $E_x$  and  $E_y$  defined by equations (2-145) and (2-146) undergo a large number of random fluctuations within the response time  $T$  of the detector. It is therefore reasonable, for the sake of mathematical simplicity, to take the limit  $T \rightarrow \infty$  rather than the actual response time of the detector in calculating the time average of  $I'$ . That is,  $I$  is given by:

$$I = \langle I'(t) \rangle = \lim_{T \rightarrow \infty} \frac{1}{2T} \int_{-T}^T I'(t) dt$$

which is proportional to

$$\lim_{T \rightarrow \infty} \frac{1}{2T} \int_{-T}^T |\text{Re}(E(\psi, \xi; t))|^2 dt \quad (2-151)$$

Using this expression for the time averaging, it is possible to show that:

$$2\langle \text{Re}^2(E(\psi, \xi; t)) \rangle = \langle E(\psi, \xi; t) \cdot E^*(\psi, \xi; t) \rangle \quad (2-152)$$

(see Born and Wolf 1975 at p. 498)

Thus, the experimentally measured intensity  $I$  is simply given by:

$$I(\psi, \xi; \omega) = \langle E(\psi, \xi; t) \cdot E^*(\psi, \xi; t) \rangle \quad (2-153)$$

where the unimportant constant of proportionality has been set equal to 1.

Inserting equation (2-148) into the above, we have:

$$I(\psi, \xi; \omega) = \langle E_x E_x^* \rangle e^{i(K_- - K_-^*)\ell} \cos^2 \psi + \langle E_y E_y^* \rangle e^{i(K_+ - K_+^*)\ell} \sin^2 \psi \quad (2-154)$$

$$+ \left[ \langle E_x^* E_y \rangle e^{i(K_- - K_+^*)\ell} e^{-i\xi} + \langle E_y E_x^* \rangle e^{i(K_+ - K_-^*)\ell} e^{i\xi} \right] \cos \psi \sin \psi$$

Equation (2-154) can be written more succinctly as

$$I(\psi, \xi; \omega) = J_{xx} \cos^2 \psi + J_{yy} \sin^2 \psi$$

$$+ (J_{xy} e^{-i\xi} + J_{yx} e^{i\xi}) \cos \psi \sin \psi \quad (2-155)$$

where:

$$J_{xx} = \langle E_x E_x^* \rangle e^{i(K_- - K_-^*)\ell}$$

$$J_{yy} = \langle E_y E_y^* \rangle e^{i(K_+ - K_+^*)\ell}$$

$$J_{xy} = \langle E_x E_y^* \rangle e^{i(K_- - K_+^*)\ell}$$

$$J_{yx} = \langle E_y E_x^* \rangle e^{i(K_+ - K_-^*)\ell}$$

The four terms  $J_{xx}$ ,  $J_{yy}$ ,  $J_{xy}$  and  $J_{yx}$  form the elements of a matrix called the coherency matrix  $J$ .

$$J = \begin{pmatrix} J_{xx} & J_{xy} \\ J_{yx} & J_{yy} \end{pmatrix} \quad (2-156a)$$

It is evident from the definitions of  $J_{xy}$  and  $J_{yx}$  that:

$$J_{xy} = J_{yx}^* \quad (2-156b)$$

Further, it follows from equation (2-154) that the total intensity  $I_T$  (i.e. the intensity measured with the polarizer removed) is given by:

$$I_T = J_{xx} + J_{yy} \quad (2-157)$$

It is clear from equation (2-155) that any two light beams with the same coherency matrix are indistinguishable in an experiment involving a polarizer and a compensator.<sup>†</sup> Thus this matrix can be used to define uniquely the state of polarization of the light. Let us briefly digress to illustrate this with some examples. For simplicity we use the coherency matrix of the incident light  $J_i$  which from equations (2-107) and (2-144) is simply:

$$J_i = \begin{vmatrix} \langle E_x E_x^* \rangle & \langle E_x E_y^* \rangle \\ \langle E_y E_x^* \rangle & \langle E_y E_y^* \rangle \end{vmatrix} \quad (2-158)$$

#### Completely Polarized Light

Completely polarized light occurs when the random fluctuations of the two amplitudes and two phases are correlated such that the ratio of the amplitudes and the difference in the phases are time independent. This may be expressed as

---

<sup>†</sup>In interference experiments the waves may be distinguished by their characteristic coherence length and spatial coherence. However, since these are intrinsic properties of the light source which are only mildly affected by the absorbing gas, they are not considered here.

$$\frac{A_y(t)}{A_x(t)} = q \quad \text{and} \quad \chi = \phi_x(t) - \phi_y(t) \quad (2-159)$$

where  $q$  and  $\chi$  are constants. In this case  $J_i$  may be written;

$$J_i^P = \langle A_x^2 \rangle \begin{pmatrix} 1 & qe^{i\chi} \\ qe^{-i\chi} & q^2 \end{pmatrix} \quad (2-160)$$

The superscript P has been added to denote completely polarized light.

It is easily shown that this matrix is identical to that of a strictly monochromatic plane wave. Since two light beams with the same coherency matrix are in the same state of polarization it follows that the matrix  $J_i^P$  does indeed represent completely polarized light. From (2-160) note that a property of polarized light is that

$$\text{Det } J_i^P = J_{xx} J_{yy} - J_{xy} J_{yx} = 0 \quad (2-161)$$

By exploiting the relationships between  $J_i^P$  and monochromatic plane waves we can denote the various states of  $J_i^P$  by the familiar terms applicable to monochromatic plane waves. Thus, in general  $J_i^P$  represents an elliptically polarized wave. If the wave is linearly polarized  $\chi = m\pi$  where  $m = 0, \pm 1, \pm 2 \dots$  and the coherency matrix becomes

$$\langle A_x^2 \rangle \begin{pmatrix} 1 & (-1)^m q \\ (-1)^m q & q^2 \end{pmatrix} \quad (2-162)$$

The direction of polarization makes an angle  $\alpha_0$  with the x-axis, where:

$$\alpha_0 = \arctan [ (-1)^m q ] \quad (2-163)$$

For circularly polarized light  $\chi = m \pi/2$  and  $A_x = A_y$  and the matrix is given by:

$$\langle A_x^2 \rangle = \begin{pmatrix} 1 & \pm i \\ \mp i & 1 \end{pmatrix} \quad (2-164)$$

where the upper and lower signs represent right and left circularly polarized light respectively.

### Unpolarized light

We define unpolarized light as light whose intensity is independent of the angle  $\psi$  of the polarizer, and of the phase shift  $\xi$ , i.e.

$$I(\psi, \xi, \omega) = \text{constant for a given } \omega. \quad (2-165)$$

It is evident from equation (2-155) and (2-156b) that this is true if and only if

$$J_{xx} = J_{yy} \quad \text{and} \quad J_{yx} = J_{xy} = 0$$

An equivalent and perhaps more insightful definition of unpolarized light is a wave whose components  $E_x$  and  $E_y$  are completely incoherent so that  $\langle E_x E_y^* \rangle = 0$  for any choice of  $x, y$  axes perpendicular to the direction of propagation. It follows that the coherency matrix for unpolarized light is given by:

$$J_i^U = I_T/2 \begin{pmatrix} 1 & 0 \\ 0 & 1 \end{pmatrix} \quad (2-167)$$

note:  $\text{Det } J_i^U \neq 0 \quad (2-168)$

### Partially Polarized Light

In general the state of a light beam lies between the two extremes of completely polarized and unpolarized light and this is known as partially polarized light. It can be shown that partially polarized light can be uniquely expressed as the superposition of a completely polarized and an unpolarized wave, (Born and Wolf, 1975, p. 550). That is

$$J = J^U + J^P \quad (2-169)$$

where in accordance with matrices (2-160) and (2-167) we can define:

$$J^U = \begin{pmatrix} A & 0 \\ 0 & A \end{pmatrix} \quad (2-170)$$

and

$$J^P = \begin{pmatrix} B & D \\ D^* & C \end{pmatrix} \quad (2-171)$$

The matrix elements of  $J^U$  and  $J^P$  are given in terms of the elements of  $J$  by the following equations.

$$A = 1/2 (J_{xx} + J_{yy}) - 1/2 \sqrt{(J_{xx} + J_{yy})^2 - 4 \text{Det } J} \quad (2-172)$$

$$B = J_{xx} - A \quad (2-173)$$

$$C = J_{yy} - A \quad (2-174)$$

$$D = J_{xy} \quad (2-175)$$

$$D^* = J_{yx} \quad (2-176)$$

The elements of  $J^U$  and  $J^P$  thus provide a unique representation of the state of polarization of the light.

It is useful to introduce one final parameter, the degree of polarization  $P$ .  $P$  is defined as the ratio of the intensity of the polarized portion  $I_{pol}$  to the total intensity of the light. That is:

$$P = \frac{I_{pol}}{I_T} = \frac{B + C}{J_{xx} + J_{yy}} \quad (2-177)$$

note  $0 < P < 1$  (2-178)

When  $P = 1$  the light is completely polarized and when  $P = 0$  it is unpolarized. The degree of polarization is independent of the choice of  $x$ ,  $y$  axes.

We can now use these definitions to examine the polarizing effect of a gas in a transverse magnetic field. From equation (2-155) the coherency matrix is given by

$$J = \begin{vmatrix} \langle E_x E_x^* \rangle e^{-k_l} & \langle E_x E_y^* \rangle e^{i(K_- - K_+^*)l} \\ \langle E_y E_x^* \rangle e^{i(K_+ - K_-^*)l} & \langle E_y E_y^* \rangle e^{-k_+ l} \end{vmatrix} \quad (2-179)$$

where equation (2-121) for  $k_{\pm}$  has been used.

If the state of polarization of the incident wave is known the above matrix will describe completely the state of the wave after traversing the gas. Two cases are of particular interest: when the incident wave is linearly polarized and when the wave is unpolarized. We examine these two cases in order to establish the conditions under which the gas may act as a polarizer.

#### Unpolarized Incident Wave

When the incident wave is unpolarized [from matrix (2-167)]:

$$\begin{aligned} \langle E_x E_x^* \rangle &= \langle E_y E_y^* \rangle = 1/2 I_0(\omega) \\ \text{and } \langle E_x E_y^* \rangle &= 0 \end{aligned}$$

where  $I_0(\omega)$  is here defined as the total intensity of the incident wave.

Thus, from matrix (2-179):

$$J = \frac{1}{2} I_0(\omega) \begin{vmatrix} e^{-k_l} & 0 \\ 0 & e^{-k_+ l} \end{vmatrix} \quad (2-180)$$

One result is immediately evident from this matrix. The gas affects the state of polarization only through the absorption coefficients  $k_+$  and  $k_-$ . Moreover, it is also clear how the gas is able to polarize the light. Consider a situation where at a given frequency  $\omega$ ;

$$k_- \gg 1 \text{ and } k_+ \ll 1 \quad (2-181)$$

then:

$$J \sim 1/2 I_0(\omega) \begin{pmatrix} 0 & 0 \\ 0 & 1 \end{pmatrix} \quad (2-182)$$

Thus the light at frequency  $\omega$  becomes linearly polarized along the y-axis. In fact only the condition  $k_- \gg k_+$  and not  $k_+ \ll 1$  is necessary for the gas to act as a polarizer. However it is highly desirable that the polarizer have as high a transmittance as possible and in this example this is achieved when  $k_+ \rightarrow 0$ .

If the conditions of (2-181) can be arranged, two limitations to the technique are still apparent. The light can only be linearly polarized and the light will never be completely polarized since  $e^{-k_- l}$  is never exactly zero. That is, there will be a strong linearly polarized component along the y-axis and a weak unpolarized component. In the representation (2-169) this can be written as;

$$J = I_0(\omega)/2 \begin{vmatrix} e^{-k_- l} & 0 \\ 0 & e^{-k_- l} \end{vmatrix} + I_0(\omega)/2 \begin{vmatrix} 0 & 0 \\ 0 & (e^{-k_+ l} \quad -e^{-k_- l}) \end{vmatrix} \quad (2-183)$$

Clearly then the larger  $k_- l$  the higher the degree of polarization.

Simple Examples

To demonstrate that the conditions given by (2-181) can in fact be realized we examine equations (2-129) and (2-130) which give  $k_-$  and  $k_+$  for lines with a non-degenerate ground state:

$$k_+ = 4\pi K_0 \frac{\omega}{c} \operatorname{Re} \left( \frac{1}{2} W(a_1 + ib) + \frac{1}{2} W(a_{-1} + ib) \right)$$
$$k_- = 4\pi K_0 \frac{\omega}{c} \operatorname{Re} \left( W(a_0 + ib) \right)$$

Let us assume for the moment that a line can be found such that at frequency  $\omega_0$ ,  $k_- \ell \gg 1$  for a gas of reasonable length and density. (It is demonstrated later that this is indeed the case for the 253.7 nm line of mercury.) In view of the earlier discussion of the effect of the magnetic field on  $k_+$  it is clear that in principle we can apply a magnetic field which is sufficiently large to cause  $k_+ \ell \ll 1$  at the frequency  $\omega_0$ . Thus an unpolarized incident beam would become partially polarized when passed through the gas. Our objective is, however, much more ambitious. We want the gas to polarize the light over its entire frequency range and not just at the central frequency  $\omega_0$ . That is if the incident light has a line shape with a characteristic width  $\Delta\nu$  we require that the conditions  $k_- \ell \gg 1$  and  $k_+ \ell \ll 1$ , (see 2-181) both remain valid over the frequency range  $\Delta\nu$ .

Examining the equation for  $k_-$  and assuming  $k_- \ell \gg 1$  at  $\omega_0$ , it is evident that the first condition can be met over  $\Delta\nu$  if the absorption line profile  $W(a_0 + ib)$  is sufficiently broad so as to remain nearly constant over  $\Delta\nu$ , (see Fig. 5a). Of course if  $k_- \ell$  is very large at  $\omega_0$  the condition

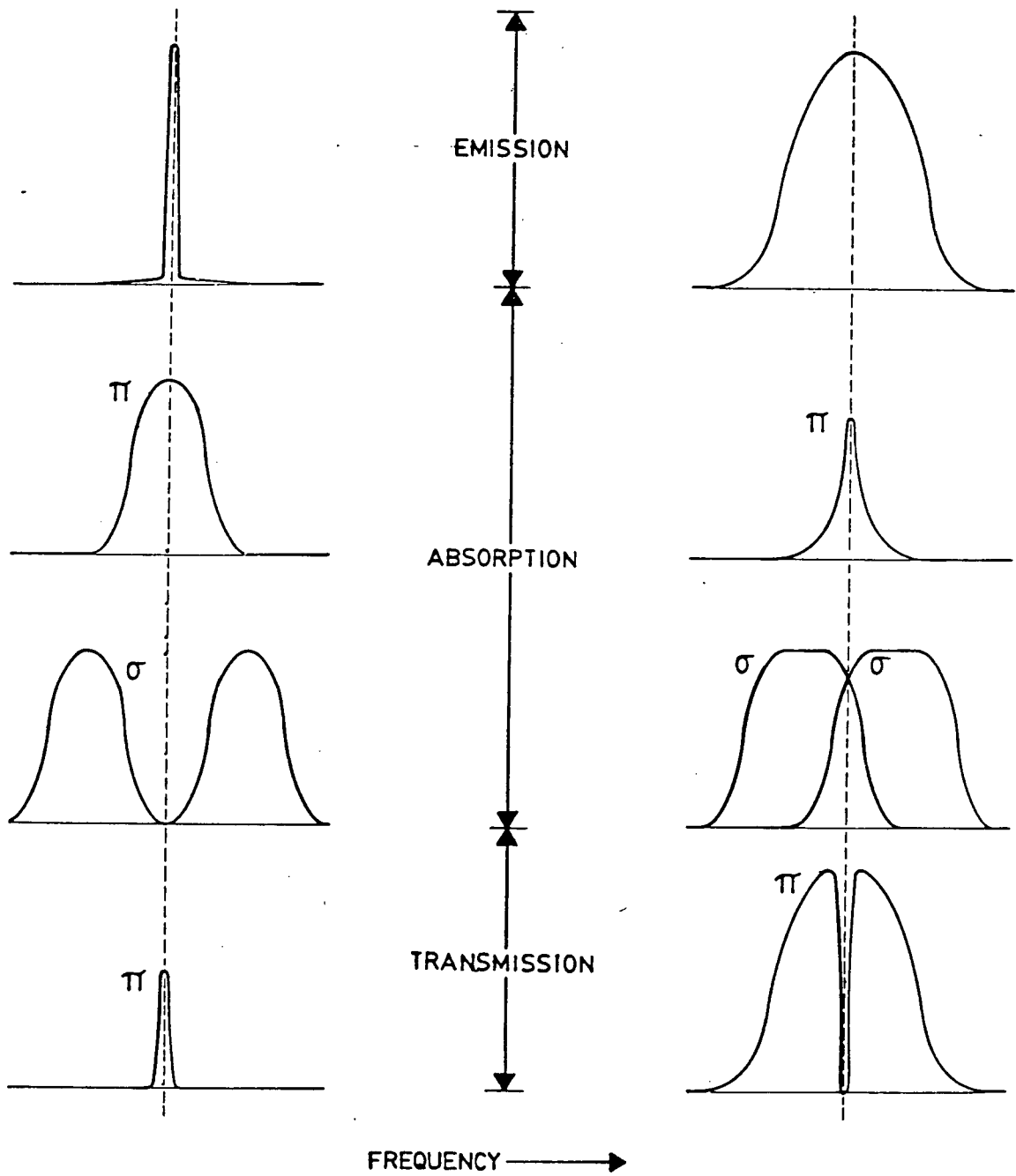


Fig. 5: Emission, Absorption and Transmission Line Profile

$k_{-l} \gg 1$  could be satisfied even with a substantial change in  $W(a_0 + ib)$  over  $\Delta\nu$ .

While it is desirable to have a broad line profile in attempting to satisfy the first condition, just the opposite is true of the second condition;  $k_{+l} \ll 1$  over  $\Delta\nu$ . For if  $W(a_1 + ib)$  and  $W(a_{-1} + ib)$  in the equation for  $k_{+}$  became broader (recall that  $W(a_0 + ib)$ ,  $W(a_1 + ib)$  and  $W(a_{-1} + ib)$  all have the same breadth), a larger magnetic field must be applied to shift the centres of the two line profiles far enough from  $\omega_0$  so that only their much smaller wings contribute to  $k_{+}$  over the range  $\Delta\nu$ . For many purposes it may also be important that  $k_{+l}$  remain reasonably constant over  $\Delta\nu$  since changes in  $k_{+l}$  over  $\Delta\nu$  will alter the line shape of the transmitted light.

In conclusion any attempt to optimize the polarizing properties of the gas must reconcile the two conflicting conditions  $k_{-l} \gg 1$  and  $k_{+l} \ll 1$  over  $\Delta\nu$ .

The foregoing comments would, of course, be less important if we could not alter the line profile width according to our design. However in our earlier discussion of line broadening we established that the line width depended on the temperature and density of the gas. Moderate adjustments in these two parameters can lead to changes in the line width of an order of magnitude, which provides the latitude necessary for optimizing the gas polarizer's performance.

There is another situation which can give rise to polarized light. Consider the case where  $k_{-l} \gg 1$  at frequency  $\omega_0$ , but the line profile of

the absorption line  $\text{Re}(W(a_0 + ib))$  is much narrower than the width  $\Delta\nu$  of the incident line, (see Fig. 5b). For the x component, the light at the center of the line is almost completely absorbed, but the light in the wings of the line is mostly transmitted. For the y component a weak magnetic field is used to spread the line profiles  $\text{Re}(W(a_1 + ib))$  and  $\text{Re}(W(a_{-1} + ib))$  over the frequency range  $\Delta\nu$  rather than to split them away from  $\Delta\nu$  as was done previously. (Note that this effect can be enhanced by using an inhomogeneous, but highly isotropic magnetic field.) In this way  $k_{\perp}l \gg 1$  is maintained over  $\Delta\nu$  and the transmitted light is polarized along the x-axis.

The obvious disadvantage of this technique is that the absorbing gas, while polarizing the source line, also distorts its shape by almost completely absorbing the centre of the line. Thus, this technique for polarizing light is only of use in studies where it is acceptable for the source line to be distorted, (although in a predictable way) by the polarizer.

#### Linearly Polarized Incident Wave

Consider now the effect of the gas on a linearly polarized incident light beam. This situation can be completely illustrated by considering the case where the incident light is polarized at an angle of  $45^\circ$  with respect to the x-axis.

That is, from matrix (2-162) and equation (2-163):

$$\langle E_x E_x^* \rangle = \langle E_y E_y^* \rangle = \langle E_x E_y^* \rangle = 1/2 I_0(\omega)$$

The coherency matrix for the transmitted light is then given by

$$J = \frac{1}{2} I_0(\omega) \begin{vmatrix} e^{-k_- \ell} & \frac{i\omega}{c} (n_- - n_+) \ell & e^{-1/2(k_+ + k_-)\ell} \\ \left( \frac{i\omega}{c} (n_+ - n_-) \ell \right) & e^{-1/2(k_+ + k_-)\ell} & e^{-k_+ \ell} \end{vmatrix} \quad (2-184)$$

where equation (2-121) has been used to define  $n_{\pm}$ .

Note that the transmitted light at frequency  $\omega$  remains completely polarized since  $\text{Det } J = 0$ . If we again imagine a situation where  $k_- \ell \gg 1$  and  $k_+ \ell \ll 1$  we obtain essentially the same result as in the case of an unpolarized incident wave, namely

$$J \sim (I_0(\omega)/2) \begin{vmatrix} 0 & 0 \\ 0 & 1 \end{vmatrix} \quad (2-185)$$

Thus the gas will behave as a polarizer much as it did in the case of an unpolarized incident beam. In particular, the earlier comments on how to optimize the polarizing properties of the gas remain valid here. However the two cases are not exactly the same. The chief difference between the two is the appearance of the indices of refraction  $n_{\pm}$  in the coherency matrix (2-184). To demonstrate the effect of these terms consider again the situation where  $k_- \ell \gg 1$  and  $k_+ \ell \ll 1$  over  $\Delta\nu$ . For unpolarized incident light the fraction of the light along the x axis which was not absorbed after traversing the gas appeared as an unpolarized component, [recall

(2-183)]. If the incident light is polarized, however, this fraction does not appear as an unpolarized component since  $\text{DET } J = 0$ .

To help illustrate this situation imagine first that  $n_+ = n_-$ . In this case the transmitted light remains linearly polarized but it is now polarized along a direction forming an angle  $\alpha_0$  with the x-axis, where from equation (2-163)

$$\alpha_0 = \arctan \left[ (-1)^m \left( \frac{C}{B} \right)^{1/2} \right] \quad (2-186)$$

$$\text{and } (-1)^m = \frac{\text{Re}(J_{xy})}{|\text{Re}(J_{xy})|}$$

(See Born and Wolf, 1975, p. 27)

Using the equations (2-173) and (2-174) for B and C:

$$\alpha_0 = \arctan \left[ (-1)^m \left( e^{1/2 \lambda (k_- - k_+)} \right) \right] \quad (2-187)$$

If  $n_+ \neq n_-$ , (which is generally the case), the transmitted light is elliptically polarized and the shape of the ellipse is governed by the factor:

$$\delta = \frac{\omega}{c} (n_- - n_+) \lambda \quad (2-188)$$

The ellipse is inscribed into a rectangle whose sides are parallel to the co-ordinate axes and whose lengths are  $2\sqrt{C}$  and  $2\sqrt{B}$ , (See Fig. 6). The ellipse touches the sides at the points

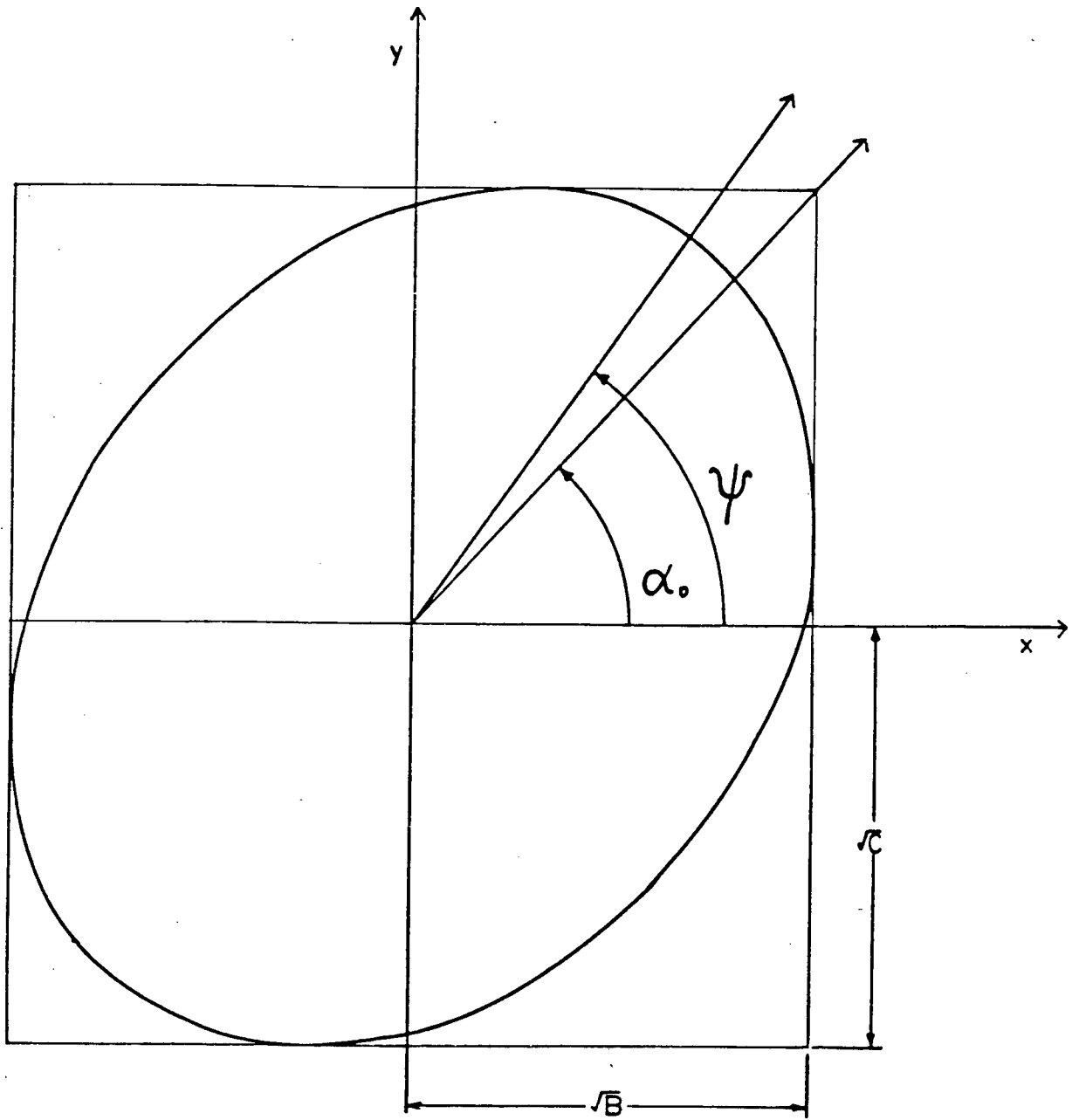


Fig. 6: Geometry of Polarization Ellipse

$$(\pm \sqrt{B}, \pm \sqrt{C} \cos\delta) \text{ and } (\pm \sqrt{B} \cos\delta, \pm \sqrt{C}) \quad (2-189)$$

The angle,  $\psi$ , which the major axis of the ellipse makes with the x-axis is given by the equation

$$\tan 2\psi = (\tan 2\alpha_0) \cos\delta \quad (2-190)$$

Thus, in general, when the incident light is linearly polarized the gas will produce elliptically polarized light, where the shape of the ellipse is a function of the frequency of the light.

The discussion to this point has been facilitated by using a representation which describes the state of polarization of the light at a specific frequency  $\omega$ . This representation is not, however, always the most convenient one. For instance if the state of polarization changes over the width of the incident line ( $\Delta\nu$ ) it is difficult to assess the degree of polarization of the entire line. Furthermore the theoretical results are not compatible with the experimental results since an experiment necessarily measures the intensity over a range of frequencies and not at a definite frequency  $\omega$ . To overcome these difficulties we introduce a slightly modified representation. Instead of considering the intensity at a specific frequency  $\omega$  as in the defining equation (2-154), we observe the intensity taken over the entire frequency range of the line. That is, we are interested in the integral of equation (2-154) over  $\omega$ . Therefore we define

$$I(\psi, \xi) = \int_0^{\infty} I(\psi, \xi; \omega) d\omega \quad (2-191)$$

If only a part of the line is of interest the limits of the integral can be changed accordingly.

In complete analogy with the earlier representation we can define a coherency matrix  $J^\infty$  by the equation

$$I(\psi, x_1) = J_{xx}^\infty \cos^2 \psi + J_{yy}^\infty \sin^2 \psi + (J_{xy}^\infty e^{-i\psi} + J_{yx}^\infty e^{i\psi}) \cos \psi \sin \psi \quad (2-192)$$

and

$$J^\infty = \begin{vmatrix} \int_0^\infty \langle E_x E_x^* \rangle e^{-k_- \ell} d\omega & \int_0^\infty \langle E_x E_y^* \rangle e^{(K_- - K_+^*) \ell} d\omega \\ \int_0^\infty \langle E_y E_x^* \rangle e^{i(K_+ - K_-) \ell} d\omega & \int_0^\infty \langle E_y E_y^* \rangle e^{-k_+ \ell} d\omega \end{vmatrix} \quad (2-193)$$

from which all the remaining parameters can be calculated in the same way as they were in the earlier representation.

Note that the total intensity of the x and y components of the incident line are given by:

$$I_x^0 = \int_0^\infty \langle E_x E_x^* \rangle d\omega \quad \text{and} \quad I_y^0 = \int_0^\infty \langle E_y E_y^* \rangle d\omega \quad (2-194)$$

and the total intensity of the incident line,  $I^0$ , is given by

$$I^0 = I_x^0 + I_y^0 \quad (2-194a)$$

An important consequence of the fact that a real detector measures the intensity over a range of frequencies and not at a single frequency is made

apparent in this representation. For if  $K_+$  and  $K_-$  are not constant over the measured range of frequencies, then, (from matrix 2-193) even if the incident light is completely polarized, the transmitted light is only partially polarized since  $\text{Det } J_{\infty} \neq 0$ . That is, even though the light is completely polarized at any given frequency  $\omega$ , the overall line is found to be only partially polarized when it is measured experimentally.

Consider the situation where the gas acts as a polarizer by absorbing the x component of the incident light. The overall effectiveness of the gas as a polarizer for the entire line can be determined from the degree of polarization  $P_{\infty}$  and the fractional change in the intensity of the polarized

component  $\frac{J_{yy}^{\infty}}{I_y^0}$ . An ideal polarizer would have  $P_{\infty} = 1$  and  $\frac{J_{yy}^{\infty}}{I_y^0} = 1$ . That is

the entire line would be completely polarized and the transmitted y component would be unattenuated. In general it can be assumed that the

smaller  $\frac{J_{yy}^{\infty}}{I_y^0}$ , the greater the distortion of the line shape of the incident

line as a result of traversing the gas. Therefore it is desirable to choose the condition of the gas such that

$$P_{\infty} \rightarrow 1 \text{ and } \frac{J_{yy}^{\infty}}{I_y^0} \rightarrow 1, \text{ which implies } \frac{J_{yy}}{I^0} \rightarrow 1/2$$

To illustrate the ideas presented in this section  $J_{yy}^{\infty}$  and  $J_{xx}^{\infty}$  are calculated as functions of the magnetic field strength for the 253.7 nm line

of mercury using the properties listed in the appendix. The absorbing gas consists of a 3 cm length of  $\text{Hg}^{202}$ . The numerical calculation is performed for a number of gas temperatures, with the gas density determined from the known vapour pressure. For simplicity the incident light is unpolarized and has a Gaussian line profile.

For convenience, the equations used in the numerical calculation are collected below.

From the matrix  $J^\infty$  (2-193)

$$J_{xx}^\infty = \int_0^\infty \langle E_x E_x^* \rangle e^{-k\ell} d\omega, \quad J_{yy}^\infty = \int_0^\infty \langle E_y E_y^* \rangle e^{-k\ell} d\omega \quad \text{dev here } \ell = 3 \text{ cm.}$$

From equations (2-177), (2-173), (2-174) and (2-172);

$$P_\infty = \left[ 1 - \frac{4(J_{xx}^\infty J_{yy}^\infty - J_{xy}^\infty J_{yx}^\infty)}{(J_{xx}^\infty + J_{yy}^\infty)^2} \right]^{1/2} \quad (2-195)$$

But, since the incident light is chosen to be unpolarized, from matrix

(2-180),  $J_{xy}^\infty = J_{yx}^\infty = 0$  and

$$P_\infty = \left| \frac{J_{xx}^\infty - J_{yy}^\infty}{J_{xx}^\infty + J_{yy}^\infty} \right| \quad (2-196)$$

Furthermore, for an unpolarized incident beam, from equations (2-166) and

(2-157)  $\langle E_x E_x^* \rangle = \langle E_y E_y^* \rangle = I_0(\omega)/2$ .

The Gaussian line profile selected for the incident source line is given by:

$$\langle E_x E_x^* \rangle = \frac{1}{2D} \left( \frac{\ln 2}{\pi} \right)^{1/2} \exp \left[ -\ln 2 \left( \frac{\omega - \omega_0}{D} \right)^2 \right] \quad (2-197)$$

where D is the half-width and the profile has been normalized such that from equation (2-194a) the total incident intensity  $I^0$  is equal to 1, i.e.

$$I^0 = \int_{-\infty}^{\infty} 2 \langle E_x E_x^* \rangle d\omega = 1 \quad (2-198)$$

From equations (2-129) and (2-130)

$$k_+ = 4\pi K_0 \frac{\omega}{c} \operatorname{Re} \left[ \frac{1}{2} W(a_1 + ib) + \frac{1}{2} W(a_{-1} + ib) \right], \quad k_- = 4\pi K_0 \frac{\omega}{c} \operatorname{Re} [\omega(a_0 + ib)]$$

where, from equations (2-88) and (2-89)

$$K_0 = \frac{Ncf_a e^{2\pi^{1/2}}}{8\pi\epsilon_0 V_0 m_e \omega_0^2} \text{ in MKSA units or}$$

$$K_0 = \frac{Ncf_a e^{2\pi^{1/2}}}{2V_0 m_e \omega_0^2} \text{ in cgs units and}$$

$N$  = the density of the atoms in the ground state

$c$  = the speed of light

$f_a$  = the absorption oscillator strength (see equation (2-82)).

$e$  = the electron charge

$\epsilon_0$  = the Permittivity of free space

$m_e$  = the electron mass

$\omega_0$  = the resonance frequency of the line (see equation (2-7))

$V_0 = \left(\frac{2K_B T}{M}\right)^{1/2}$  (see equation (2-29)) and

$K_B$  = the Boltzmann constant

$T$  = the temperature in degrees Kelvin

$M$  = the atomic mass.

$W(a_u + ib)$  is the complex error function defined by equation (2-78) and from equations (2-80) and (2-81)

$$a_u = \frac{c}{V_0 \omega_0} \left( \omega - \omega_0 - \frac{\mu_0}{h} g_{j\alpha} B u \right)$$

$$b = \frac{c}{V_0 \omega_0} (1/2) (1 \gamma_{\alpha j}) \text{ where}$$

$\mu_0$  = the Bohr magneton (see equation (2-4))

$g_{j\alpha}$  = the Landé g factor for the state  $\alpha j$ , (see equation (2-6))

$B$  = the magnetic field strength

$\gamma_{\alpha j}$  = the total Lorentz broadening width, (see equation (2-39))

From equation (2-31)

$$\gamma_{\alpha j} = \gamma_N + \gamma_R$$

where  $\gamma_N$  is the natural line width defined by equation (2-18)

$\gamma_R$  is the resonance broadening width.

In the calculation the Ali and Griem expression (2-19) was used.

In Fig. 7,  $J_{yy}^{\infty}$  is plotted as a function of magnetic field strength for three different gas temperatures, 300K, 350K and 375K. Note that  $J_{xx}$  is unaffected by the magnetic field and has a constant value equal to  $J_{yy}$  at zero field. The half width of the source line,  $D$ , is  $25 \cdot 10^{-3} \text{cm}^{-1}$ . Figs. 8 and 9 are the same as Fig. 7 except that the half width of the source line has been increased to  $40 \cdot 10^{-3} \text{cm}^{-1}$  and  $60 \cdot 10^{-3} \text{cm}^{-1}$  respectively.

In the next chapter the polarizing properties of a mercury gas are examined experimentally.

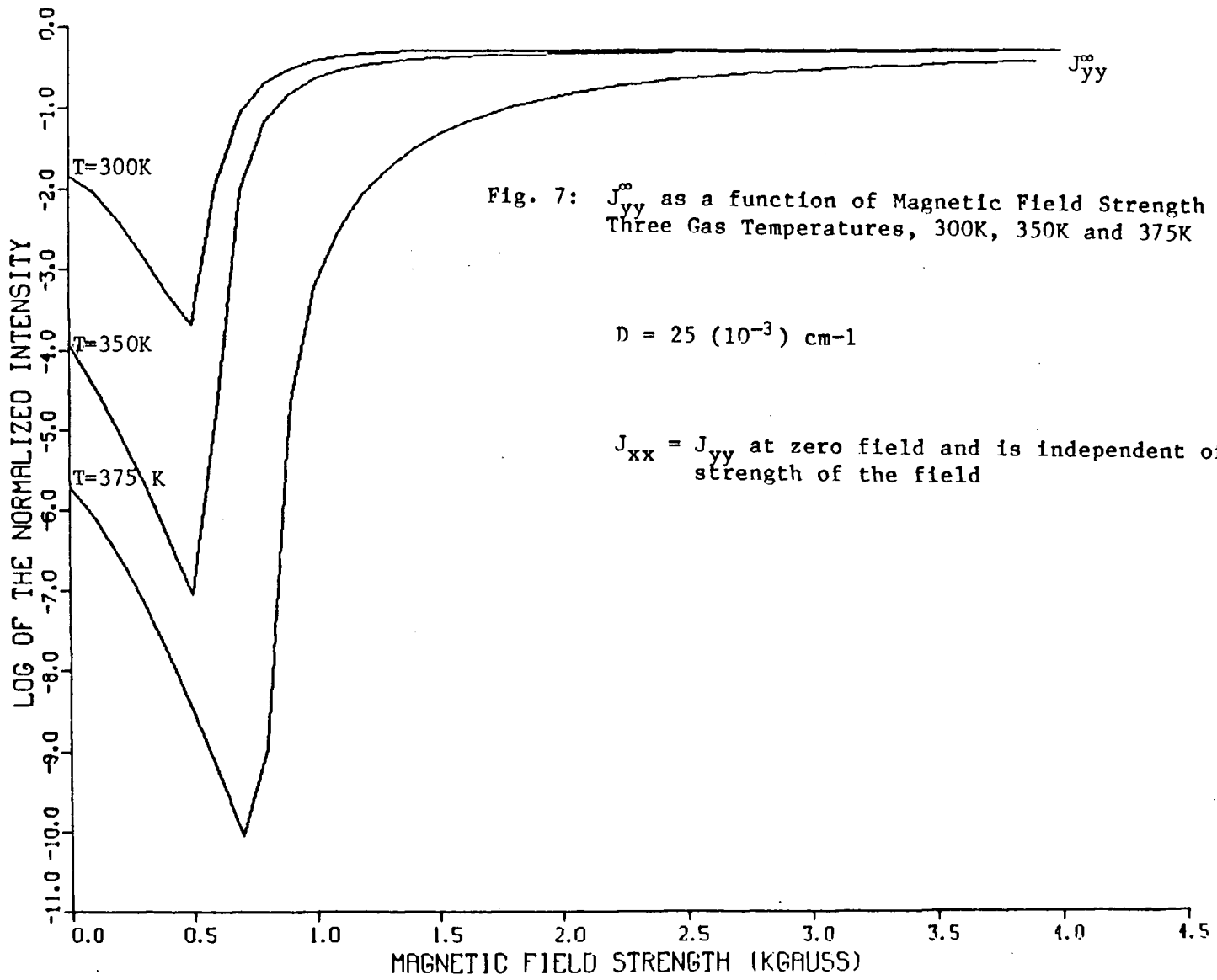
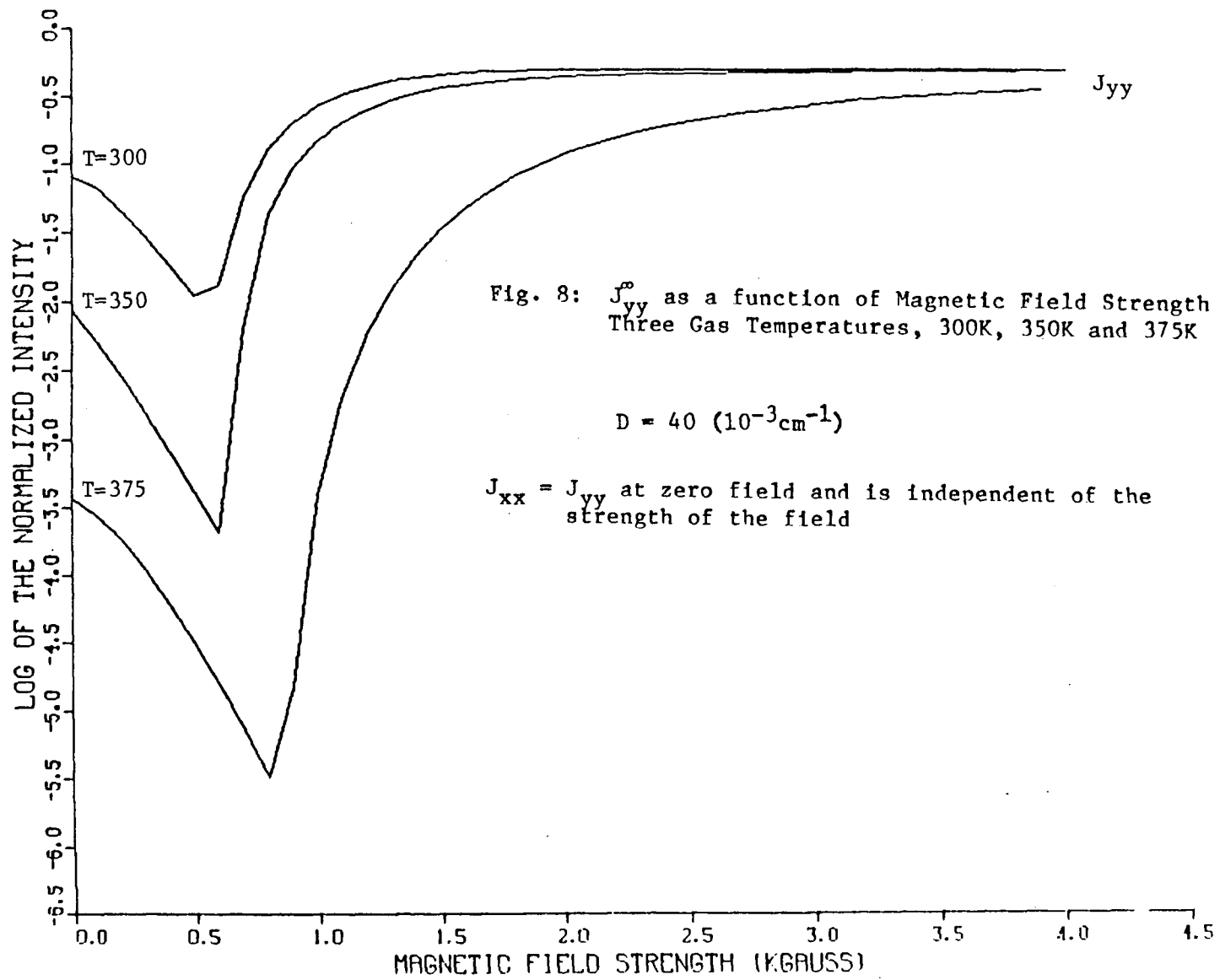
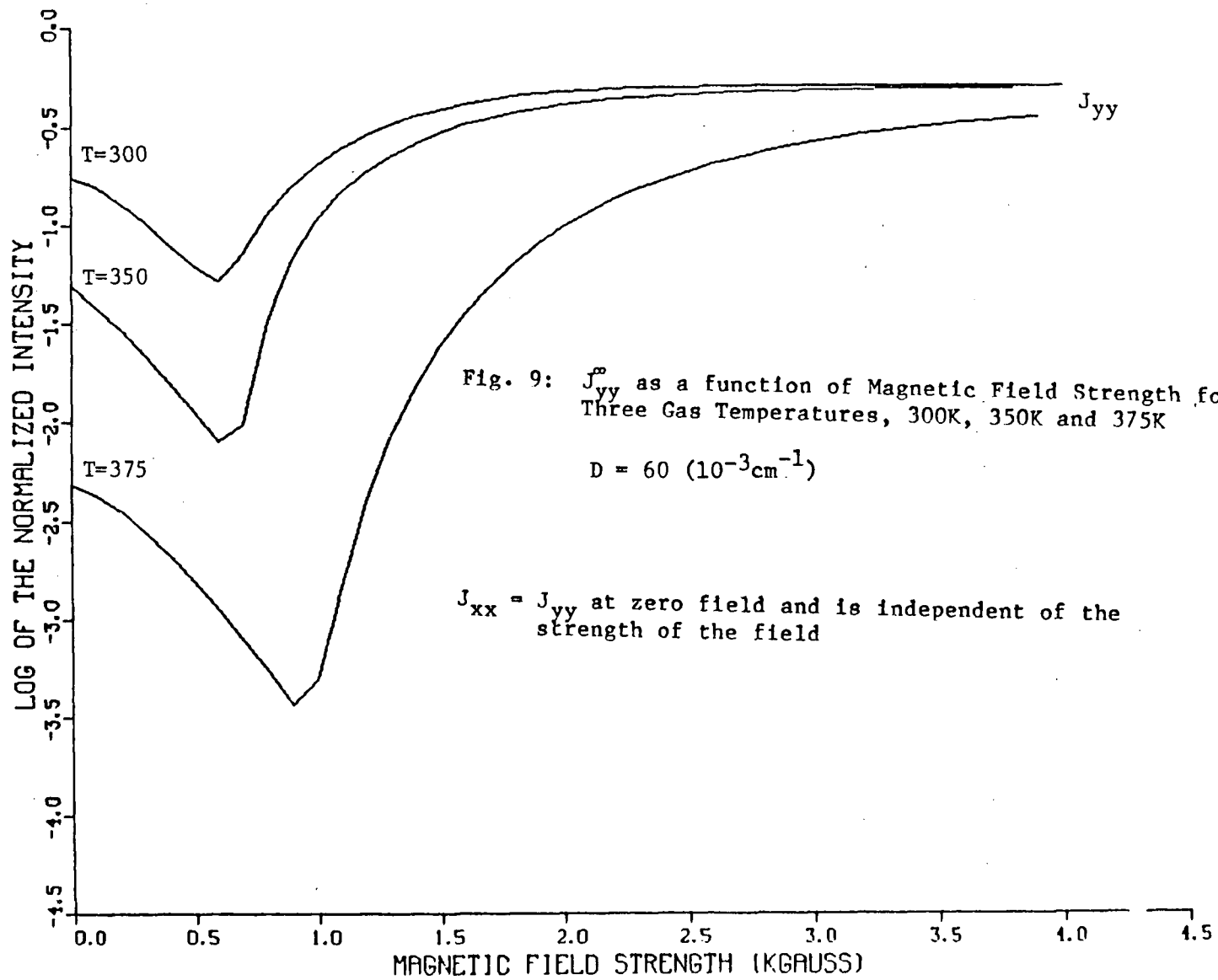


Fig. 7:  $J_{yy}^{\infty}$  as a function of Magnetic Field Strength for Three Gas Temperatures, 300K, 350K and 375K

$D = 25 (10^{-3}) \text{ cm}^{-1}$

$J_{xx} = J_{yy}$  at zero field and is independent of the strength of the field





CHAPTER III

III.I THE EXPERIMENTAL DESIGN

A schematic diagram of the experimental arrangement is given in Fig. 10. The object of the experiment was to determine the state of polarization, or more specifically the coherency matrix  $J^\infty$ , of light corresponding to the 253.7 nm line of mercury after the light traversed a mercury gas cell immersed in a magnetic field.

As is evident from Fig. 10, the experiment closely paralleled the ideal experiment described in the last chapter, and the method for experimentally determining the coherency matrix is indicated by equation (2-192) which defines  $J^\infty$ . Recall:

$$I(\phi, \xi) = J_{xx} \cos^2\phi + J_{yy} \sin^2\phi + (J_{xy} e^{-i\xi} + J_{yx} e^{i\xi}) \sin\phi \cos\phi$$

(where the superscript  $\infty$  has been omitted for convenience).

Measuring the intensity  $I(\phi, \xi)$  for four independent combinations of the variables  $\phi$  and  $\xi$  leads to four independent equations which can be solved for  $J_{xx}$ ,  $J_{yy}$ ,  $J_{yx}$  and  $J_{xy}$ . While there are many acceptable choices of the four combinations of  $\phi$  and  $\xi$ , the following set of measurements was used in the experiment:

- a.) Polarizer along x-axis, thus  $I_1(0,0) = J_{xx}$
- b.) Polarizer along y-axis, thus  $I_2(\pi/2,0) = J_{yy}$  (3-1)
- c.) Polarizer set at  $45^\circ$ , thus  $I_3(\pi/4,0) = 1/2 (J_{xx} + J_{yy}) + \text{Re}(J_{xy})$
- d.) Polarizer set at  $45^\circ$  and quarter-wave plate inserted with fast axis along x-axis, thus  $I_4(\pi/4, \pi/2) = 1/2(J_{xx} + J_{yy}) - \text{Im}(J_{xy})$ .

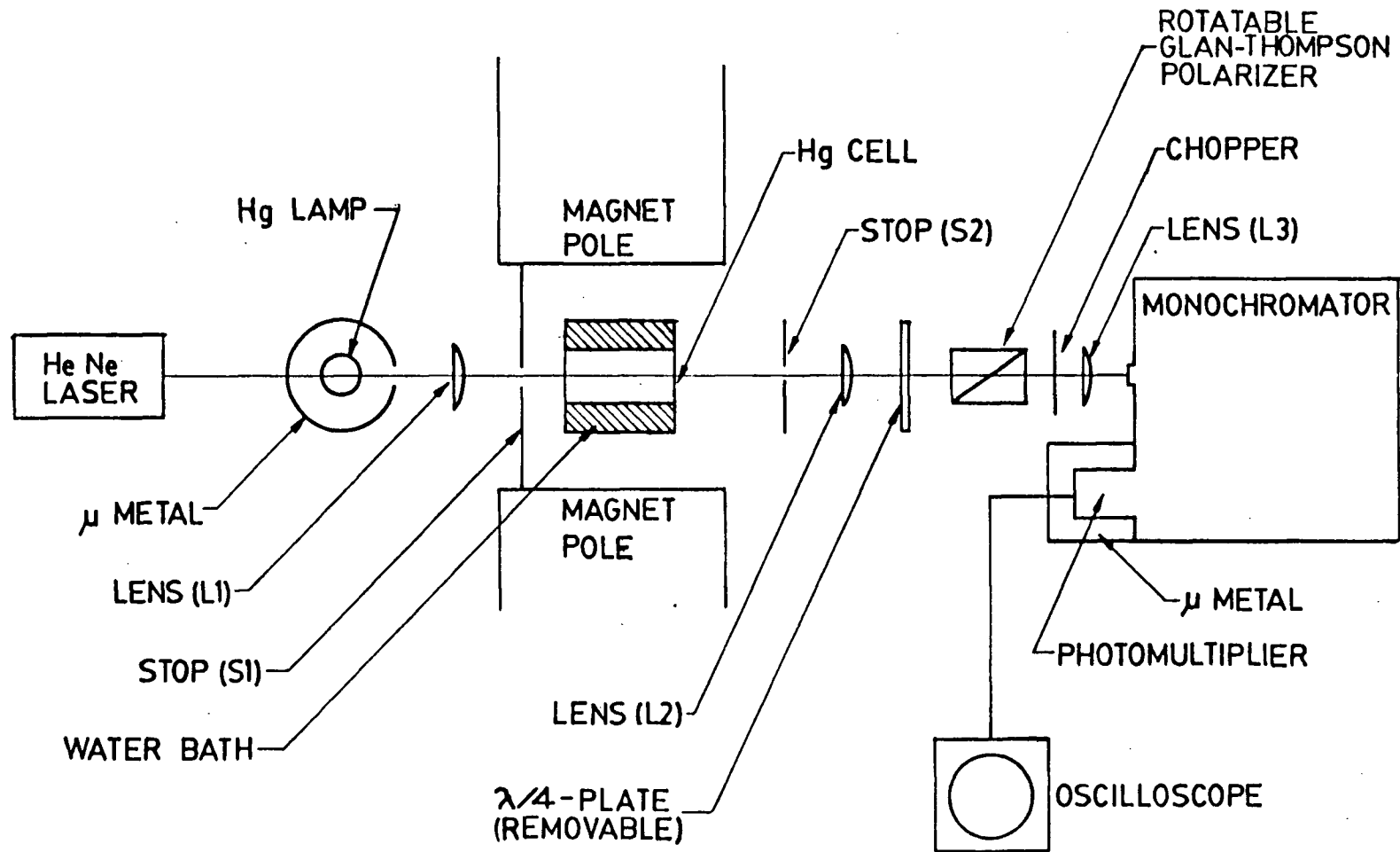


Fig. 10: Experimental Apparatus

These four equations are linearly independent and easily solved for  $J_{xx}$ ,  $J_{yy}$ ,  $\text{Re}(J_{xy})$  and  $\text{Im}(J_{xy})$ , yielding the complete coherence matrix.

The experimental set of x-y axes was arbitrarily selected, hence the experimental x-axis does not necessarily lie along the direction of the magnetic field as in the theoretical description. This is explained in more detail in a later section.

Briefly, the experimental method was as follows. A beam of light propagates through a cell filled with mercury vapour which is immersed in a magnetic field. The magnetic field is transverse to the direction of propagation. The light next traverses the quarter-wave plate and polarizer, which are arranged in one of the four preselected combinations discussed earlier in (3-1). The light then passes through a monochromator which selects the line of interest. Finally the intensity of the entire line is measured by a photomultiplier and an oscilloscope.

### The Light Source

It was essential that the light source used in the experiment produce a stable, intense, unpolarized and reasonably narrow 253.7 nm line. The source most commonly used in experiments of this kind is a microwave excited electrodeless discharge lamp, (see G. Stanzel, 1974). However, the extreme sensitivity of neighboring experiments to microwave radiation precluded its convenient use in this experiment.

Two other light sources were considered; a high voltage mercury discharge tube and a standard low voltage laboratory mercury lamp filled with natural mercury and argon. The lamp was finally selected after a spectroscopic analysis demonstrated that the lamp produced a narrower 253.7 nm line than the tube at the required intensity.

The stability of the 253.7 nm line produced by the lamp was examined by monitoring its intensity over a period of 30 hours. Following an initial warm-up period of two hours, the intensity of the line was found to drift by as much as 30% over the 30 hour period. However, the drift was not constant; there were long periods, typically greater than four hours, during which no measurable change in the intensity was observed. These long period of stability were followed by relatively brief periods, during which changes in the intensity of up to 20% were observed. These periods of instability persisted despite efforts to locate the source of the instability and eliminate it. Ultimately, the experimental procedure was simply adapted to accommodate the instability. This adaptation is described in a later section.

### The Gas Cell

The gas cell was a cylinder, 3.7 cm long and 2.5 cm in diameter, containing a droplet of natural mercury and its vapour. Before the mercury was added, the cell was purged of impurities by heating it as it was evacuated by a high vacuum pump. The cell was equipped with high quality quartz windows which, even under the strain of the partial vacuum, had a negligible effect on the state of polarization of the light.

Since the mercury vapour pressure (and hence the gas density) is highly temperature sensitive, the temperature of the gas cell had to be carefully controlled. This was accomplished by immersing the cell in the temperature regulated water bath sketched in Fig. 11. Water was circulated past the gas cell and into a large dewer vessel which contained a heating coil. An electronic monitoring device was constructed which continuously measured the temperature of the water and automatically switched the heating coil on and off when the temperature reached certain fixed settings above and below the desired temperature. By this means the mercury temperature could be set at any value between 20°C and 30°C with an accuracy of  $\pm 1/2^\circ\text{C}$ . Mercury condensation on the windows of the cell excluded temperatures greater than 30°C.

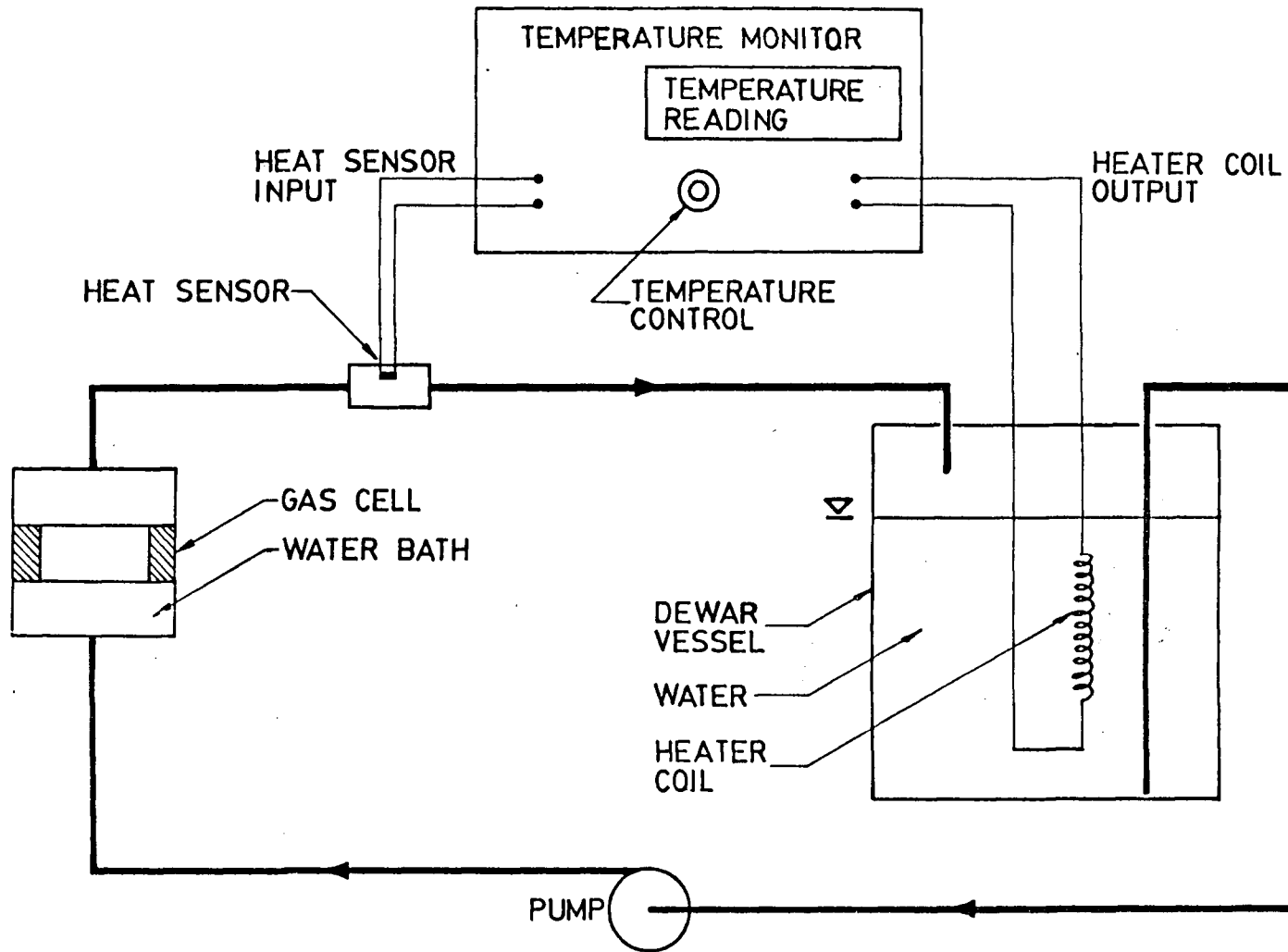


Fig. 11: Temperature Regulator for the Water Bath

### The Magnet

The electro-magnet and its current supply were manufactured by Varian Associates for use in Nuclear Magnetic Resonance studies and thus provided a very stable and homogeneous magnetic field. Measurements of the uniformity of the field, using an Incremental Gaussmeter Hall Probe, showed that the field never varied by more than .3% over the length of the cell.

The magnetic field was calibrated using both a Rotating Coil Gaussmeter with a rated accuracy of .1%, (at the calibrated field strength of 25 KG) and an Incremental Gaussmeter Hall Probe. To ensure a consistent result the field was adjusted, both during the calibration and the actual experiment, by first setting the current at a large preselected value and then lowering the current to the largest of the current settings to be used in the calibration. The current was then lowered sequentially through the pre-determined current settings which were used both for the calibration and the experiment. In this way variations due to hysteresis were reduced. The two sets of measurements were found to be consistent to about 1% over the complete range of experimental field strengths. When no current flowed in the magnet a residual field of  $90 \pm 1G$  was found to persist.

### The Aperture Stops and Lenses

The first aperture stop, ( $S_1$  in Fig. 10) encountered by the light served only to define a sufficiently narrow light beam to prevent light from being reflected into the detector from the walls of the gas cell or the poles of the magnet. The second aperture stop ( $S_2$ ) limited the beam to a total divergence of less than  $.75^\circ$ .

The three lenses  $L_1$ ,  $L_2$  and  $L_3$  (see Fig. 10) were all made of quartz. The purpose of  $L_1$  was to concentrate the light emitted from the lamp into a narrow and intense beam, hence a lens with as small a focal length as possible was selected. The lens  $L_2$  collimated the beam before it passed through the polarizer and the quarter-wave plate and thus permitted the diameter of the second stop to be made as large or larger than the face of the polarizer, which in turn greatly increased the intensity of the light reaching the monochromator. The lens  $L_3$  was used to focus the beam on the entrance slit of the monochromator. The focal length of  $L_3$  was such that the f-number of the lens was only slightly larger than the f-number of the monochromator. Thus effectively all of the monochromator's grating was used and the dispersion of the instrument approached its rated value.

### Polarizer and Quarter-Wave Plate

A Glan-Thompson polarizer, with a transmissivity of about 40% for a wavelength of 253.7 nm, was used in the experiment. The polarizer could be set at any angle in the plane normal to the optical axis with an accuracy of better than 1°.

The quarter-wave plate was designed specifically for use at the 253.7 nm wavelength. The plate was a true quarter-wave plate in the sense that the relative phase shift between the two components was  $\pi/2$  and not  $\pi/2 + m 2\pi$  where  $m = 1, 2, 3, \dots$ . This property was necessary to ensure that the relative phase shift never exceeded the finite coherence length of the light, which in turn ensured that the coherence length did not manifest itself in the experimental measurements.

Most of the intensity measurements required only the polarizer and not the quarter-wave plate. Therefore the quarter-wave plate was fixed to a pivoting mount which enabled it to be moved in and out of the light beam without realignment. Measurements taken with and without the quarter-wave plate were made compatible by determining the attenuation of the light by the quarter-wave plate. It was found that the intensity of the light was diminished by a factor of 1/1.14, regardless of the angle of the quarter-wave plate's fast axis. Thus all measurements taken with the quarter-wave plate in place were multiplied by the factor 1.14 before being combined with the measurements taken without the quarter-wave plate.

### Monochromator

The monochromator was a Spex 1800, with a rated dispersion of  $10\text{\AA}/\text{mm}$ . in the first order. The 253.7 nm line was observed in the 3rd order with the entrance slit set at  $140\ \mu\text{m}$  and the exit slit set at  $500\ \mu\text{m}$  to maximize the intensity. This resulted in a bandpass of about  $1.7\text{\AA}$  which was sufficient to exclude all other detectable lines emitted by the source.

### Detector

The intensity of the line, isolated by the monochromator, was measured by observing the oscilloscope trace of the output of a photomultiplier placed at the monochromator's exit slit. To reduce noise the light was chopped to give a series of 2 msec. pulses. Shorter pulse lengths were necessarily excluded by the long observed rise time of the oscilloscope trace.

The linearity of the detector system was tested using a series of neutral density filters to produce a range of intensities encompassing the range found in the experiment. A least squares fit to a straight line was performed on the data with a resulting linear-correlation coefficient of  $r = .998$  for the 14 data points, (see Bevington, 1969). This high degree of linearity allowed the height of the oscilloscope trace to be taken as

directly proportional to the intensity over the intensity range of interest.

#### Effect of the Magnetic Field on the Experimental Apparatus

To minimize the effect of the magnetic field on the light source and the photomultiplier, each of these devices was surrounded by a  $\mu$ -metal shield. The magnetic field strength inside the  $\mu$ -metal shield of the light source was measured using an Incremental Gaussmeter Hall Probe. It was found that the field was as always less than .7% of the field at the centre of the magnet poles, which, even for the largest fields used in the experiment, would lead to a negligible Zeeman Splitting of the source lines.

The effect of the field on the remainder of the system was tested by removing the absorption cell and monitoring the intensity as the magnetic field was increased. Even with fields up to 4 KGauss there was no detectable change in the intensity.

### III.2 THE EXPERIMENTAL PROCEDURE

The He-Ne alignment laser was positioned to define an optical axis parallel to the surfaces of the poles of the magnet and through the centre of the gap between the poles. All of the optical instruments, including the light source and the entrance slit to the monochromator, were initially centred on the optical axis using the alignment laser. The lens  $L_1$  and the light source were placed on moveable mounts allowing the light source to be moved across the optical axis and the lens  $L_1$  to be moved along the axis. These two devices were adjusted until the focal point of  $L_1$  was positioned on a region of excited gas in the lamp which produced the most intense 253.7 nm.

The lens  $L_3$  was placed on a moveable mount which enabled it to be manoeuvred to the point in the plane normal to the optical axis which gave the maximum intensity. It was found that when the angle of the polarizer was changed, the position of  $L_3$  which gave the maximum intensity also changed due to a deflection of the beam by the polarizer. Although this effect could be significantly reduced by carefully positioning the polarizer in its mount, it could not be completely eliminated. Thus whenever the polarizer was rotated the lens  $L_3$  was repositioned to give the maximum intensity.

In general a monochromator polarizes the light which it disperses. This property of the monochromator was studied because in the course of the experiment it was necessary to send light polarized at different angles into

the monochromator and the measured intensity of this light would be affected if the monochromator acted as a polarizer.

To examine the effect, the absorption cell was removed so that only the unpolarized light from the source was incident on the polarizer. The polarizer was sequentially rotated through  $180^\circ$  while the max. intensity of the 253.7 nm line was measured. It was found that the max. intensity was unaffected by the angle of the polarizer. This result was greeted with some scepticism and the measurements were repeated for the 763.5 nm line of argon. In this case the intensity varied by a factor of more than four over the  $180^\circ$  rotation. Since the polarizing effect of a monochromator is known to be highly frequency dependent, with frequencies where there is no polarizing effect, (see K. Rabinovitch et al., 1965 and G.W. Stroke, 1963), the result for the 253.7 nm line was regarded as one of those rare instances in experimental physics where nature conspires to lessen the work of the experimenter.

The x-y axes of the polarizer were selected arbitrarily rather than setting the x-axis along the field as in the theoretical analysis. This was done because the only method available for aligning the axes was to find the polarizer angles which produced the maximum and minimum intensity for light polarized by the gas cell in the magnetic field, and this could only be done to an accuracy of a few degrees. It was felt that rather than introducing this further source of error it was simpler and more precise to calculate the maximum and minimum intensity from equation (2-192) using the J obtained from the arbitrary set of axes.

The experiment required the quarter-wave plate, when in place, to be oriented such that its fast axis was parallel to the designated x-axis of the polarizer. The most sensitive method found for accomplishing this was as follows. Another Glan-Thompson polarizer ( $P_2$ ) was placed along the optical axis just past the second aperture stop. With the monochromator set for the intense line of the He-Ne laser, and the quarter-wave plate positioned out of the laser beam, the polarizer  $P_1$  in Fig. 10 was rotated until the measured intensity was minimized, i.e. the polarizers were crossed. This position of the polarizer  $P_1$  was henceforth designated as the x-axis. The quarter-wave plate was then swung into position between the two polarizers, and rotated in the plane normal to the optical axis until the measured intensity was again a minimum. This could only occur if the fast and slow axes were aligned with the pass directions of the two polarizers. It was found that using this method the quarter-wave plate axes could be positioned along the x-y axes of the polarizer  $P_1$  to within  $1^\circ$ .

Of course this method cannot distinguish between the situation where the fast axis is along the x-axis and the situation where the slow axis is along the x-axis. Returning to the equations (3-1) it is evident that the only effect of this uncertainty is to leave the sign of  $\text{Im}J_{xy}$ , or equivalently the handedness of the elliptical wave in doubt. It was felt that this was of little importance and no attempt was made to distinguish between the fast and slow axes of the quarter-wave plate.

As a check on the experimental technique a mock experiment was performed using the Glan-Thompson polarizer  $P_2$  which was known to produce

highly linearly polarized light. With no current flowing in the magnet, the polarizer  $P_2$  was placed between the poles of the magnet while the gas cell was placed between the second aperture stop  $S_2$  and the lens  $L_2$ . To be certain that the residual field of the magnet would not affect the Hg gas, the cell was surrounded by a  $\mu$ -metal shield. With this arrangement the complete set of measurements (3-1) was taken. It was found after analyzing the data that  $P_\infty = 1.00 \pm .03$  and

$$J_{xy} = -.02 \pm .13$$

(an explanation of the error estimates is given later). Thus to within the accuracy of the experiment the light was found to be completely linearly polarized. This result indicated not only that the experimental system was performing as expected, but also that any depolarization of the light, by the gas or intervening optics, was entirely negligible.

The actual experiment was performed with the instruments positioned as in Fig. 10. The initially unpolarized light from the source passed through the gas cell, which was held at a constant temperature and immersed in a uniform magnetic field of known strength. With the polarizer along the x-axis as in (3-1a) and the lens  $L_3$  positioned for maximum intensity, the height of the oscilloscope trace corresponding to the transmitted intensity of the 253.7 nm line was recorded. The current in the magnet was then lowered to the next setting at which the magnetic field had previously been measured and the intensity was again measured. After a representative set of measurements had been taken covering fields from about 250 G to 3500 G, the polarizer and the quarter-wave plate were set at the next combination

described by (3-1) and the process was repeated for the same magnetic field settings. This was done for the four combinations described by (3-1). The complete set of measurements provided all of the information necessary for determining  $J$  as a function of field strength at a given temperature. The problems created by the unstable light source are considered below.

#### The Unstable Light Source

The instability of the light source affected the experimental procedure in a number of ways. First, in order to reduce the probability of a period of instability occurring during the taking of a given set of measurements, the number of measurements in the set had to be limited to permit the complete set to be taken in about 3 hours. Second, at the beginning, the end and periodically during the course of the experiment, the intensity of the light at a fixed setting was measured to ensure that the intensity of the source had remained constant throughout the set of measurements. When a measurable change in this intensity was observed the complete set of measurements was rejected.

Finally, it might appear that because the magnetic field settings were not exactly reproducible, greater precision would result if all four measurements (3-1) were taken before the field strength was changed. However, because a significant period of time was required to reset the polarizer and the quarter-wave plate and to realign  $L_3$ , the time necessary

to complete a set of measurements would be greatly increased if this approach were adopted and the instability in the intensity of the source would begin to influence the results, thereby negating any gain in precision.

In addition to the experiment using an unpolarized light source, an attempt was made to study the effect of the gas on a linearly polarized incident light beam produced by inserting the polarizer  $P_2$  in front of the gas cell. Unfortunately, this attempt was unsuccessful because the polarizer  $P_2$  had a low transmissivity and with the intensity of the light further diminished by the polarizing properties of the gas cell the resulting intensity was too weak to provide a meaningful intensity measurement.

### III.3 EXPERIMENTAL ERROR

The experimental intensity measurements could not, of course, be made with absolute precision. Experimental error was introduced into the measurements principally from three sources. First, there was error in reading the height of the oscilloscope trace, in part because of the inherent imprecision of such a reading, but primarily because the background noise of the photomultiplier caused the height of the trace to fluctuate. Second, the repositioning of the equipment between each of the four series of measurements described by equations (3-1) unavoidably perturbed the alignment of the equipment. Finally, because of the effects of hysteresis, the same electromagnet current settings may not have produced precisely the same magnetic field strengths for each of the four measurements (3-1).

It is difficult to determine directly the impact of each of these factors on the magnitude of the error in the intensity measurements. In general, the best estimate of the experimental error would be obtained by repeating the complete set of measurements until a statistically meaningful sample is collected, from which the standard deviation in the intensity at each point could be calculated. This approach was, however, unworkable in this experiment because the time required to collect a large sample would greatly exceed the time period during which the light source remained reasonably stable. If the only consequence of the lamp's instability was a drift in intensity it would have been possible to renormalize the results

before comparing them. However, the observed change in the lamp's intensity was accompanied by a change in the line shape of the source. This produced a variation in the measurements which was unrelated to the actual imprecision of the experimental technique. Thus, to achieve a better estimate of the actual error in the experimental measurements an alternative approach was adopted. Instead of taking a large number of measurements at each magnetic field setting, a large number of measurements was taken at only a small but representative group of field settings. Unlike the complete set of measurements, these measurements could be taken in a sufficiently short period of time to avoid the consequences of the changing intensity and line shape of the source. Thus, the standard deviation in the intensity measurement at each of these representative settings can be taken as truly indicative of the magnitude of the error in the experimental measurements.

When the standard deviation in the intensity measurements was calculated it was found not to be simply proportional to the intensity of the light. It was instead found to be virtually constant for measurements taken at the same oscilloscope voltage scale setting, even when the height of the trace varied considerably. However, the standard deviation was found generally to increase when the voltage scale setting was decreased (in order to observe less intense signals). This result suggests that the principal cause of error in the measurements was the inherent imprecision in determining the height of the oscilloscope trace against the background

noise, since the noise becomes more pronounced as progressively lower scale settings are used.

Since the magnitude of the error remained reasonably constant for a given voltage scale setting, it was possible to provide a reasonable estimate of the error in the intensity by ascribing the same absolute error  $\sigma_i$  to all measurements taken at the same scale setting, (the subscript  $i$  identifies the intensity measurement associated with the error  $\sigma_i$ ). It was this ascribed error which was used in all subsequent calculations involving the experimentally measured intensities.

The error in the intensity measurements  $\sigma_i$ , leads to an error in all of the quantities, such as  $P$ ,  $J_{xx}$ , and  $J_{yy}$ , that are calculated from the measured intensities. In general, each of these quantities is a function of the four measured intensities given in equations (3-1) and therefore may be represented by:

$$f(I_1, I_2, I_3, I_4) = f(I_i) \quad (3-2)$$

Since there is no correlation in the errors  $\sigma_i$  associated with each intensity measurement  $I_i$ , the error in the experimentally determined quantity  $\sigma_f$  is given by:

$$\sigma_f^2 = \sum_{i=1}^4 \sigma_i^2 \left( \frac{\partial f(I_1, I_2, I_3, I_4)}{\partial I_i} \right)^2 \quad (3-3)$$

(See Bevington, 1969, p. 58.)

The error in each experimentally determined quantity presented in the next section was found from this equation.

### III.4 EXPERIMENTAL RESULTS

In this section the experimental results are presented in a form which permits a direct comparison with the theoretical results.

The experimental coherency matrix  $J$ , as initially determined from the equations (3-1), can not be directly compared to the theoretical coherency matrix because the experimental  $x$ -axis is not along the direction of the magnetic field. However, the two matrices can be made compatible by performing a transformation from the experimental  $(x,y)$  axes to a new set of axes  $(x',y')$ . The  $x'$  axis is aligned with the direction of the magnetic field, and forms an angle  $\phi$  with respect to the  $x$ -axis. The coherency matrix  $J$  transforms under this rotation into the matrix  $J'$  which is readily expressed in terms of the matrix elements of  $J$  and the angle  $\phi$ , (see Born and Wolf, 1975, P. 548).

$$\begin{array}{rcl}
 J_{xx}C^2 + J_{yy}S^2 + (J_{xy} + J_{yx})CS & (J_{yy} - J_{xx})CS + J_{xy}C^2 - J_{yx}S^2 & \\
 (J_{yy} - J_{xx})CS + J_{yx}C^2 - J_{xy}S^2 & J_{xx}S^2 + J_{yy}C^2 - (J_{xy} + J_{yx})CS & (3-4)
 \end{array}$$

where  $C = \cos \phi$                        $S = \sin \phi$

The elements of  $J'$  are directly comparable to the theoretical coherency matrix once the angle  $\phi$  is determined.

The angle  $\phi$  may be determined by noting that when the incident light is unpolarized and the  $x'$ -axis is aligned with the magnetic field the theory requires the coherency matrix of the transmitted light to be of the form (see equation 2-180)

$$\begin{vmatrix} J'_{xx} & 0 \\ 0 & J'_{yy} \end{vmatrix} \quad (3-5)$$

That is, the transmitted light may only consist of an unpolarized component and/or a linearly polarized component with the direction of polarization along either the  $x'$  or  $y'$  axis. Thus, the angle  $\phi$  may be found from the matrix (3-4) by setting  $J'_{xy} = J'_{yx} = 0$  and solving the two equations for  $\phi$ . When this is done it is found that:

$$\phi = \arctan \left( \frac{C}{B} \right)^{1/2} \quad \text{or} \quad \phi + \pi/2 = \arctan \left( \frac{C}{B} \right)^{1/2} \quad (3-6)$$

where B and C are calculated from the experimental intensity measurements, (with unpolarized incident light) using the equations (3-1), (2-173) and (2-174). A choice can be made between the two possible solutions by comparing them with the observed orientation of the experimental  $x$ -axis with respect to the magnetic field.

The foregoing method for determining  $\phi$ , (and hence  $J'$ ) is of course only valid if the transmitted light is found to consist entirely of an unpolarized component and/or a linearly polarized component as predicted by the theoretical analysis. For, if the transmitted light is found to contain an elliptically polarized component, that is if  $\text{Im}(J_{xy}) \neq 0$ , then from the matrix (3-4)  $J'_{xy} \neq 0$  for all  $\phi$  and the method is inapplicable. Thus, before the suggested technique for finding  $\phi$  can be used, the theoretical prediction that  $\text{Im}(J_{xy}) = 0$ , (for unpolarized incident light), must be experimentally verified. To this end,  $\text{Im}(J_{xy})$  was calculated at each magnetic field setting using the experimental intensity measurements and the equations (3-1) and (3-3). The result for a gas at 22.6°C is plotted in Fig. 12.

It is evident from Fig. 12 that  $\text{Im}(J_{xy})$  is zero at each magnetic field setting to within experimental error. However, it is also evident that the average value of  $\text{Im}(J_{xy})$  is not zero. In fact if  $J_{xy}$  is averaged over all field settings, it is found to be:

$$-8.8 \times 10^{-2} \pm 1.7 \times 10^{-2}$$

Thus, it would appear that there is a small elliptical component in the transmitted wave. This small component can, however, be completely accounted for by the systematic error which is introduced when, in calculating  $\text{Im}(J_{xy})$ , the measurement  $I_4$  [see equations (3-1)] is multiplied by the constant factor  $G = 1.14$  in order to compensate for the attenuation of the light by the quarter-wave plate. The error  $\sigma_G$  in determining  $G$  is  $\pm 0.04$  and, using equation (3-3), this produces a systematic error in

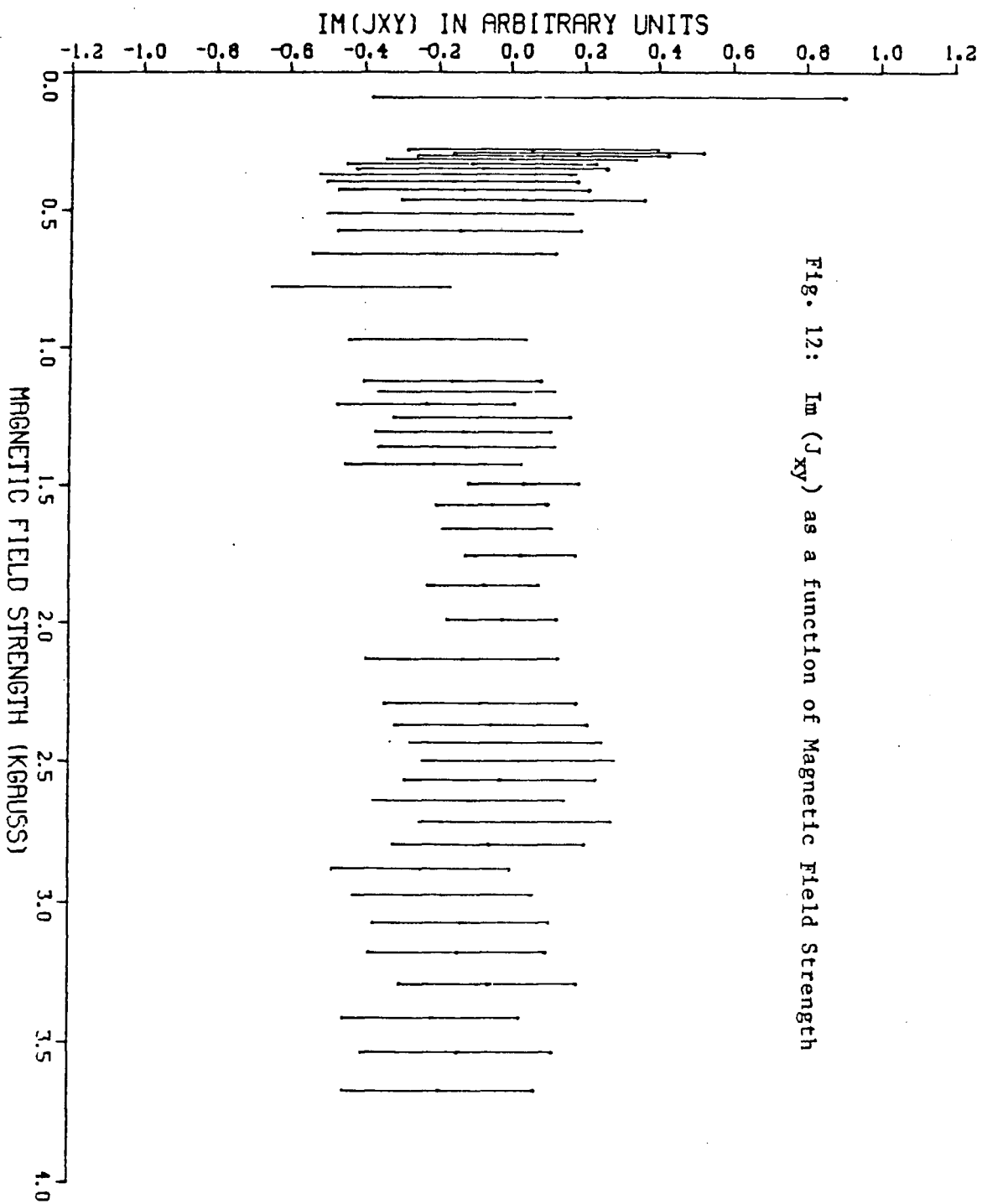


Fig. 12:  $\text{Im}(J_{xy})$  as a function of Magnetic Field Strength

$\text{Im}(J_{xy})$  of about 0.12 for a typical value of  $I_u$ . Thus, the apparent elliptical component can be attributed entirely to this systematic error and the theoretical prediction that  $\text{Im}(J_{xy}) = 0$  for all field strengths is verified to within experimental error. This result justifies using equations (3-6) to determine  $\phi$  in the experiment. The average value of  $\phi$  was found to be

$$86.2^\circ \pm 0.8^\circ$$

For the purposes of comparing the experimental results with the theoretical results the quantities of primary interest, (when considering unpolarized incident light), are  $J'_{xx}$ ,  $J'_{yy}$  and the degree of polarization  $P$ , (where again the superscript  $\infty$  has been omitted from  $P^\infty$ ). These quantities were determined from the experimental measurements in the following ways.

The degree of polarization  $P$ , is independent of the choice of  $x, y$  axes and therefore was simply determined from the elements of the experimental coherency matrix  $J$ , which were in turn determined from equations (3-1).

From equation (2-195):

$$P = \left[ 1 - \frac{4(J_{xx}J_{yy} - J_{xy}J_{yx})}{(J_{xx} + J_{yy})^2} \right]^{1/2}$$

$J'_{xx}$  and  $J'_{yy}$  can be calculated from the matrix (3-5) by simple substitution, once the angle  $\phi$  and the matrix  $J$  have been determined. Instead, however,  $J'_{xx}$  and  $J'_{yy}$  were calculated using a set of equations in

which the values of  $J'_{xx}$  and  $J'_{yy}$  are not directly dependent upon the calculated value of  $\phi$ . This set of equations is again based on the fact that  $\text{Im}(J'_{xy}) = 0$  at all field strengths which implies that  $J'_{xy} = J'_{yx} = 0$ . By further noting that the trace and the determinant of the matrix  $J'$  are invariant under rotational transformations the desired set of equations can be readily derived from the matrix  $J'$ .

$$J'_{xx} = (J_{xx} + J_{yy}) - A \quad \text{and} \quad J'_{yy} = A$$

when

(3-7)

$$C' = 0 \quad \text{and} \quad B' \neq 0$$

and that:

$$J'_{xx} = A \quad \text{and} \quad J'_{yy} = (J_{xx} + J_{yy}) - A$$

when

$$B' = 0 \quad \text{and} \quad C' \neq 0$$

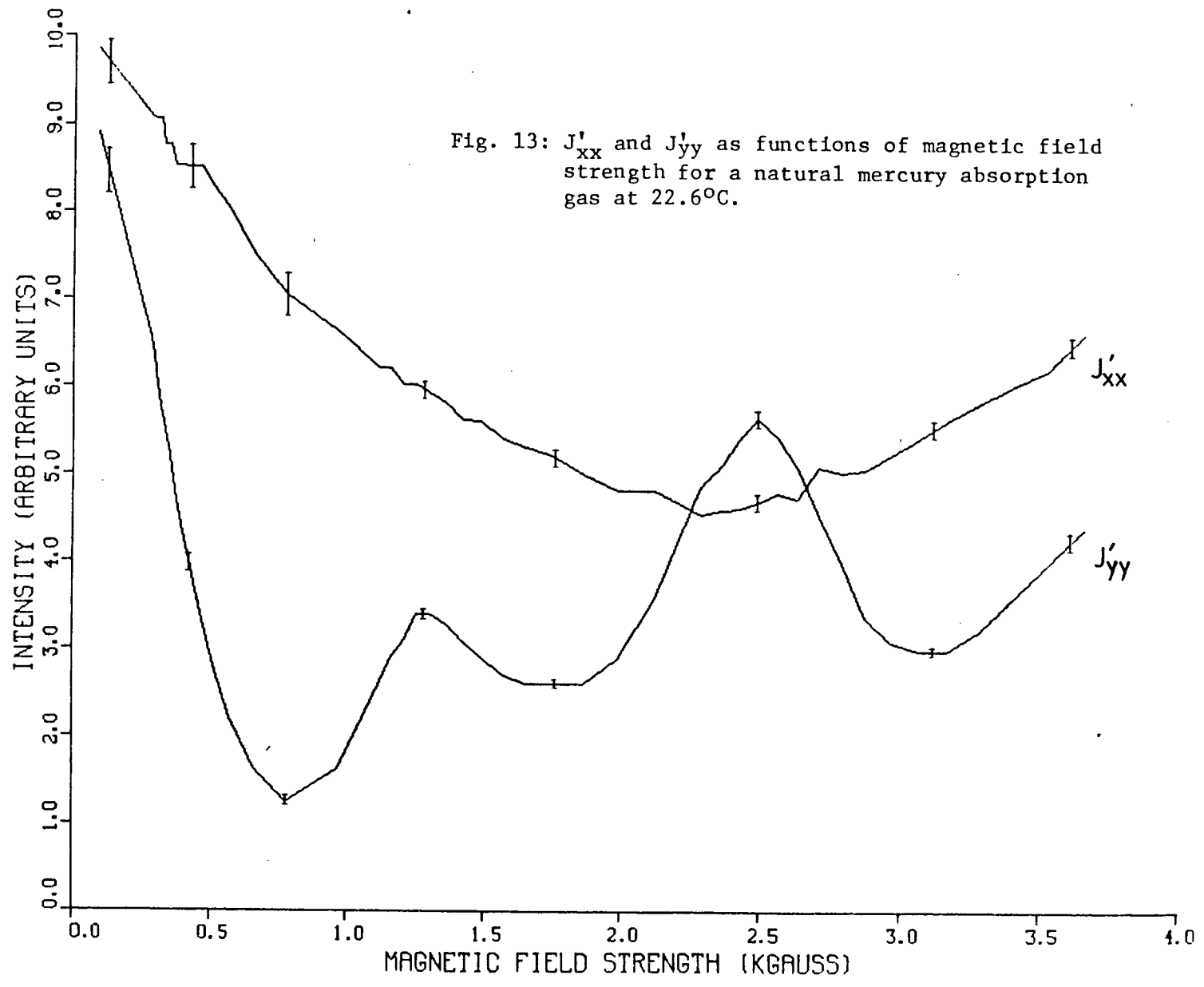
where

A is given by equation (2-172) and B' and C' are found from equations (1-173) and (2-174) and the matrix J' which is found from the calculated values of  $\phi$  and J.

It is clear from these equations that the error in determining  $\phi$  only affects the precision with which B' and C' are determined and these values are only used to choose between the two possible solutions for  $J'_{xx}$  and  $J'_{yy}$ . Thus, when equations (3-7) were used to calculate the experimental values of  $J'_{xx}$  and  $J'_{yy}$ , the uncertainty in  $J'_{xx}$  and  $J'_{yy}$  was not affected by the uncertainty in determining  $\phi$ .

The experimental values of  $J_{xx}'$ ,  $J_{yy}'$  and  $P$  for the two gas temperatures of 22.6°C and 30°C are plotted in Fig. 13, 14, and 15.

In the next chapter the theoretical and experimental results are compared.



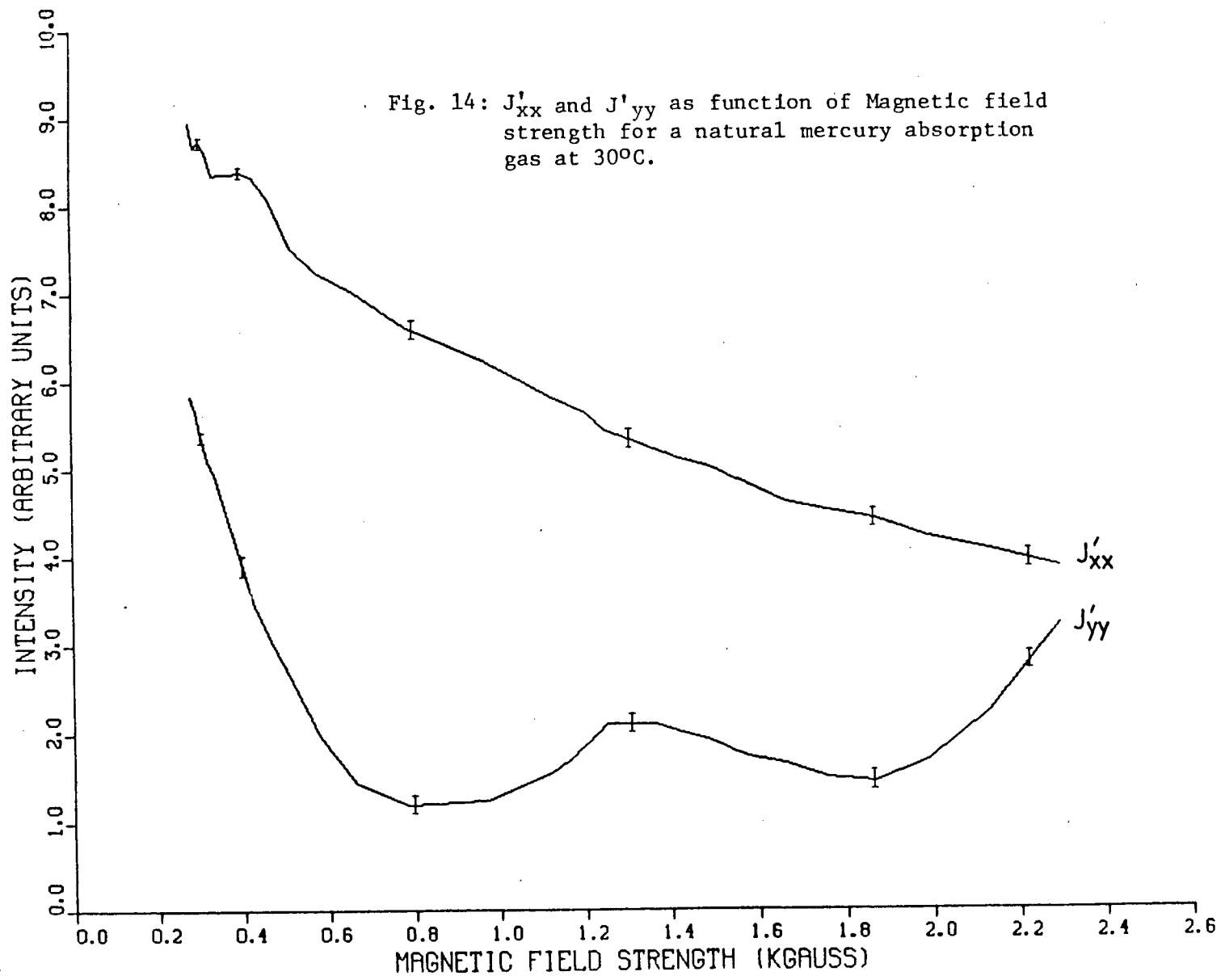
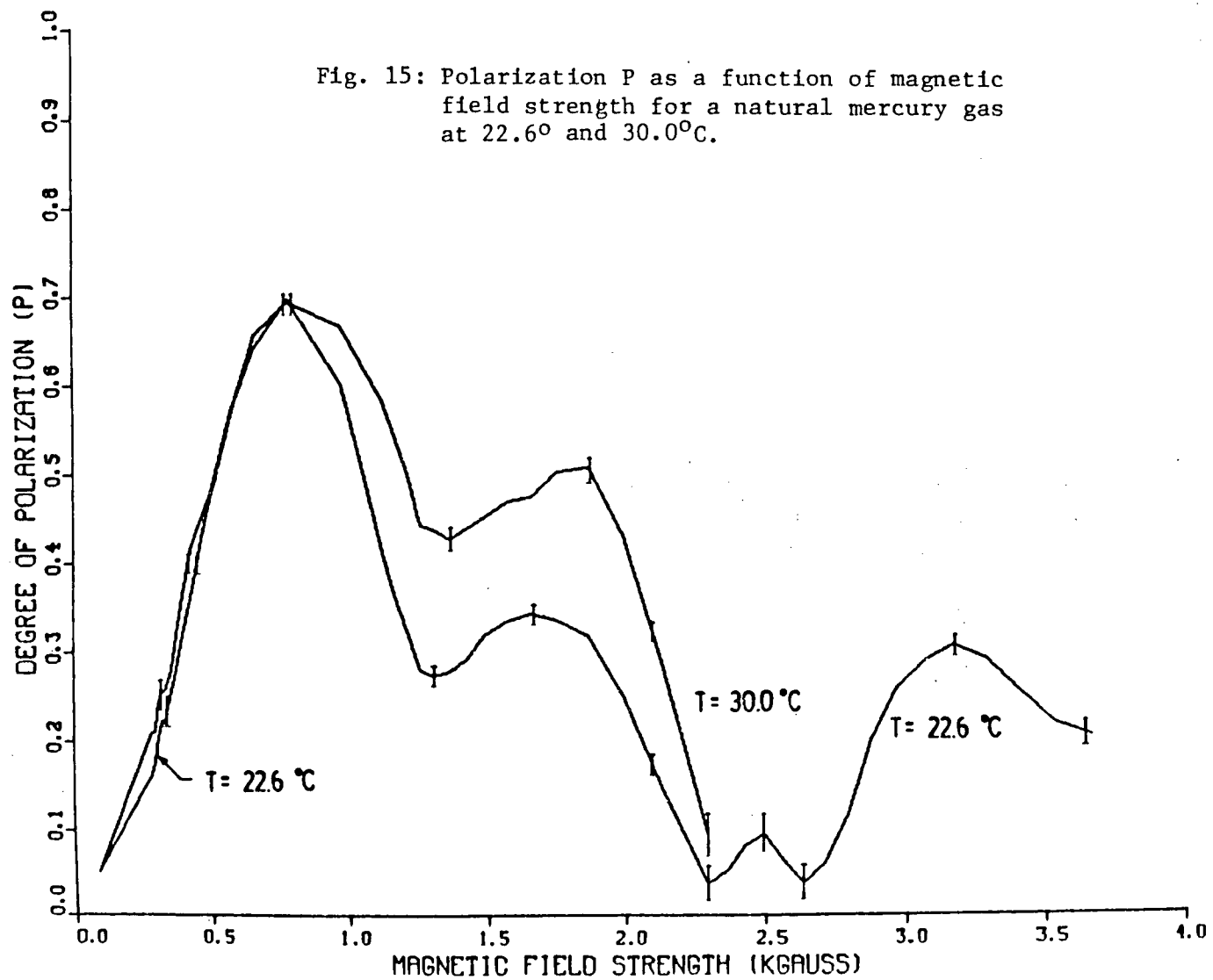


Fig. 15: Polarization P as a function of magnetic field strength for a natural mercury gas at 22.6° and 30.0°C.



CHAPTER IV

COMPARING THEORY AND EXPERIMENT

When the experimental curves of  $J'_{xx}$ ,  $J'_{yy}$  and P, (given in Figs. 13, 14, 15) are compared with the theoretical curves for  $J^{\infty}_{xx}$ , and  $J^{\infty}_{yy}$  and (given in Figs. 7, 8, and 9) it is evident that there are significant differences between the two. This result is, however, not unexpected since certain characteristics of the experiment do not accord with certain assumptions made in calculating the theoretical curves. In particular, the theoretical calculations were carried out using the properties of the single, even isotope of mercury,  $Hg^{202}$ , (with nuclear spin  $I = 0$ ), while the experiment was performed using natural mercury which consists of 7 isotopes, each of which has a unique spectrum. Furthermore, while the theoretical curves were based on an incident source line with a gaussian line profile, the experimental source line had a much more complex shape.

In principal it is possible to carry out the theoretical calculation using the properties of natural mercury and an incident line profile matching the experimental source line. However, in practice this complex calculation can only be performed with limited precision and no attempt was made in this study to perform such a calculation.

In this section the differences between the assumptions in the theoretical calculation and the characteristics of the experiment are examined. It is then suggested that when these differences are accounted for the theory and experiment are in qualitative agreement.

#### IV.1 The Effect of Using Natural Mercury in the Absorption Cell

When the spectrum of natural mercury is examined the 253.7 nm line is found to consist of a series of very closely spaced lines, (Schweitzer, 1963). This complex line spectrum, results from superposing the hyperfine structure of the various isotopes of mercury which are present in natural mercury.

Different isotopes of the same element have different spectra because the energy levels of an atom are affected not only by the nuclear charge but also by other nuclear characteristics, such as the nuclear angular momentum or spin,  $I$ , the nuclear mass and the nuclear charge distribution. The effect of these nuclear characteristics is examined in detail in Kuhn, 1969 at page 329 and in Sobel'man, 1972 at page 204. For the limited purpose of explaining the results of the experiment it is sufficient simply to note that the chief effect of the difference in nuclear mass and charge distribution between isotopes of the same element is a small shift in the frequencies of the line spectra. The effect of the nuclear spin  $I$  is briefly considered below.

##### Effect of Nuclear Spin

Isotopes with an odd mass number have a half-integral nuclear spin, while isotopes with an even mass number have an integral nuclear spin. Isotopes with an even number of protons and neutrons have zero nuclear spin.

The nuclear spin gives rise to a nuclear magnetic moment,  $\mu_I$ , which is of the order of 1000 times smaller than the Bohr Magneton. The nuclear magnetic moment interacts with the magnetic field caused by the orbital motion of the electrons, and to a lesser extent with the magnetic field generated by the electron spin. This interaction leads to a shift in the energy levels,  $\Delta E_I$ , which is given by:

$$\Delta E_I = A/2 (F(F+1) - I(I+1) - J(J+1)) \quad (4-1)$$

where

A is the magnetic dipole interaction constant,

F is the total angular momentum of the atom and is produced by the coupling of I and J in complete analogy with the coupling of S and L to produce J. The quantum values of F run from  $|J+I|$  to  $|J-I|$ .

A quadrupole coupling which courses a smaller shift in the energy levels has been ignored. It follows from equation (4-1) that isotopes where  $I \neq 0$  will exhibit a hyperfine splitting of the spectral lines while isotopes where  $I = 0$ , will exhibit no hyperfine splitting.

With these results, the structure of the 253.7 nm line depicted in Schweritzer's paper can be understood. The even isotopes of mercury  $\text{Hg}^{204}$ ,  $\text{Hg}^{202}$ ,  $\text{Hg}^{200}$  and  $\text{Hg}^{198}$  produce 253.7 nm lines at slightly different frequencies because of the different nuclear shapes, but, since  $I=0$  for these isotopes, their lines do not exhibit any hyperfine splitting. The odd isotopes,  $\text{Hg}^{199}$  and  $\text{Hg}^{201}$  also produces a frequency shifted 253.7 nm line,

but, since  $I \neq 0$  for these isotopes, their lines exhibit hyperfine splitting described by equation (4-1).

In weak magnetic fields, (those producing line splitting which is smaller than the hyperfine splitting), each hyperfine line splits into Zeeman Components having a definite state of polarization. The first order change in the energy levels,  $\Delta E_Z$ , is given by:

$$\Delta E_Z = \frac{F(F+1) + J(J+1) - I(I+1)}{2F(F+1)} (g_{\alpha j} \mu_0 B_m) \quad (4-2)$$

where  $m$  has the values

$$m = F, F-1, \dots, -F$$

When the magnetic field splitting exceeds the hyperfine splitting equation (4-2) is no longer valid, and the spectral line splits into the  $\pi$  and  $\sigma$ -components given by equation (2-9) and each of these components is in turn split into several equidistant hyperfine lines as a result of the nuclear spin. It is important to note that when  $I=0$ , the Zeeman splitting of the lines is simply governed by equation (2-9) and not equation (4-2).

It follows that when natural mercury is immersed in a weak magnetic field, the 253.7 nm lines of the odd isotopes will independently exhibit a more complex splitting described by equation (4-2). This complex lines splitting makes it difficult to describe the resulting absorption spectrum

with precision, particularly since equation (4-2) becomes invalid at relatively weak field strengths of about 1 KGauss. The splitting of the lines will, however, be used in section IV.3 to describe the shape of the experimental curves for  $J'_{xx}$  and  $J'_{yy}$  in qualitative terms.

#### IV.2 The Shape of the Experimental Incident Line

The light source used in the experiment was a mercury lamp filled with natural mercury and argon. While the lamp produced an intense 253.7 nm line, most of the light was produced at the centre of the lamp's gas bulb and had to traverse a volume of cold gas before being emitted from the lamp. As the cold gas would re-absorb some of the light the lamp would be expected to produce a highly self-reversed line profile.

The 253.7 nm line produced by the lamp was examined in a spectrograph which in the 5th order had a reciprocal linear dispersion of 400 mA/mm. Unfortunately, this did not provide sufficiently high resolution to observe the hyperfine structure or the detailed shape of the line. It was, however, possible to estimate that the width of the line was between 70 and 85 mA. Since Schweitzer's work shows that the width of the hyperfine structure in natural mercury is less than 50 mA it may be assumed from the size of the measured line width that each component line was sufficiently broad to create a continuous line profile marked by narrow troughs produced by the re-absorption of the cold gas.

In the next section the effect of this line profile on the experimental curves for  $J'_{xx}$  and  $J'_{yy}$  is examined.

### IV.3 The Experimental Results

The experimental and theoretical results are in broad agreement when the differences between the theoretical assumptions and the experimental conditions are considered.

In the theoretical curves, Figs. 7, 8 and 9  $J'_{xx}$  is independent of magnetic field strength while in the experimental curves, Figs. 13 and 14,  $J'_{xx}$  varies with field strength. This difference is, however accounted for by the presence of odd isotopes of mercury in the experimental but not the theoretical absorption gas.

It was shown in matrix (2-180) that the magnitude of  $J'_{yy}$  is only affected by the strength and frequency of the  $\sigma$ -components of the absorbing gas, while the magnitude of  $J'_{xx}$  is only affected by the strength and frequency of the  $\pi$ -components. The even isotopes of mercury have zero nuclear spin, (see the appendix) and a non-degenerate ground state and therefore, from equations (2-129) and (2-130), only the  $\sigma$ -components of the 253.7 nm line are field dependent. Thus, when the absorption gas consist entirely of even isotopes of mercury, as in the theoretical calculation, only  $J'_{yy}$  should be field dependent for the 253.7 nm line.

In contrast, odd isotopes of mercury which were present in the natural mercury used in the experiment, produce both  $\pi$  and  $\sigma$ -components which are field dependent. This is because odd isotopes of mercury have a non-zero nuclear spin,  $I$ , (see the appendix) and this produces a degenerate ground state with a non-zero angular momentum,  $F$ . The Zeeman splitting of the

253.7 nm line is governed by equation (4-2). When equation (4-2) is examined for all allowed transitions, it is found that some of the  $\pi$ -components are field dependent. Thus, when the absorption gas contains odd isotopes both  $J'_{xx}$  and  $J'_{yy}$  are field dependent.

While it is clear that the presence of odd isotopes in the experimental absorption gas leads to the field dependence of  $J'_{xx}$ , the shape of the curves for  $J'_{xx}$  in Figs. 13 and 14 can not be verified by direct calculation. This is because the dependence of  $J'_{xx}$  on field strength depends critically upon the line shape of the incident source line, and in the experiment this line shape could not be determined with precision. The general shape of the  $J'_{xx}$  curves can, however, be explained.

Referring to the emission spectrum of natural mercury (Schweitzer, 1963) and Fig. 13, the initial decrease in  $J'_{xx}$  with increasing field strength is caused by the splitting of the  $\pi$ -component absorption away from the centres of the absorption lines of the odd isotopes,  $Hg^{201}$  and  $Hg^{199}$ . This splitting leads to an increased absorption of the  $\pi$ -component of the source line and hence a decrease in the magnitude of  $J'_{xx}$ . The increase in  $J'_{xx}$  at a field strength of about 2.4 K Gauss which is evident in Fig. 13 is likely due to three effects. First, some of the  $\pi$ -components of the absorption lines will be split beyond the width of the source line, reducing the total absorption of the  $\pi$ -component of the source line. Second, some of the  $\pi$ -component absorption lines will shift to the same frequency, again reducing the total absorption of the  $\pi$ -component of the source line. Finally, in stronger fields the coupling between J and I breaks down and the Zeeman splitting is no longer described by equation

(4-2). At these higher field strengths the field dependence of some of the  $\pi$ -components is reversed and these lines again approach the centres of the incident lines which reduces the total absorption of the  $\pi$ -component of the incident source line.

The most striking difference between the theoretical and experimental curves for  $J'_{yy}$  is the oscillatory appearance of the experimental curves. This feature can, however, be explained if the effect of having a number of even isotopes in the absorption gas is examined.

From Fig. 13, the magnitude of  $J'_{yy}$  peaks at field strengths of about 1.25 K Gauss and 2.5 K Gauss. Using equation (2-9) these field strengths lead to a splitting of the  $\sigma$ -component absorption lines of the even isotopes from the line centre by  $86.75 \times 10^{-3} \text{ cm}^{-1}$  and  $173.5 \times 10^{-3} \text{ cm}^{-1}$  respectively. By referring to the emission spectrum of natural mercury (Schweitzer, 1963), it can be seen that the emission lines of the even isotopes are separated from each other as shown below

- a) between 202 and 204       $174 \times 10^{-3} \text{ cm}^{-1}$
- b) between 200 and 202       $177 \times 10^{-3} \text{ cm}^{-1}$
- c) between 198 and 200       $160 \times 10^{-3} \text{ cm}^{-1}$

Thus, a frequency shift of about  $86.75 \times 10^{-3} \text{ cm}^{-1}$  would place the  $\sigma$ -component absorption lines approximately half-way between the line centres, while a shift of about  $173.5 \times 10^{-3} \text{ cm}^{-1}$  would place the  $\sigma$ -component absorption lines approximately at the centre of the adjacent absorption line. It therefore appears that the oscillatory appearance of  $J'_{yy}$  is caused

by the crossing of the  $\sigma$ -component absorption lines which results in a decrease in the total absorption of the  $\sigma$ -component of the incident source line.

In conclusion, the differences between the theoretical assumptions and the experimental results preclude using the latter to verify directly all of the theoretical predictions. However, when the theoretical predictions could be tested directly as in the case of  $I_m (J_{xy})$  the theory and experiment were in good agreement. Further, even when the theory could not be tested directly as in the case of  $J'_{xx}$  and  $J'_{yy}$ , the theory was shown to be at least consistent with the experimental results.

In the next Chapter the conclusion which may be drawn from this study are examined in more detail.

## CHAPTER V

### Concluding Discussion

The object of this study was to examine the feasibility of using the transverse Zeeman effect to produce a narrow band polarizer in the ultra-violet region. The theoretical model indicated that an absorption gas consisting of the even isotope of mercury,  $\text{Hg}^{202}$ , would act as a high quality polarizer for narrow 253.7 nm emission lines produced by an  $\text{Hg}^{202}$  source. The experimental results, while not inconsistent with the theory, were insufficient to verify the theoretical predictions because of the complications introduced by the hyperfine structure of natural mercury in the absorption gas, and by the broad self-reversed source line.

The general theoretical model which was developed for the transmission of light in a gas immersed in a magnetic field is applicable to a variety of spectroscopic studies. Equation (2-112) provides a complete description of the propagation of an EM-wave in a gas with a non-degenerate ground state where the magnetic field may assume any orientation with respect to the direction of propagation. A demonstration of how equation (2-112) could be extended to the case of a gas with a degenerate ground state was presented in equations (2-131) to (2-134).

A general description of the state of polarization of an incident wave after traversing a gas in a transverse magnetic field was provided by matrix

(2-179). The matrix is valid for incident waves with any initial state of polarization.

The theoretical calculation of the polarizing effect of an  $\text{Hg}^{202}$  absorption gas on  $\text{Hg}^{202}$  created 253.7 nm emission lines with a variety of line widths indicated that the technique should produce high quality narrow band polarizers in the ultra-violet region.

The experimental results supported some of the theoretical predictions. For example, the theoretical prediction that  $I_m(J_{xy}) = 0$  for an unpolarized incident source line was verified to within experimental error. However, the hyperfine structure of the natural mercury used in the experimental absorption gas, and the broad source line generally precluded a direct comparison between theory and experiment.

The width of the source line limited the variation of  $J'_{yy}$  to a single order of magnitude, while the theoretical curves of  $J'_{yy}$  varied over several orders of magnitude. It was for this reason that the theoretical and experimental plots of  $J'_{yy}$  and  $J'_{xx}$  were not presented in the same graph.

The hyperfine structure caused  $J'_{xx}$  to be field dependent contrary to the theoretical model. Further, the isotope shift of the 253.7 nm line and the presence of a number of even isotopes in natural mercury lead to line crossing which in turn caused the plots of  $J'_{yy}$  as a function of field strength to assume an oscillatory form.

The precise shapes of the experimental curves of  $J'_{xx}$  and  $J'_{yy}$  could not

be theoretically calculated because the source line profile, upon which the calculation critically depend, could not be measured with the limited resolution of the available spectrograph.

Thus, while the experimental results confirm the theory in some limited respects, the experiment could not provide a quantitative test of the theory. To test the theoretical prediction that the transverse Zeeman-effect can be used to produce a high quality polarizer a gas consisting of a single isotope with zero nuclear spin should be used in the experiment. Further the source line should be reasonably narrow; if it is broad, then its line profile should be known.

References

1. Abramowitz, M. and Stegun, I.A., Handbook of Mathematical Functions, Dover Publications, New York, 1972.
2. Ali, A.W. and Griem, H.R., Physical Review, 140, A1044 (1965) and Erratum, Physical Review, 144, 366 (1966).
3. Bevington, P.R., Data Reduction and Error Analysis for the Physical Sciences, McGraw-Hill Book Co., New York, 1969.
4. Born, M. and Wolf, E., Principles of Optics, Pergamon Press, Oxford, 1975.
5. Camm D.M. and Curzon, F.L., Canadian Journal of Physics, 50, 2866 (1972).
6. Condon, E.V., and Shortley, G.H., The Theory of Atomic Spectra, Cambridge University Press, New York, 1964.
7. Corney, A., Kibble, B.P. and Series, G.W., Proc. R. Soc., A293, 70 (1966).

8. D'Yakonov, M.I. and Perel, V.I., Soviet Physics JETP, 21, 227 (1965).
9. Dodd, J.N. and Series, G.W., Proc. R. Soc., A263, 353 (1961).
10. Heitler, W., The Quantum Theory of Radiation, Oxford University Press, Oxford, 1954.
11. Jackson, W.D., Classical Electrodynamics, John Wiley & Sons, New York, 1975.
12. Klein, M.V., Optics, John Wiley & Sons, Inc., New York, 1970.
13. Kuhn, H.G., Atomic Spectra, Academic Press, New York, 1969.
14. Lurio, A., Physical Review, 140, A1505 (1965).
15. Merzbacher, E., Quantum Mechanics, John Wiley & Sons, Inc., New York, 1970.
16. Messiah, A., Quantum Mechanics Volumes I and II, John Wiley & Sons, Inc., New York, 1962.
17. Rabinovitch, K., Canfield, L.R. and Madden, R.P., Applied Optics, 4, 1005 (1965).

18. Rose, M.E., Elementary Theory of Angular Momentum, John Wiley & Sons, Inc., New York, 1957.
19. Schweitzer, W.G., Journal of the Optical Society of America, 53, 1055 (1963).
20. Sobel'man, I.I., Introduction to the Theory of Atomic Spectra, Pergamon Press, Oxford, 1972.
21. Stanzel, G., Z. Physik, 270, 361 (1974).
22. Stroke, G.W., Physics Letters, 5, 45 (1963).

APPENDIX

Properties of the 253.7 nm Line

a) A term diagram of the Atomic Spectra of Hg can be found in Condon and Odishaw (ed.), Handbook of Physics, McGraw-Hill Book Company, New York, 196, at page 7-45.

b) Lifetime of the state  $^3P_1$ , from Lurio, 1965

$$\tau_{\alpha j}(^3P_1) = 1.14 \times 10^{-7} \text{ sec.}$$

which gives an absorption oscillator strength,  $f_a$ , of

$$f_a = 2.54 \times 10^{-2}$$

c) Landé  $g_{\alpha j}(^3P_1)$ , from Lurio, 1965

$$g_{\alpha j}(^3P_1) = 1.486094(8)$$

d) Natural Isotopes of Mercury

| <u>ISOTOPE</u>           | <u>% NATURAL ABUNDANCE</u> | <u>NUCLEAR SPIN, I</u> | <u>ATOMIC MASS</u> |
|--------------------------|----------------------------|------------------------|--------------------|
| ${}_{80}\text{Hg}^{196}$ | 0.146                      | 0                      | 195.9658           |
| ${}_{80}\text{Hg}^{198}$ | 10.02                      | 0                      | 197.9668           |
| ${}_{80}\text{Hg}^{199}$ | 16.84                      | 1/2                    | 198.9683           |
| ${}_{80}\text{Hg}^{200}$ | 23.13                      | 0                      | 199.9683           |
| ${}_{80}\text{Hg}^{201}$ | 13.22                      | 3/2                    | 200.9703           |
| ${}_{80}\text{Hg}^{202}$ | 29.80                      | 0                      | 201-9706           |
| ${}_{80}\text{Hg}^{204}$ | 6.85                       | 0                      | 203-9735           |

(Taken from Handbook of Chemistry and Physics, The Chemical Rubber Co., Cleveland, 1969 on page B-491 to B-494)

e) FREQUENCY AND WAVELENGTH OF THE 253.7 nm LINE

$$\lambda_0 = 2536.519 \text{ \AA}$$

$$\omega_0 = 7.42613 \times 10^{15} \text{ Hz.}$$

(Taken from, Handbook of Chemistry and Physics Op. Cit. Page E-222)

f) The Properties of the Hyperfine Structure of the 253.7 nm Line  
Structure of the 253.7 nm Line can be found in Schweitzer, 1963.